Spring 2015

Novel methods for manipulating ion types in the solution and gas phases for the structural analysis of biomolecules using Mass Spectrometry

Christine M Fisher
Purdue University

Graduate School Form 30
(Updated 11/20/2014)

PURDUE UNIVERSITY
GRADUATE SCHOOL
Thesis/Dissertation Acceptance

This is to certify that the thesis/dissertation prepared

By Christine M. Fisher

Entitled NOVEL METHODS FOR MANIPULATING ION TYPES IN THE SOLUTION AND GAS PHASES FOR THE STRUCTURAL ANALYSIS OF BIOMOLECULES USING MASS SPECTROMETRY

For the degree of Doctor of Philosophy

Is approved by the final examining committee:

Scott A. McLuckey

Yu Xia

Marcy H. Towns

Peter T. Kissinger

To the best of my knowledge and as understood by the student in the Thesis/Dissertation Agreement, Publication Delay, and Certification/Disclaimer (Graduate School Form 32), this thesis/dissertation adheres to the provisions of Purdue University's "Policy on Integrity in Research" and the use of copyrighted material.

Scott A. McLuckey

Approved by Major Professor(s): _____

_____

Approved by: R. E. Wild 03/31/2015

Head of the Department Graduate Program Date

NOVEL METHODS FOR MANIPULATING ION TYPES IN THE SOLUTION AND GAS PHASES FOR THE STRUCTURAL ANALYSIS OF BIOMOLECULES USING MASS SPECTROMETRY

A Dissertation

Submitted to the Faculty

of

Purdue University

by

Christine M. Fisher

In Partial Fulfillment of the

Requirements for the Degree

of

Doctor of Philosophy

May 2015

Purdue University

West Lafayette, Indiana

To Mom, Dad, J.C., and Ryan

Thank you for your unending love and support through thick and thin.

You all mean the world to me.

ACKNOWLEDGEMENTS

I want to begin by thanking my Mom and Dad, Patty and Jim, and my brother, J.C. Expressing the gratitude I have for you all is not easy to put in words, but I'll try. I know that without your love and support there is no way I could have accomplished half of what I have set out to do. Thank you for always believing in me, even when I struggled to do so myself. Mom, you have been my emotional rock. I know if I ever need to be comforted or if I need to talk to someone that will make me feel better when I am struggling, you are always there. Dad, you have been the voice of reason. You may not always tell me what I want to hear (especially in the moment), but you are usually right and are telling me what I need to hear. Thank you for raising me to be considerate of others and to do my best at everything I try to do. J.C. you have always been able to cheer me up, without even trying to. You have a great personality and sense of humor and I've always wanted to be as "cool" as you. You are a strong and brave person and I'm honored to call you my brother. I know you will succeed at anything you put your mind to. I love you all so much.

Ryan, you are my best friend and I can't imagine having a better, better half. I am so lucky I met you before coming to graduate school. I don't think I could have made it through without having you to support me through all the ups and downs. Even though

long distance has been hard, I can't tell you how much I look forward to hearing your voice each day and to our Netflix dinner dates. Thank you for everything. I love you with all my heart. I also want to thank my four-legged best friend, Molly. I don't know how you know when I've had a rough day, but you can tell and you are always there to make me feel better. Thank you for always thinking I'm the best person in the world (even if it is just for food). You are a great listener.

Professor McLuckey, it has been an honor to have had the opportunity to work in your lab at Purdue. Thank you for all of your advice, mentorship, and support. Thank you for sharing your passion for science with me. I have learned so much through working with you and observing how you think about and approach problems. I have really enjoyed and appreciated the sub-group meetings where we are able to practice communicating our research and are able to get feedback with new, exciting ideas to try each week.

To all the McLuckey group members I have had the pleasure to work with, thank you for all of your kindness, guidance, mentorship, and fun times! I'd like to thank Dr. Boone Prentice, for teaching me so many things, especially how to use the dueling trap and how to work with power supplies, switch boxes, scopes, voltmeters, etc. Boonedizzle, you have been a great mentor whom I'll never be able to repay. You are one of the most hardworking people I know and I know that will carry you far as a professor. Dr. Anastasia Kharlamova, Stasia, thank you for being an amazing lab mate with such a positive attitude and friendly personality. I always felt better after talking

with you and you always brighten my day! I aspire to be as good of a lab mate and coworker as you have been! I also want to thank Dr. Ryan Hilger for his mentorship and advice. Without your creative ideas (i.e. square wave electroosmosis) my papers would be much less interesting and impactful. Dr. Will McGee, Willbo, I appreciate all of your encouragement and your advice. You are a very wise person, whom I trust and admire very much. Joshua Gilbert (I'll spare you the nickname, here...), thank you for being one of my best friends and coworkers in graduate school. I have really appreciated bouncing ideas off of you and all the fun times we have had. I know I would not have made it through graduate school without our friendship. Josh, Carl Luongo, and Corinne DeMuth, I have appreciated going through all of the grad school hurdles with all of you. Thank you all for being there for me when times were tough and I was laugh-crying. I'm going to miss our daily coffee breaks! Tiffany Jarrell, BGF, it has been my pleasure to have you as a "best good friend" through graduate school. I know I could not have tackled all of the hurdles without your support and without the fun times we shared together (i.e. dangy-shoo-doo, shopping, dancing, cooking, etc.). You, Josh, and Boone are all a huge part of some of the best memories I have during graduate school. Thank you all for your friendship, which has meant so much to me.

I am very appreciative of all the older students, who have taught me a great deal about working with other people and various lab techniques. Dr. Kerry Hassell, thank you for helping me feel welcome in McLuckey group. Dr. Marija Mentinova, thank you for helping keep the lab well organized and running efficiently. Dr. John Stutzman, I

appreciate your critical thinking skills and that you are not easily convinced. You pushed me to thoroughly prove my conclusions, which has helped improve my own critical thinking skills. Dr. James Redwine, you are like a walking encyclopedia and I appreciate that you were always willing to explain confusing concepts to me. Dr. Yang Gao, you are incredibly intelligent and I appreciated being able to talk with you. Dr. Ian Webb, Big Cat, thank you for your help on the QSTAR. Dr. Ken Chanthamontri I hope we will have the opportunity to play volleyball together someday!

I also want to thank all of the younger students I have had the opportunity to work with. Alice Pilo, I admire your ability to learn new areas so quickly from the literature, I feel like I have learned a lot through your research and group meeting presentations. Stella Betancourt, you have come so far and I know you will continue to do great things. You have done an excellent job of being nimble and flexible when projects come and go. Jiexun Bu, I admire your ability to pick up instrumentation and molecular modeling calculations so quickly. I have definitely learned a lot from you. I know you will be able to accomplish anything you set your mind to. Eric Dziekonski, I appreciate that you are able to pick up electronics so quickly, which has helped me numerous times. I have enjoyed hanging out with you and Amy Bueno outside of work, which has helped keep me sane! You are incredibly intelligent and I admire all of the skills you have. I know you will do great things. Zhou Peng, your research is interesting and I feel like I have learned a great deal through the work you have done. Dr. Andrew DeBlase, Dr. James Redwine, Nicole Burke, and John Hopkins, I admire the guts you all

have to work on such a difficult project with the cold ion spectroscopy instrument. You all have taught me that perseverance pays off and I know the challenges you face with this project will help all of you do great things in the future. To the first year students, Feifei Zhao, Nan Wang, and Mack Shih, you all have a great group of older students in the lab currently to learn from. You all have bright futures ahead of you and it can be whatever you make it. Work hard, but have fun while doing it! I hope you all can enjoy your research in the McLuckey group as much as I have.

I also want to thank the collaborators I have had the opportunity to work with, especially everyone from AB Sciex, namely Dr. Jim Hager, Dr. Larry Campbell, Dr. Yves LeBlanc, and Dr. Frank Londry. You have all been an invaluable resource for our lab. Thank you for all of your help with keeping the instruments running which has enabled me to pursue many interesting experiments. The advice and information I have learned through our scientific discussions will help me in my future endeavors. I also want to thank Dr. Robert Santini for many interesting scientific discussions. I know your ideas have definitely helped improve my research by helping me think about things differently. Your breadth of knowledge has always amazed me and I appreciate that you have shared it with me. I also want to thank my undergraduate advisor, Professor Glen P. Jackson, who first encouraged me to pursue a career in chemistry. He was the first mentor I had as a young chemist and has had a large impact on where I am today. Thank you. I'd also like to acknowledge my committee members, Professor Yu Xia, Professor Marcy Towns, and Professor Peter Kissinger. Thank you for your advice and for sharing

your time with me. Professor Yu Xia, thank you for giving me the opportunity to be your teaching assistant. I really enjoyed teaching the analytical chemistry undergraduate course with you.

TABLE OF CONTENTS

Page

Page

Page

LIST OF FIGURES

Figure Page

Figure Page

Figure Page

Figure Page

Figure Page

Figure Page

Appendix Figure Page

LIST OF ABBREVIATIONS

2D	Two Dimensional
3D	Three Dimensional
AA	Acetic Acid
AP	Atmospheric Pressure
C-I	Carbon-Iodine Bond
CA	Collisional Activation
CE	Capillary Electrophoresis
CEM	Chain Ejection Model
CI	Chemical Ionization
CID	Collision Induced Dissociation
CRM	Charge Residue Model
CSD	Charge State Distribution
DC	Direct Current
DDC	Dipolar Direct Current
ECD	Electron Capture Dissociation
EESI	Extractive Electrospray Ionization
EI	Electron Ionization

EOF	Electroosmotic Flow
ESI	Electrospray Ionization
ETD	Electron Transfer Dissociation
FBDSA	4-Formylbenzene-1,3-Disulfonic Acid
FD-ESI	Fused Droplet-Electrospray Ionization
FT	Fourier Transform
HDX	Hydrogen/Deuterium Exchange
HPLC	High Pressure Liquid Chromatography
ICR	Ion Cyclotron Resonance
IEM	Ion Evaporation Model
IRMPD	Infrared Multi-Photon Dissociation
LIT	Linear Ion Trap
MALDI	Matrix Assisted Laser Desorption Ionization
MS	Mass Spectrometry
MS^n	Tandem Mass Spectrometry
MSAE	Mass Selective Axial Ejection
MS/MS	Tandem Mass Spectrometry
*m/*z	Mass to charge ratio
nESI	nanoElectrospray Ionization
q	RF only Quadrupole Ion Trap
Q	RF/DC Quadrupole Ion Trap

QIT	Quadrupole Ion Trap
RF	Radio Frequency
SID	Surface Induced Dissociation
SIMS	Secondary Ion Mass Spectrometry
Sulfo-NHS	*N*-hydroxysulfosuccinimide
Sulfo-SIAB	Sulfosuccinimidyl (4-Iodoacetyl)Aminobenzoate
SNa	Sulfosuccinimidyl Acetate
TOF	Time of Flight
UVPD	Ultraviolet Photodissociation

ABSTRACT

Fisher, Christine M. Ph.D., Purdue University, May 2015. Novel Methods for Manipulating Ion Types in the Solution and Gas Phases for the Structural Analysis of Biomolecules Using Mass Spectrometry. Major Professor: Scott McLuckey.

Mass Spectrometry has become a valuable tool for the analysis of a variety of molecules, making it applicable to many fields. The advent of nanoelectrospray ionization (nESI) as a soft/low energy ionization technique has enabled the analysis of large, intact biomolecules. Most mass spectrometry experiments consist of three main steps: ionization, probe step(s), and mass analysis. The present work focuses on a variety of methods for altering ion types at various stages of the mass spectrometry experiment to affect ion fragmentation.

Ion types can be manipulated in the solution/droplet phases using novel nESI emitters, generated from borosilicate theta capillaries. These nESI emitters enable the mixing of two solutions as they are sprayed into the mass spectrometer. This technique has been used to manipulate protein charge states (i.e. protein folding and unfolding) and to demonstrate peptide/protein analyte-reagent complex formation and covalent modification. This technique provides a simple and inexpensive method for manipulating ion types as the ions are generated during the electrospray process on the sub-millisecond timescale. These nESI emitters are also expanded to longer solution

mixing times through the use of electroosmotic flow (EOF) between the two channels of the theta capillary prior to mass analysis. This work presents initial efforts to use theta capillaries to develop a "lab-in-a-tip" to provide for the manipulation of ion types on short timescales just prior to mass analysis.

Additionally, ion types can be manipulated once the ions are in the gas-phase and trapped inside the mass spectrometer via ion/ion reactions. This work presents ion/ion reactions with reagents containing chromophores, which can be activated via ultraviolet photodissociation (UVPD) to generate radical peptide cations. Altering ion types in this way provides complementary sequence information upon collision induced dissociation (CID) when compared to CID of the even electron species.

The McLuckey group is well known for work with ion/ion reactions to modify ion types and to conjugate biomolecules through covalent chemistry in the gas-phase. However, the kinetics and energetics of these reactions are not well known. This work will provide a method for measuring ion/ion reaction kinetics using dipolar DC CID (DDC-CID), which was previously developed in the McLuckey lab. Knowledge of gas-phase ion/ion reaction kinetics and energetics will provide insights for improving current ion/ion reaction efficiencies as well as for improving reagent design for future ion/ion reactions.

CHAPTER 1. INTRODUCTION

Since the first parabola mass spectrum was collected by Sir J. J. Thomson in the early 1900's,[1,2] mass spectrometry has become an invaluable analytical tool. Through a series of significant advancements over the past century, mass spectrometry (MS) has developed into a routine technique that is now found at the forefront of a number of diverse fields due to its unparalleled sensitivity, resolution, limit of detection, speed, and versatility. Mass spectrometry has made significant contributions to many fields including forensics, food chemistry, the analysis of natural products, and the study of reaction kinetics and thermodynamics. Particularly with the advent of electrospray ionization and tandem mass spectrometry, the analysis of the structures and interactions of large biomolecules has become possible. Additionally, mass spectrometry has been coupled to various other analyte separation methods, including liquid and gas chromatography and capillary electrophoresis. Because many of these separation methods are orthogonal to mass spectrometry (i.e. the techniques separate analytes based on different characteristics), the power of each of these techniques is amplified making mass spectrometers invaluable for complex mixture analysis.

The simplest mass spectrometry experiment includes two main stages: ionization and mass analysis. Ionization, includes transferring the analyte from the bulk sample

into the gas phase and converting the analyte into an ion. During the mass analysis step the mass spectrum containing the generated ions' mass to charge ratios is obtained. In more complex mass spectrometry experiments additional ion manipulation techniques (e.g. tandem MS, ion activation, ion/molecule, and ion/ion reactions) can be applied to probe ions via fragmentation and reactions that can lead to covalent modifications or altered ion types. These probing techniques are useful for determining the structures of molecules. More recently, these techniques have become invaluable in the analysis of biomolecular structures from the primary sequence structure to higher order structures of biomolecular complexes.

1.1 Electrospray Ionization

The first step in all mass spectrometry experiments is the generation of gaseous analyte ions that can be steered and controlled in an electric or magnetic field under vacuum. There are many different ionization methods that can create a variety of different ion types. In general, the main ionization methods commonly used in mass spectrometry include electron ionization (EI) and chemical ionization (CI, e.g. proton transfer, charge transfer, adduct formation), desorption ionization (e.g. SIMS, secondary ion MS, and MALDI, matrix assisted laser desorption ionization), and spray ionization. There are many factors that should be considered in order to determine the best ionization method for a given analyte. These factors include the energy distribution imparted on the ions (i.e. hard vs. soft ionization), the chemical characteristics of the

analyte (e.g. vapor pressure, solubility, thermal stability), the phase of the sample matrix (i.e. solid, liquid, gas), and the efficiency and stability of the ionization method.

Ambient ionization methods are characterized by ionization at atmospheric pressure followed by transfer into the main vacuum of the instrument; often through a differentially pumped region to assist in ion transfer. Ambient ionization methods have become popular due to their simplicity and compatibility with on-line separation methods. In addition, the advent of low energy/soft ambient ionization techniques, such as atmospheric pressure MALDI (AP-MALDI) and electrospray ionization (ESI), has enabled the analysis of large, intact biomolecules.

1.1.1 History

Electrospray ionization (ESI) was first demonstrated on macromolecules such as polystyrene by Dole *et al.* in the late 1960's and early 1970's.[3,4] John Fenn *et al.* applied ESI to the analysis of proteins in 1989 where multiply charged, intact, gaseous protein ions were generated for the first time.[5] The multiple charging characteristic of ESI brought the protein signal into the mass range of most commercially available mass spectrometers. ESI has also become one of the most commonly used ionization techniques for large and small analytes alike due to its compatibility with continuous flow separation techniques including high pressure liquid chromatography (HPLC)[6] and capillary electrophoresis (CE).[7] ESI has been used to study a wide range of chemicals of varying size and complexity from small organic molecules to extended polymeric

systems. Because ESI has had such an impact on many versatile fields of study, expansive efforts have been directed toward understanding the electrospray process and ionization mechanisms.[8,9,10,11]

1.1.2 The Electrospray Process

Practically, ESI is performed by pumping an analyte solution through a capillary (~100 µm diameter) at flow rates in the low µL/min range. A potential, usually 2-5 kV, is applied to the capillary, which creates an electric field between the capillary and the orifice of the mass spectrometer, the counter electrode. The electric field results in charge separation within the solution. The electric field at the tip of the capillary (E_c) can be calculated as follows:[8,12]

$$E_c = \frac{2\,V_c}{r_c \ln 4d/r_c} \qquad (1.1)$$

where V_c is the applied potential, r_c is the radius of the capillary orifice, and d is the distance from the capillary to the counter electrode. As charge builds up on the surface of the solution, a "Taylor cone" will form at the end of the capillary. The "Taylor cone" is named in homage of Sir Geoffrey Taylor, who introduced the first theoretical explanation for liquid protrusions and disintegrating droplets in an electrical field in 1964.[13] The liquid will continue to protrude from the capillary until the Coulombic repulsion on the surface of the droplet is equal to the surface tension of the solution, known as the Rayleigh limit.[14,15] The total charge on a droplet surface (q_r) at the Rayleigh limit is described by:

$$q_r = 8\pi(\epsilon_0 \gamma R^3)^{1/2} \quad (1.2)$$

where ε_0 is the permittivity of free space, γ is the surface tension of the droplet, and R is the droplet radius. Once the solution reaches the Rayleigh limit, a Rayleigh fission occurs in which a large, highly charged droplet will break off from the Taylor cone. As this satellite droplet travels toward the mass spectrometer, solvent evaporates from the droplet which decreases its volume and thus increases the charge density on the surface of the droplet. This droplet will undergo another fission process once it reaches the Rayleigh limit. Numerous subsequent fissions will occur producing a cascade of progeny droplets until all of the solvent is evaporated.[10] Each successive fission event results in a loss of 2% of the mass and 15% of the charge of the parent droplet.[8,9] The mechanisms by which ions are formed from these charged droplets will be discussed in more detail below.

ESI is an electrochemical process with a continuous electrical current, which can be represented as an electrolytic cell.[8,10] In the positive mode, positive ions are generated and sprayed from the capillary. As a result, negative charge must also be removed from the solution to maintain charge balance in the solution. The oxidation of solution components (i.e. analyte and solvent) occurs at the tip of the capillary, the anode, which provides the removal of negative charge from the solution. Reduction occurs at the orifice of the mass spectrometer, the cathode, where positive ions are neutralized. The current generated by the spray travels from the orifice of the mass spectrometer (cathode) toward the negative terminal of the power supply, then to the

capillary (anode) from the positive terminal of the power supply, and finally returns to the orifice of the MS. The spray current is representative of the rate of charge separation and the current produced by the oxidation and reduction reaction limits the total rate of ion production. The electrospray ion current (i_{ES}) is often limited to less than 1 μA[16] and can be calculated according to the Hendricks equation:[12,17]

$$i_{ES} = H v_f^v \sigma_S^n E_c^\varepsilon \quad (1.3)$$

where H is a constant determined by the dielectric constant and the surface tension of the solvent, v_f is the solution flow rate, E_c is the electric field at the capillary tip as given above in equation (1.1), and σ_S is the specific conductivity of the solution. A similar electrolytic cell can be used to describe ESI in the negative mode, however the capillary acts as the cathode, where reduction occurs, while the orifice is the anode, where oxidation occurs and the current flow is reversed relative to positive mode ESI.

1.1.3 Ionization Mechanisms

While the general electrospray process described above explains the generation of charged droplets from a solution, the mechanism(s) for generating ions from the charged droplets remains to be discussed. There are currently two main models used to describe the ionization mechanisms of ions.[18] The first model was proposed by Dole *et al.* in 1968 and is commonly referred to as the charge residue model (CRM).[3] The second model is called the ion evaporation model (IEM), which was first proposed by Iribarne and Thomson in 1976.[19] Both mechanisms have been well studied and experimental

support has been provided for both mechanisms. Recently, an additional model has been proposed by Konermann *et al.*, termed the chain ejection model (CEM).[20]

1.1.3.1 Charge Residue Model

The charge residue model (CRM) relies on the Rayleigh fission process[14,15] described above for the ionization of molecules. A series of Rayleigh fissions occurs until the final generation of progeny droplets in which each droplet contains a single analyte molecule. The remaining solvent in this droplet will evaporate, leaving behind the charge, which complexes with the analyte molecule. Often the charge carriers in this mechanism are remaining protons and/or metal ions such as sodium and potassium. Since Dole's first description of the CRM for neutral macromolecules, the model has been extended to describe the ionization of analytes including small metal and organic ions[21] and multiply charged macromolecules.[22] Ions that are thought to be ionized via the CRM tend to be more adducted with salts such as sodium and potassium as these highly soluble species are concentrated toward the center of the droplets during solvent evaporation.[23] The CRM is generally accepted as the mechanism for the ionization of larger ions, including native/globular proteins.[22] Fernández de la Mora provided experimental evidence that ions with masses ranging from 3.3 kDa to 1.4 MD ionize via the CRM by comparing the observed charge states of globular proteins and dendrimers to the charge at the Rayleigh limit (q_r) on a droplet of approximately the same radius as the bare molecule. The Rayleigh limit is inherently an upper-bound for the charge state

of ions formed via the CRM as a charge state greater than q_r would result in another Rayleigh fission to relieve Coulombic repulsion as the droplet evaporates. De la Mora found the charge states for globular proteins ranged from 65-110% of the calculated q_r value, thus indicating the macromolecule ions were mainly formed via the CRM.[22]

1.1.3.2 Ion Evaporation Model

The second most widely accepted model for ionization via ESI is the ion evaporation model.[19] According to this model, ions are generated by evaporation from the surface of droplets during the droplet desolvation process, once the droplet radii decreases below 10 nm.[11] As ions are ejected from the surface of the droplet, they remove charge from the droplet, providing an alternative mechanism to reduce charge repulsion on the droplet surface as opposed to droplet fissions at the Rayleigh limit. Evidence for this mechanism has been provided by Iribarne's and Thomson's work with NaCl clusters in electrospray droplets, in which they observed more abundant signal from Na^+ and hydrated Na^+ species compared to the abundance of larger salt complexes. The salt clusters were presumed to have formed via the CRM, while the presence of hydrated Na^+ ions indicated that some of the sodium cations evaporated off the surface of the droplet with solvent molecules.[19] The IEM is generally accepted as the primary ionization mechanism for small inorganic ions.[11]

As mentioned above, the analyte size plays a significant role in the mechanism for ion generation (i.e. larger molecules via CRM, smaller molecules via IEM). However,

the surface activity of the analyte will also influence the mechanism by which it is ionized. Analytes that are very surface active (e.g. hydrophobic detergents) will tend to reside on the surface of the droplet. Thus surfactants will be more likely to evaporate from the surface of the droplet taking surface charge with them (IEM) when compared with less surface active analytes, which are more likely to ionize via the CRM. One example in which the surface activity has been shown to affect the ionization mechanism of the analyte is when comparing the ionization of folded/native proteins and unfolded/denatured proteins.

As described above, large globular proteins are expected to ionize via the CRM. However, unfolded proteins tend to be more hydrophobic and thus more surface active than folded proteins. In 2013 Konermann and coworkers proposed a third ionization mechanism, dubbed the chain ejection model (CEM), to describe ion formation from denatured or unfolded proteins.[20] This mechanism is very similar to the IEM, where denatured protein ions are generated at the surface of the droplet via the charge residing on the surface. More precisely, it is proposed that a small portion of the protein reaches the droplet surface and begins to protrude from the surface, where it picks up charge and is ejected from the droplet. As the protein is ejected, charge equilibration occurs between the droplet surface and the protein, which provides Coulombic repulsion to propel the protein out of the droplet.[20,24] A comparison of the CRM and CEM has been performed via the analysis of salt adducts on various charge states of proteins.[25] The correlation between the observed CSD of a protein and its conformation

in solution has been well studied.[26,27,28] Higher charge states correspond to more denatured proteins, while folded proteins tend to have lower charge states due to Coulombic repulsion. It has often been observed that the lower protein charge states tend to contain more salt adducts, while the higher charge states are less adducted. This observation is consistent with the lower charge states/folded protein ions being formed via the CRM, while the higher charge states/denatured protein ions are formed via the CEM.[25]

The mechanism(s) of ion formation via ESI is not fully understood and thus is still an active area of research. It is clear that none of the models described above are able to explain all observations and it is quite possible that all of these processes are occurring simultaneously during the dynamic ESI process.

1.1.4 Nanoelectrospray Ionization (nESI)

A variation of ESI, namely nanoelectropsray ionization (nESI), has recently gained popularity due to its higher salt tolerance, improved sensitivity, and low sample consumption compared to conventional ESI.[29,30] While the general electrospray process and mechanisms ion formation are very similar for nESI and ESI, there are several differences that distinguish the techniques. The tip diameters for nESI (100s of nm to ~10 μm) are much smaller than the tip diameters for ESI and thus, the first droplets generated from the Taylor cone are an order of magnitude smaller in diameter than those produced by ESI. The smaller parent droplets enable the nESI tip to be placed

closer to the orifice as less time is needed for desolvation compared to larger ESI droplets, resulting in a better sampling efficiency for nESI compared to ESI in which most of the generated ions are lost.[11] Additionally, nESI has become heavily utilized in the biological mass spectrometry community due to its lower sample volume requirement, higher salt tolerance, and compatibility with aqueous solvent systems. The preparation of many biomolecules involves the addition of salts (i.e. from buffers), thus the salt concentration of these samples is usually much greater than in other fields. Karas and coworkers have shown that nESI will produce biological ions at higher concentrations of salt than can be observed by ESI, which they have attributed to the much smaller initial droplet size.[31,32] ESI of aqueous solutions is also challenging due to the high surface tension of water, which requires larger ESI voltage gradients and thus increases the propensity for electrical discharges. Most biological molecules are inherently soluble and more stable in water, which makes nESI the preferred ionization method for these aqueous samples due the ability to operate at lower voltage gradients.[11]

In practice, nESI is performed using borosilicate glass capillaries that are pulled to a tip of ~1-10 μm. These capillaries can be coated with a conductive material, or a wire electrode can be inserted into the channel. A ~1-2 kV potential is applied to either the coating or the wire electrode that is in contact with the solution. The potentials associated with nESI are usually lower than those used in ESI due to the shorter tip-orifice distance and the smaller tip diameter. The tip diameter is also small enough that the application of a potential creates an electric field at the tip that is sufficient to

produce a spray without requiring a pressurized flow as is used in ESI.[11] All experiments that will be described in this work (*vide infra*) were performed using nESI with a wire-in-a-capillary setup to generate gas-phase ions.

1.2 Mass Analyzers

There are a variety of mass analyzers that separate ions based on their motions in static or dynamic electric or magnetic fields. Ions are separated based on their mass and charge, thus the x-axis of a mass spectrum scales with increasing mass (*m*) to charge (*z*) ratio (*m/z*). All mass analyzers have various advantages and limitations, thus the type of mass analyzer used for a given experiment is usually chosen based upon the ultimate goal of the experiment. The common figures of merit for mass spectrometers include mass range, analysis speed, transmission efficiency, resolution, and mass accuracy. The combination of a variety of mass analyzers into hybrid instruments is a common method used to compound the advantages of each of the stand-alone mass analyzers. Quadrupole ion traps are frequently used in hybrid instruments to mass select an individual ion for further analysis in the following mass analyzer (i.e. ion cyclotron resonance (ICR) or time of flight (TOF)). The main mass analyzers that are currently used include quadrupoles, quadrupole ion traps (QIT), orbitraps, time of flight (TOF), magnetic and electric sectors, and Fourier transform ion cyclotron resonance (FT-ICR). The instruments used in this work are limited to quadrupole ion traps (i.e. 2D/linear QIT and 3D QIT) and time of flight mass spectrometers. A more detailed description of the

operation and characteristics of the mass analyzers relevant to this work will be discussed below. Figure 1.2 and Figure 1.3 show the instrument schematics of the homebuilt 3D ion trap mass spectrometer[33] and QqTOF (Q-STAR Pulsar XL, AB Sciex, Toronto, ON, Canada) [34] used for the present work, respectively.

1.2.1 Quadrupole Ion Traps

Quadrupole ion traps (QIT) are one of the most versatile mass analyzers which also function as ion transmission devices. They can be found in many commercially available mass spectrometers as they are relatively simple to combine with each other and with other mass analyzers, and are capable of performing ion isolations to simplify mass spectra. They are particularly amenable to tandem MS experiments, *vide infra*. Generally, there are two types of QITs: the 3D, or Paul ion trap, and the 2D, or linear ion trap. The Paul ion trap is so-called as it was first described by Paul and Steinwedel in 1960.[35] More recently, the 2D or linear ion trap was developed from linear quadrupole ion guides.[36] 3D quadrupole ion traps perform better at higher mass extensions (i.e. higher *m/z*) than 2D quadrupoles and are capable of trapping ions of either polarity under the same conditions and in a small volume, making them advantageous reaction vessels. However, 2D ion traps have better trapping efficiencies and are more resistant to space charge effects due to the larger trapping volume.[37] The details of operation for each of the QITs are provided below.

1.2.1.1 3D Quadrupole Ion Traps

Although the Paul trap was first proposed in 1960,[35] it was not until 1984 that it was used as a mass spectrometer via a mass instability scan (the most popular mode of operation currently in use).[38] The trap consists of a central ring electrode that is enclosed by two hyperbolic endcap electrodes, each corresponding to either the entrance endcap or the exit endcap. In the most common method of operation, ions are injected into the trap through a hole in the center of one of the endcap electrodes, the entrance endcap. Ions are held in the trap by a trapping potential well formed by the quadrupolar field, which is produced by applying a radio frequency (RF) voltage in the radial (*r*) dimension (i.e. on the ring electrode) and a direct current (DC) potential in the axial (*z*) dimension (i.e. on the endcaps). The most common method of mass analysis from the 3D trap is a mass instability scan, in which the amplitude of the RF is ramped from low to high amplitude resulting in the successive instability of ions of increasing m/z. Ions are ejected through both the entrance endcap (*vide supra*) as well as the exit endcap (the endcap opposite of the entrance endcap), however there is usually only a detector outside the exit endcap. Thus, up to only 50% of the ions originally injected into the trap are ultimately detected. However, there have been efforts to increase the detection efficiency such as the application of a monopolar DC field to push ions closer to the exit endcap during mass analysis.[39] The stability, or instability, of an ion can be determined using the solutions to the Mathieu equations:[40,41]

$$a_z = -\frac{16eU}{m(r_0^2+2z_0^2)\Omega^2} = -2a_r \qquad (1.4)$$

$$q_z = \frac{8eV}{m(r_0^2+2z_0^2)\Omega^2} = -2q_r \quad (1.5)$$

where a_z and a_r are trapping parameters in the axial (*z*) and radial (*r*) dimensions corresponding to the DC potential (*U*), q_z and q_r are trapping parameters in the axial (*z*) and radial (*r*) dimensions corresponding to the RF amplitude (*V*), *e* is the charge state of the ion, *m* is the mass of the ion, r_0 and z_0 correspond to the radius in the radial and axial dimensions respectively, and Ω is the drive RF frequency applied to the ring electrode.

An ion must be stable in both the *r* and *z* dimensions in order to be stable in the trap. The a and q equations for each dimension can be graphed onto a 2D plot to determine the regions in which the stability in the radial and the axial dimensions overlap, indicating that the ion will be stable in the trap. The first stability region is the most commonly used region of the so-called Mathieu stability diagram, which is shown in Figure 1.4a.[40] The first stability region corresponds to $\beta_u = 0$ through $\beta_u = 1$, where β is a secondary trapping parameter and *u* represents any of the Cartesian coordinates, specifically *r* and *z* as it pertains to the trapping of ions in the ion trap. The $\beta_z = 1$ line, representing the stability boundary, crosses the q_z axis at $q_z = 0.908$. According to Equations 1.4 and 1.5 the *m/z* of an ion increases as the value of q_u decreases. The mass-selective instability scan (or mass-selective ejection) is usually performed by ramping the RF amplitude such that the ions will successively be brought to a *q* value of 0.908, where they will become unstable and will be ejected from the trap. Since the smaller ions are closets to a *q* value of 0.908 at lower RF amplitudes, the ions will be

ejected through the endcap electrodes in the order of low *m/z* to high *m/z* over the duration of the RF ramp. The ions ejected via the exit endcap will be detected successively, producing a mass spectrum ranging from low to high *m/z*.

The mass range of a 3D trap using mass selective ejection for detection is often limited by the amplitude of the RF. High *m/z* ions (above *m/z* ~650) require higher amplitudes of RF than is often available in commercial power supplies. A common solution to this limitation is resonant ejection,[42] which is performed by applying supplementary dipolar AC to the two endcaps (i.e. AC waveforms that are at the same frequency, but 180^{o} out of phase applied to each endcap). This supplementary AC accelerates ions whose secular frequency is in resonance with the frequency of the dipolar AC applied to the endcaps. Given a large enough AC amplitude, the ions in resonance will be ejected from the trap. In this way, the dipolar AC effectively puts a "hole" in the stability diagram at a specific *q* value ($q<0.908$). Similar to the mass selective instability scan described above, the amplitude of the RF is scanned to sweep ions into resonance with the dipolar AC successively. In this way, larger ions can be mass-selectively ejected from the trap through the "hole" at lower RF amplitudes than would be required to eject them via the $\beta_z = 1$ boundary line ($q_z = 0.908$).

1.2.1.2 2D Quadrupole Ion Traps

Linear quadrupoles were originally used as strong focusing ion guides and ion traps in the early 1950's.[43,44] Most commercially available linear ion traps consist of four cylindrical rods that run parallel to each other. Although the rods should theoretically be hyperbolic in shape for the ideal electric field, round rods are far simpler to manufacture. Thus, round rods are more commonly used and are spaced such that the electric field is optimized with the round geometry.[45] The quadrupolar field is generated by coupling opposite rods together and applying both DC and RF potentials to the separate rod pairs. The RF potential on the rod pairs is 180° out of phase relative to each other. Similar to the 3D quadrupole described above, the Mathieu equation can be solved for the 2D quadrupole to give the a_u and q_u trapping parameters:[40]

$$a_x = \frac{8eU}{mr_0^2\Omega^2} = -a_y \quad (1.6)$$

$$q_x = \frac{-4eV}{mr_0^2\Omega^2} = -q_y \quad (1.7)$$

where *e* is the charge state of an ion with mass *m*, *U* is the DC potential, *V* is the RF amplitude, r_0 is the radius of the trap, and Ω is the RF frequency. The RF provides the trapping well that maintains ions in the radial dimension, while repulsive DC potentials are applied to lenses on both ends of the rods to trap ions in the axial dimension. The first stability region for a linear ion trap is depicted in Figure 1.4b.

Linear ion traps (2D ion traps) were first proposed as mass spectrometers using mass selective, radial ejection in 1995 by Bier and Syka,[46] which was first demonstrated in 2002 by Schwartz, Senko, and Syka from Thermo Finnigan.[37] This form of *m/z*

dependent ion detection is similar to that described above for a 3D trap. A dipolar auxiliary AC potential is applied to the rods to accelerate ions in the radial dimension while ramping the drive RF amplitude such that ions are successively ejected (from low to high *m/z*) through a slit cut in one of the rods and into a detector placed outside the rod with the slit.[37]

Another method for mass selective ion ejection from a 2D ion trap was first described by Hager from MDS Sciex in 2001,[47,48,49] in which ions are ejected axially through the ends of the rods. This so-called mass selective axial ejection (MSAE) method couples the radial and axial motions of ions near the fringing fields at the end of the quadrupole to eject ions. Fringe fields are created at both the entrance and exit of the rods as the quadrupolar field ends abruptly due to field penetration by the external trapping lenses. The imperfect quadrupolar field created by the fringe fields enables the coupling of axial and radial ion motion, in which ions with radial motion furthest from the center of the trap are affected the most. Ions can be selectively accelerated in the radial dimension by applying a supplementary quadrupolar AC field to the rods (180^{o} out of phase on the two rod pairs) or by applying an AC field to the exit lens of the ion trap. Ions of a specific *m/z* that have a secular frequency in resonance with the supplemental AC waveform will be accelerated radially. Near the fringe fields, the radial motion is translated into axial kinetic energy which results in ion ejection from the trap in the axial dimension. The auxiliary AC amplitude and drive RF amplitude can be ramped simultaneously to successively scan ions out of the trap from low to high *m/z*.

1.2.2 Time of Flight

The time of flight (TOF) mass analyzer was first described in 1946[50] and was first built and demonstrated in the early 1950's.[51,52] The separation of ions in TOF analyzers is based upon the velocity of ions through a field-free drift tube; ions of large *m/z* will travel slower, while ions of lower *m/z* will travel faster through the drift tube. The relationship between *m/z* and drift time (*t*) is given below:

$$\frac{m}{z} = \left(\frac{2eV_s}{L^2}\right)t^2 \qquad (1.8)$$

where *e* is the elementary charge of a proton, V_s is the acceleration potential, and L is the length of the field-free region.

TOF analyzers have many advantages over other mass spectrometers, including a theoretically unlimited mass range, speed (microseconds timescale), high transmission efficiency (i.e. good sensitivity), and they are simple to calibrate.[16,53] TOF is a pulsed ion technique, making it compatible with pulsed ion sources such as matrix-assisted laser desorption/ionization (MALDI). However, distributions in the position and initial kinetic energy of the ions during the pulse as well as the pulse length contribute to losses in resolution, thus the ion beams produced by most pulsed techniques limit the resolution that can be obtained in the mass spectrum. The first TOF instruments suffered from poor resolution due to these ion distributions.

Improvements in TOF resolution have been attributed to two main advancements: delayed pulsed extraction[52,54,55,56] and the reflectron.[57] Delayed pulsed extraction is a technique that aims to correct for distributions in ion kinetic energies.

Ions are brought in from the source and after a time delay on the order of microseconds, a pulse is applied. The delay provides time for ions to separate based upon their initial kinetic energies. The delayed pulse then accelerates the ions of lower kinetic energies more than those of higher kinetic energy as they are closer to the source. While this method provides better resolution without sacrificing sensitivity, it makes mass calibration more complicated and is limited to a smaller mass window.[16,53]

The reflectron was developed initially by Mamyrin *et al.* in 1973 as another method for improving TOF resolution by accounting for ion kinetic energy distributions.[57] A reflectron is a series of ion mirrors that decelerate and then reaccelerate ions back toward the direction of the source. Ions of the same *m/z* that have higher initial kinetic energies will penetrate further into the mirror, which effectively increases their flight path relative to the ions with lower kinetic energies. The detector is often placed next to the source at the focal point where ions with different kinetic energies but the same *m/z* will arrive at the detector at the same time. The resolution of a TOF is also directly proportional to the length of the drift path. Thus, reflectrons also improve resolution by increasing the flight length without drastically increasing the size of the mass spectrometer.[53] Resolution has been further improved by adding multiple stages of reflectron mirrors[58] or by including multiple turns (i.e. increased path length).[59,60] However, the alignment at focal points becomes more complicated with the increase in number of turns, thus most commercial TOF mass spectrometers are sold with a single reflectron. The ability for TOF instruments to reach

resolutions on the order of 10^3 – 10^4 combined with their ability to easily analyze masses in the kDa range with great accuracy has made them popular in the analysis of large biomolecules. An example of their use for the analysis of proteins is provided in this work, *vide infra*.

1.3 Tandem Mass Spectrometry

Tandem mass spectrometry, also known as MS/MS, refers to experiments in which ions are manipulated in a way such that at least two mass analysis steps are performed. If *n* mass selective steps are performed, the experiment is commonly referred to as MS^n.[16] Examples of tandem mass spectrometry experiments include ion isolation, ion activation/dissociation, and ion reactions with molecules or other ions. The latter will be discussed in more detail in the following section, *vide infra*. Tandem mass spectrometry in the form of ion activation has become a standard capability on most commercially available mass spectrometers and has become a powerful technique as the mass of not only the intact analyte, but also the mass of fragments of the analyte can be determined. Thus tandem mass spectrometery can be used to determine the chemical structure of analytes. This technique is particularly useful in determining the primary structure of large biomolecules. One of the main strengths of tandem mass spectrometry is spectral simplification as the desired analytes can be individually isolated from all other analytes in a complex mixture and fragmented for structural interrogation. In this way, chemical noise is often diminished in tandem MS experiments.

In general, a tandem mass spectrometry experiment involves ionization of the analyte followed by trapping of the ions in an ion trap, where the desired analyte ion can be isolated and subsequently activated. Mass analysis follows such that the masses of the individual fragment ions produced by the activation step can be analyzed. Activation methods include ion trap and beam-type collision induced dissociation (CID), surface induced dissociation (SID), ultraviolet photodissociation (UVPD), infrared multiphoton dissociation (IRMPD) and electron transfer/dissociation methods (e.g. ETD, ECD, ExD). The methods used in this work include ion trap CID and UVPD, which will be discussed in detail below.

All of these ion activation methods impart energy on the ions via either collisions or with light, however the rates of heating and cooling for each technique can differ greatly, which has implications for the fragmentation products that will be generated. Generally, ion activation methods are divided into two main categories: fast and slow heating. These categories refer to the timescale over which the ion is activated. Slow heating methods such as ion trap CID and IRMPD occur on the order of 10^{-6} – 10^{3} s, while fast heating methods including SID, beam-type CID, and UVPD occur on the order of 10^{-16} – 10^{-10} s.[61] Slower ion activation methods provide time for chemistry to occur (i.e. rearrangements or reactions), while fast ion activation methods generally result in simple cleavages due to the short time scale. An important distinction for slow heating methods is that the rates of heating and cooling are comparable such that the internal energy of the ions reaches a steady state.

1.3.1 Ion Trap Collision Induced Dissociation

Ion trap collision induced dissociation is a slow heating method. The 'ergodic' process (i.e. energy that is imparted upon the molecule is redistributed throughout the bonds in the molecule) usually proceeds through two steps. The first step, a relatively fast process, is collisional activation (CA) which is caused by collisions of the ion with gaseous molecules. The second step involves the conversion of the translational energy from the collision into internal energy which results in unimolecular dissociation of the ion, which is a longer process.[16,62] Additionally, ion trap CID as it is performed in a quadrupole ion trap mass spectrometer usually involves multiple low energy collisions. The type of fragments observed depend not only on the activation method, but also on the nature of the precursor ion. Most fragmentation is either charge-directed or radical-directed, thus fragments tend to be more abundant if they result from bonds breaking near the charge or radical site, respectively.

Prior to ion activation, the desired ion is isolated. In a 3D ion trap the ions are isolated by performing a mass selective instability scan similar to that described above for mass analysis; however the supplemental AC as well as the amplitude of the RF ramp are tuned such that all ions except the desired precursor ions are ejected from the trap. This is an RF only isolation such that $a = 0$.[63,64] In a linear ion trap, the ions are isolated by ramping the RF amplitude such that the desired ion will be at $q = 0.703$, which is just below the apex of the first stability region. A DC potential is then applied to raise the a_x value such that the precursor ion is brought into the apex of the stability region where it

is the only ion stable in the trap. This method is termed apex isolation. In a triple quadrupole tandem MS instrument, ions are often isolated via apex isolation through the first RF/DC quadrupole (Q) prior to storage in an RF only quadrupole (q).[48] Both 2D and 3D ion traps can be operated via RF only, or via RF and DC for ion isolation, however the descriptions given above were the configurations used for this work. Once ions are isolated, they can be activated to induce fragmentation to obtain structural information.

1.3.1.1 Resonant Collision Induced Dissociation

Resonant CID, or resonant excitation, is one of the most commonly used ion activation methods in quadrupole ion traps as it is a universal technique and is simple to implement.[65] A supplementary AC waveform is applied, similar to that described above for mass extensions and ion isolations, where the frequency is in resonance with the secular frequency of the desired ion in the trap, which will accelerate the ion motion in the trap. This method increases the radius of motion of the desired ion cloud such that the ions experience more RF heating (i.e. move closer to the electrodes) and will undergo more energetic collisions with the background or buffer gas.[66] Both the frequency and the amplitude of the supplemental AC waveform must be tuned to provide efficient fragmentation without ion losses. For example, if the amplitude is too low then fragmentation will not be observed, while amplitudes that are too high will result in ion trajectories that are no longer stable in the trap. Because ions will only be accelerated if their secular frequency matches that of the supplemental AC waveform,

this is a selective technique. Therefore, it is possible to activate a single *m/z* without ion isolation prior to CID. However, isolations are commonly performed to avoid complicating the fragmentation spectrum.

1.3.1.2 Dipolar Direct Current Collision Induced Dissociation

Dipolar direct current CID (DDC-CID) is another method of performing ion trap CID. Many of the same principles apply to DDC-CID as described for resonant CID. DDC-CID is performed by applying a DC field to the quadrupole ion trap in a dipolar fashion. In a 3D trap this field is created by applying equal voltages of opposite polarities to the two endcaps of the trap.[67] In a linear trap the dipolar DC field is created by applying equal and opposite DC voltages to one of the rod pairs, while the other rod pair is held at ground.[68] The dipolar field displaces the entire ion cloud from the center of the trap, such that the ions are exposed to higher RF heating. Thus, ion activation is caused by more energetic collisions with the bath gas, similar to ion activation via resonant CID. An important distinction between resonant CID and DDC-CID is that the latter is a broadband technique while the resonance condition is selective for a certain ion frequency (i.e. *m/z*). DDC-CID is also simpler to implement and tune relative to resonance CID because all ions are activated equally, for a pure quadrupolar field. Higher order fields (as are found in 3D ion traps with a stretched geometry) have been found to contribute to a slight mass discrimination in which higher m/z ions are displaced further from the center of the trap and thus are subjected to more RF heating

and subsequent activation and fragmentation.[69] Each of the techniques has its own advantages and disadvantages, thus the preferred method is often application dependent.

1.3.2 Ultraviolet Photo Dissociation

Ultraviolet photo dissociation (UVPD) is a fast heating process that is also a more selective ion activation method relative to ion trap CID because the analyte ions must have a chromophore that absorbs at the wavelength of the incident light in order to be activated.[70] Opposed to infrared multiphoton dissociation (IRMPD), UVPD often results in fragmentation after the absorption of one to a few, higher energy photon(s) (2-10 eV/photon). After the molecule absorbs the photon(s), the energy is vibrationally dissipated through the bonds near the chromophore. Because the energy absorption is more localized and imparts more energy on the ion, a wider variety of fragmentation types can be expected relative to that obtained with ion trap CID.

The biggest drawback of UVPD is the requirement of a laser for ion activation. Lasers are expensive and provide for more complicated experiments. There must also be a clear line of sight to ions in the trap such that the light can reach them. Even so, the selectivity of UVPD relative to ion trap CID may be advantageous depending on the application. Many methods have been developed to conjugate or complex chromophores to various analytes,[71,72,73] which improves the applicability of UVPD to a broader range of analytes (i.e. biomolecules) that do not have native chromophores.

1.3.3 Analysis of Peptides and Proteins

This work focuses on the development of methods for analyzing biomolecules, especially peptides and proteins. Thus, a targeted discussion of the fragmentation schemes and nomenclature for peptides and proteins is included here. MS/MS techniques are useful in determining the primary structure (i.e. the amino acid sequence) of proteins. There are two main approaches for investigating the primary structure of a protein, namely 'bottom up' and 'top-down.'[74] The bottom-up approach is the most prominent method currently used in proteomics. The first step of this approach is to enzymatically digest an intact protein in solution, which is followed by separation (usually via HPLC) and MS analysis to determine the mass of the digested peptides. The main disadvantage to this method is that the mass of the intact protein is lost. Contrarily, the top-down approach takes the intact protein into the mass spectrometer where its intact mass is determined prior to ion modification and/or activation to induce sequence informative fragment ions. This technique, however struggles with sensitivity and is not currently high-throughput, which prevents its adoption as the primary method in the proteomics community. One of the major focuses of research in the McLuckey group is to develop and improve methods for use in top-down proteomics, thus the following discussion will focus on tandem MS for top-down proteomics.

Most ion activation techniques result in cleavages along the backbone of peptides. A common nomenclature for peptide fragmentation was proposed in 1984[75] and was later modified to the current labeling scheme used by the community.[76] Ions

that contain the N-terminus are labeled with a_n, b_n, or c_n, while ions containing the C-terminus are labeled x_n, y_n, or z_n for cleavages at the C^{α} – C, amide, and N-C^{α} bonds, respectively, where *n* is the number of residues present in the fragment. A schematic showing peptide fragmentation nomenclature is given in Figure 1.5. The observed fragment ion types are determined by the activation method as well as the nature of the charge on the precursor ion.

Ion trap CID of protonated peptides (the most commonly used ion activation method for peptides) usually gives b- and y-type fragment ions. This observation has been attributed to the 'mobile proton theory' in which fragmentation is driven by charge directed reactions.[77] Thus, positive ions with higher charge states (i.e. more mobile protons) tend to fragment more efficiently via ion trap CID than ions of lower charge or negative ions. The sequence of the peptide can play a large role as well. For example, the presence of a proline yields cleavage of the amide bond N-terminal to the proline residue as the most abundant fragmentation pathway.[78]

However, faster ion activation methods, such as UVPD, can favor other fragments including a-type ions and side chain losses in addition to b- and y-type ions. The observed fragments via UVPD are dependent upon the wavelength of the incident light as well as the nature of the target chromophore. UVPD performed at ≤193 nm is able to cleave peptides without chromophores. However, only tyrosine and tryptophan residues will absorb 266 nm light. At wavelengths ≥355 nm, peptides will not absorb the light unless they are conjugated to a chromophore.[73]

Additionally, certain bonds can be homolytically cleaved via ion trap or beam type (higher energy) CID (e.g. azo compounds) or via UVPD (e.g. C-I bonds). A homolytic cleavage results in an odd electron analyte molecule. The odd-electron molecule can be activated via CID to provide energy for a series of hydrogen abstractions yielding free radical migration which leads to radical-directed dissociation (RDD). The fragmentation produced via RDD is complementary to that produced by charge directed dissociation and often gives a- and x-type ions as well as side chain losses.[79]

1.4 Manipulation of Ion Types

As mentioned previously, the type of precursor ion is important in determining the information that can be obtained via ion activation (i.e. ion trap CID and UVPD, *vide supra*). One method of manipulating the ion type is via reactions of the analyte with other molecules or ions. These reactions can be performed in the solution or droplet phases on the way into the mass spectrometer or via ion/molecule or ion/ion reactions once the bare ions are inside the mass spectrometer.

Solution-phase derivatization of biomolecules is widely used for labeling[80] and crosslinking[81] studies to aid in determining primary and tertiary structures. As mentioned above, solution-phase conjugation may be necessary to generate the desired ion type for certain activation methods, such as conjugating a chromophore to a peptide for UVPD.[73] Although this is a vast area of research, this work will focus on analyte reactions that occur in solution within a nESI capillary, in the droplet phase during nESI,

and in the gas-phase via ion/molecule and ion/ion reactions. The main advantage all these techniques have over bulk solution-phase modifications is the simplification of analyte preparation. Additionally, reactions in the gas-phase avoid solvent interactions and are easier to tune than solution-phase reactions. Pseudo solution-phase (i.e. Droplet-phase), ion/molecule, and ion/ion reactions are discussed in more detail below.

1.4.1 Pseudo Solution-Phase Reactions

While these reactions occur in the solution-phase, there are important differences that have implications for the types of ions that will be formed and the types of reactions that can be studied when compared to bulk solution-phase reactions performed at equilibrium. For example, initiating reactions just prior to the mass spectrometer provides the opportunity to study reactions that occur on shorter timescales (e.g. microseconds to seconds), enabling the investigation of reaction kinetics, products, and intermediates (even short-lived). Additionally, Cooks *et al.* and others have found that reaction rates are significantly faster when the reaction occurs in an evaporating electrospray droplet, which has been attributed to the increase in concentration of the reagents as well as the decrease in pH[82,83] as the droplet evaporates.[84,85]

1.4.1.1 Solution-Phase Reactions on Short Timescales

There are two main methods for mixing reagent solutions just prior to nESI: stopped flow or time-resolved MS and microfluidic chip mixers. Stopped-flow mixing techniques were first used with optical spectroscopy to measure reaction kinetics and observe short-lived intermediates.[86] Konermann *et al.* have performed many studies, particularly involving biomolecule reactions, by coupling stopped-flow mixers with MS.[87,88,89,90] This technique consists of a Y-shaped capillary system in which two reactant solutions are pumped through individual channels to a junction where the two capillaries join into a single capillary, where the reactant solutions are mixed. With a known flow rate, the length of the single capillary can be correlated to reaction time such that the reaction mixture can be sampled into the mass spectrometer at various time points. Thus, this technique has been useful for studying reaction kinetics including lifetimes of short-lived (millisecond timescale) intermediates.[90] Additionally, microfluidic chips are being combined with MS to facilitate low volume reactions just prior to mass analysis.[91,92,93] Many of these techniques use electroosmotic flow (EOF) to move solutions through channels on the chip. After reactions are performed on the chip, the solution is often ionized via ESI or MALDI. Microfluidic chips have been used to improve high-throughput analysis methods by enabling in-line enzymatic digests,[94] and sample separation from salts and detergents.[95] Recently, a microfluidic chip was used to mix two reagent solutions in the Taylor cone and subsequent droplets.[96] This microchip was used to manipulate protein charge state distributions (CSDs) with supercharging agents.

Similarly, borosilicate theta capillaries have been used to mix solutions in the Taylor cone and subsequent droplets, [97] as demonstrated by Mark *et al.* via hydrogen/deuterium exchange (HDX) and complex formation. A majority of the present work will focus on the use of theta capillaries as nESI emitters for the study of protein conformations on various timescales (microseconds to seconds), *vide infra.*

1.4.1.2 Droplet-Phase Reactions

The stopped-flow and microfluidic techniques described above result in reagent mixing in the solution-phase on short timescales (non-equilibrium). Reagents can also be mixed in the droplet phase via a variety of methods. For example, fused-droplet ESI (FD-ESI) and extractive ESI (EESI) mix two plumes (ESI or aerosol) together and have been used to avoid sample preparation in complex mixtures[98,99] and to avoid the deleterious effects of salts and buffers.[100,101]

Additionally, there are a variety of vapor introduction methods that react electrospray droplets with gaseous vapors in the interface of the mass spectrometer. Chemical vapors can be introduced with the desolvating counter-current[102] or nebulizing gas flows,[103] or by evaporation from a vial placed below the electrospray capillary.[104] These methods have been utilized for a variety of studies including salt reduction,[102] protein unfolding[103,105,106] and refolding,[107] and HDX.[104,108,109] These methods do not require bulk solution modifications and can provide protein structural information via the manipulation and labeling of protein conformations. However, vapor introduction

techniques inherently require volatile solvents, making them incompatible with many reagents including supercharging reagents.

1.4.2 Ion/Molecule Reactions

Another method for manipulating ion types is ion/molecule reactions. The first ion/molecule reaction was observed by Thomson in 1913 in which he observed H_3^+.[110] However, the mechanisms and theory of ion/molecule product formation were not described until 1936.[111] Ion/molecule reactions often interfered with early mass spectrometry experiments due to poor vacuum technology, which resulted in higher pressures and an abundance of reactive gas molecules.[112] Initially, most ion/molecule studies were conducted using ion cyclotron resonance (ICR) mass spectrometers. In the 1980's the use of triple quadrupoles as reaction vessels for ion/molecule reactions became more popular.[113,114] The present work will focus on ion/molecule reactions conducted within quadrupole ion traps.

As the name suggests, ion/molecule reactions often occur inside the vacuum of the mass spectrometer (although ion/molecule reactions can also occur in the interface if the ions are desolvated at that point) between an ion and a gaseous molecule. Often the ion is introduced via one of the many ionization methods; this work will focus on electrosprayed ions which are charged via protonation or deprotonation. Gaseous molecules are often introduced via a leak-in valve with the bath gas. These reactions often occur in ion traps, where the ions are trapped while neutral molecules are brought

into the trap with the bath gas. Advantages of ion/molecule reactions over solution-phase reactions include that they are fast, efficient, and require small reagent quantities.[115]

Ion/molecule reactions have been used for a broad range of applications including chemical ionization, HDX, and the determination of stereochemistry.[115] Additionally, ion/molecule reactions have been useful for the study of biomolecules. For example, HDX has been used to study conformational changes in peptides and proteins as greater HDX rates are often indicative of more denatured proteins since exchangeable sites are shielded in the more folded/native proteins.[116,117] Ion/molecule reactions have also been used to count the number of protonation sites on a protein via proton transfer to neutral basic reagent molecules.[118]

1.4.3 Ion/Ion Reactions

Another method for manipulating ion types is ion/ion reactions, or reactions that occur between two ions of opposite polarity. The interactions of opposite polarity ions in the gas-phase were first studied by Thomson and Rutherford in the late 1890's.[119,120] More recently, ion/ion reactions have been studied for a variety of applications including atmospheric chemistry and biochemistry.[121] Prior to the advent of nESI, ion/ion reactions were somewhat limited to kinetic studies due to the singly charged analytes produced by most ionization methods, which would become neutralized upon reaction with the singly charged ion of the opposite polarity. However, ESI produces

multiply charged ions and the charge reduced ion/ion reaction products are easier to study as they are not neutralized upon a single charge transfer event. Advantages of gas-phase ion/ion reactions over solution-phase reactions include their speed, their tunability (i.e. relative amount of each reagent and reaction time can easily be varied), that the reactants and products are easily compared, and that the reactions are better controlled (via ion isolation).

Over the past few decades McLuckey *et al.* have demonstrated the utility of ion/ion reactions for both charged particle transfer as well as covalent modification to manipulate biomolecular ion types in the gas-phase. Several different covalent modifications have been performed to label specific biomolecular residues in the gas-phase: N-hydroxysuccinimide ester reactions with primary amines,[122,123,124] guanidinium groups, [125] and carboxylates; [126] Schiff base reactions with primary amines; [127 , 128] carbodiimide reactions with carboxylic acids;[129] alkylation reactions between 'onium' reagents and carboxylate, phosphate, and sulfonate groups;[130,131] and peptide side chain (e.g. methionine) oxidation with peroxy reagents.[132,133] Additionally, charged particle transfer during ion/ion reactions has been applied to the removal of metal cations from polymers,[134] charge reduction of multiply charged ions for spectral simplification,[135,136] and to affect ion fragmentation via the generation of uneven electron species. [137,138] All of these modifications provide primary and/or tertiary structural information for biomolecules by altering fragmentation pathways, labeling specific sites, and/or crosslinking nearby residues. The present work will focus on the instrumentation,

complex formation (including the competition between charged particle transfer and covalent chemistry), and the kinetics and thermodynamics of ion/ion reactions as they apply to the present work.

1.4.3.1 Instrumentation

While ion/ion reactions have been performed using various instrument setups, 3D and linear ion traps have been most widely used due to their tandem MS compatibility and their ability to store both positively and negatively charged ions simultaneously in the same space.[121,139,140] In 3D ion traps, the RF trapping field is sufficient to store both ion polarities, without applying additional trapping waveforms.[141] Although, ions must either be injected via different paths into the mass spectrometer (i.e. one polarity injected through the ring electrode while the other is injected through the entrance end cap), or both ion polarities traverse the same ion path in which lens voltages are switched between the optimal potentials for each ion polarity. Typically, one polarity ion is injected into the trap, where the desired precursor ion is isolated. The opposite polarity ions are then injected into the trap where they interact with the isolated precursor ions. The desired reaction product (charge transfer, complex formation, or covalent modification) can then be isolated and further activated. It is important to note that this configuration allows the isolation of a single ion polarity, therefore it is often advisable to inject the ion polarity with the most chemical noise first,

such that the desired precursor can be isolated to avoid as many unwanted reactions as possible.

Linear ion traps can also be used for ion/ion reactions. Triple quadrupole ion traps are particularly useful as both ion polarities can be isolated in the first quadrupole prior to trapping in the reaction cell (usually a higher pressure ion trap). Both ions can be trapped in the same linear quadrupole simultaneously by applying an AC waveform to the axial trapping lenses. The RF trapping field is sufficient to trap both ion polarities in the radial dimension (see Figure 1.3 for example). Ion/ion reactions performed by trapping both ion polarities simultaneously are referred to as 'mutual storage' reactions.[137,142] Additionally ions can be reacted in 'transmission mode' in which one ion polarity is trapped in the quadrupole, while the opposite polarity ions are transmitted through the quadrupole without trapping.[143,144,145]

1.4.3.2 Complex Formation

There are two main reaction pathways that are observed via ion/ion reactions: charged particle transfer and covalent modification. Charged particle transfer includes proton transfer, electron transfer, and metal ion transfer, which have recently been reviewed.[121] During an ion/ion reaction, the first step is a long-range Coulombic attraction of the ions of opposite polarity. This long-range interaction can develop into a stable orbit, which collapses through collisional cooling with the bath gas in the ion trap. Charged particle transfer tends to be a relatively fast process that can occur during a

long-range orbit. Once a smaller, intimate orbit is generated, the anion and cation undergo a series of collisions with each other. Under these conditions it is possible for chemistry to occur if chemically reactive functional groups are present. In fact, reaction rates tend to be greater in the gas-phase as opposed to solution-phase due to the nature of this complex and the increased probability of multiple collisions during the complex lifetime.

The nature of both the reagent and the analyte are important in determining if a long-lived complex can be generated via a 'sticky collision' (a collision in which a long-range Coulombic orbit of the ions of opposite polarity is formed). Similar to ion/molecule reaction complexes and sticky collisions in CID, larger analytes and reagents have more degrees of freedom, which favors sticky collisions.[62] On the other hand, proton transfer is favored over complex formation for reactants that are highly charged.[121] For ion/ion reactions in which covalent modifications are desired, multifunctional reagents are necessary.[121] Multifunctional reagents contain a 'sticky group,' such as sulfonate for anionic reagents or quaternary ammoniums for positive reagents, and a chemical functional group capable of reacting with a functional group on the analyte. The sticky group promotes the formation of a long-lived complex, which then provides time for the chemical reaction to proceed. If the complex is stable enough, it can be isolated and activated to provide additional energy for chemical reactions (*vide infra*). It is important to note that charged particle transfer can occur with or without

intimate complex formation when the interaction potentials of the ions are at a crossing point.

1.4.3.3 Reaction Energetics

The ion/ion reactions described in this work usually consist of a competition between covalent modification and proton transfer. Thus, the following section will focus on the competition between these two specific pathways, although this competition is also present for other charged particle transfers as well. A general representation for an ion/ion reaction in which a proton is transferred from a multiply charged cation to a singly charged anion is given below:[121,140]

$$(M + nH)^{n+} + Y^{-} \rightarrow [M + (n-1)H]^{(n-1)+} + YH \qquad (1.9)$$

where, for this work, *M* is the peptide cation with *n* protons and *Y* is the anionic reagent.

Thermodynamically, ion/ion reactions are quite exothermic (≥100 kcal/mol). The entrance channel to an ion/ion reaction is dominated by the Coulombic attraction of the two oppositely charged ions.[121,136] The Coulomb potential (E_{pot}) of this interaction is given below:

$$E_{pot} = \frac{-Z_1 Z_2 e^2}{r} \qquad (1.10)$$

where Z_1 and Z_2 are the number of charges on the cation and anion, *e* is the electronic charge, and *r* is the distance between the two ions. The exit channel for ion/ion reactions is determined by ion-dipole and ion-induced dipole interactions, unlike that of

ion/molecule reactions which is determined by a Coulomb barrier. However, there may be a reaction barrier for ion/ion reactions including covalent modification.

For the same proton transfer ion/ion reaction described in equation (1.9), pseudo-first order reaction kinetics can be obtained if there is a large excess of the singly charged anion reagent relative to the multiply protonated cation analyte. The rate of proton transfer has been found to have a Z^2 dependence,[136] which indicates that the formation of the orbiting complex is the rate limiting step. The rate constant for the formation of the orbiting complex (k_c) is given below:[140]

$$k_c = v\pi \left[\frac{z_1 z_2 e^2}{4\pi\varepsilon_0 \mu v^2}\right]^2 \qquad (1.11)$$

where v is the relative velocity of the ions, ε_0 is the permittivity of vacuum, and μ is the reduced mass of the two ions. The strength of the long-range attractive potential is great enough that ion orbits can form at distances larger than is suitable for chemistry to occur. In these cases, dampening collisions of the background gas with the ion orbit can reduce the velocity of the ions such that the orbit collapses to a diameter over which chemistry can occur. Thus, helium buffer gas is often used to avoid collisional scattering, often observed with higher mass buffer gases, which can destroy the complex.[121,140] In addition, the ion distance can be decreased due to 'tidal' effects in which large polyatomic ions, such as proteins, are influenced by the electric field of the orbit such that translational energy is converted to vibrational energy in the bonds of the large ion.[146,147]

The covalent modification ion/ion reactions presented in this work always compete with a proton transfer pathway. Thus, the ion/ion reaction spectrum shows evidence of the charge reduced peptide as well as a charge reduced complex. The complex can be isolated and heated via CID. Upon activation of the complex, often a proton transfer product as well as a covalent modification product (usually indicated by a signature neutral loss dependent upon the reaction and reagent used) are observed. The additional energy imparted by the CID step may drive the covalent modification reaction step or it could be responsible for the dissociation of the electrostatically bound complex post covalent chemistry. This is an interesting question that will be addressed in further detail in this work, *vide infra.*

1.5 Conclusions

Mass spectrometry combined with ESI and tandem mass spectrometry has proven to be a valuable instrument for the analysis of biomolecules. The manipulation of ion types is key in determining the type of analyte structural information that can be obtained. This work presents novel methods for manipulating ion types at various stages of a typical mass spectrometry experiment. Herein, Ion types are manipulated prior to and during nESI and while gas-phase ions are trapped in a quadrupole ion trap via ion/ion reactions. When combined with well-known ion activation techniques, these techniques provide alternative methods to provide complementary primary and tertiary structural information of large biomolecules.

1.6 References

[1] Thomson, J. J. *Phil. Mag.S. 6.* **1907**, *13*, 561-575.

[2] Thomson, J. J.; *P. Roy. Soc. A.* **1913**, *89*, 1-20.

[3] Dole, M. Mack, L. L.; Hines, R. L.; Mobley, R. C.; Ferguson, L. D.; Alice, M. B. *J. Chem. Phys.* **1968**, *49*, 2240-2249.

[4] Teer, D.; Dole, M. *J. Polym. Sci.* **1975**, *13*, 985-995.

[5] Fenn, J. B.; Mann, M.; Meng, C. K.; Wong, S. F.; Whitehouse, C. M. *Science* **1989**, *246*, 64-71.

[6] Gelpí, E. *J. Chromatogr. A.* **1995**, *703*, 59-80.

[7] Simpson, D. C.; Smith, R. D. *Electrophoresis.* **2005**, *26*, 1291-1305.

[8] Kebarle, P.; Tang, L. *Anal. Chem.* **1993**, *65*, 972-986.

[9] Kebarle, P. *J. Mass Spectrom.* **2000**, *35*, 804-817.

[10] Cech, N. B.; Enke, C. G. *Mass Spectrom. Rev.* **2001**, *20*, 362-387.

[11] Kebarle, P.; Verkerk, U. H. *Mass Spectrom. Rev.* **2009**, *28*, 898-917.

[12] Pfeifer, R. J.; Hendricks, C. D. *AIAA J.* **1968**, *6*, 496-502.

[13] Taylor, G.I. *Proc. R. Soc. Lond.* **1964**, *A 280*, 383-397.

[14] Rayleigh, Lord *Philos. Mag.* **1882**, *14*, 184-186.

[15] Taflin, D. C.; Ward, T. L.; Davis, E.J. *Langmuir.* **1989**, *5*, 376-384.

[16] de Hoffman, E.; Stroobant, V. *Mass Spectrometry: Principles and Applications.* 3rd ed. Wiley: West Sussex, **2002**, "Electrospray," 43-55.

[17] Van Berkel, G. J.; Zhou, F. *Anal. Chem.* **1995**, *67*, 2916-2923.

[18] Kebarle, P.; Peschke, M. *Anal. Chim. Acta.* **2000**, *406*, 11-35.

[19] Iribarne, J. V.; Thomson, B. A. *J. Chem. Phys.* **1976**, *64*, 2287-2294.

[20] Konermann, L.; Ahadi, E.; Rodriguez, A. D.; Vhidi, S. *Anal. Chem.* **2013**, *85*, 2-9.

[21] Schmelzeisen-Redeker, G.; Bütfering, L.; Röllgen, F. W. *Int. J. Mass Spectrom.* **1989**, *90*, 139-150.

[22] Fernández de la Mora, J. F. *Anal. Chim. Acta.* **2000**, *406*, 93-104.

[23] Loscertales, I. G.; Fernández de la Mora, J. *J. Chem. Phys.* **1995**, *103*, 5041-5060.

[24] Konermann, L.; Rodriguez, A. D.; Liu, J. *Anal. Chem.* **2012**, *84*, 6798-6804.

[25] Yue, X.; Vahidi, S.; Konermann, L. *J. Am. Soc. Mass Spectrom.* **2014**, *25*, 1322-1331.

[26] Chowdhury, S. K.; Katta, V.; Chait, B.T. *J. Am. Chem. Soc.* **1990**, *112*, 9012-9013.

[27] Fenn, J. B. *J. Am. Soc. Mass Spectrom.* **1993**, *4*, 524-535.

[28] Kaltashov, I.A.; Eyles, S. J. *Mass Spectrom. Rev.* **2002**, *21*, 37-71.

[29] Wilm, M. S.; Mann, M. *Int. J. Mass Spectrom.* **1994**, *136*, 167-180.

[30] Wilm, M.; Mann, M. *Anal. Chem.***1996**, *68*, 1-8.

[31] Juraschek, R.; Dülcks, T.; Karas, M. *J. Am. Soc. Mass Spectrom.* **1999**, *10*, 300-308.

[32] Schmidt, A.; Karas, M.; Dülcks, T. *J. Am. Soc. Mass Spectrom.* **2003**, *14*, 492-500.

[33] Gilbert, J. D.; Fisher, C. M.; Bu, J.; Prentice, B. M.; Redwine, J. G.; McLuckey, S. A. "Strategies for generating peptide radical cations via ion/ion reactions." J. Mass Spectrom. 2015, 50, 418-426.

[34] Xia, Y.; Chrisman, P. A.; Erickson, D. E.; Liu, J.; Liang, X.; Londry, F. A.; Yang, M. J.; McLuckey, S. A. *Anal. Chem.* **2006**, *78*, 4146-4154.

[35] Paul, W.; Stenwedel, H. S. **1960**, US Patent, 2939952.

[36] Douglas, D. J.; Frank, A. J.; Mao, D. *Mass Spectrom. Rev.* **2005**, *24*, 1-29.

[37] Schwartz, J. C.; Senko, M. W.; Syka, J. E. P. *J. Am. Soc. Mass Spectrom.* **2002**, *13*, 659-669.

[38] Stafford, G. C.; Kelley, P. E.; Syka, J. E.; Reynolds, W. E.; Todd, J. F. J. *Int. J. Mass Spectrom. Ion Process.* **1984**, *60*, 85-98.

[39] Prentice, B. M.; Xu, W.; Ouyang, Z.; McLuckey, S. A. *Int. J. Mass Spectrom.* **2011**, *306*, 114-122.

[40] Mathieu, E. *Math. Pure Appl.* (*J. Liouville*). **1868**, *13*, 137.

[41] March, R. E.; Todd, J. F. J. *Quadrupole Ion Trap Mass Spectrometry*, 2nd ed. Wiley Interscience: New Jersey, 2005.

[42] Kaiser, Jr. R. E.; Louris, J. N.; Amy, J. W.; Cooks, R. G. *Rapid Commun. Mass Spectrom.***1989**, *3*, 225-229.

[43] Courant, E. D.; Livingston, M. S.; Snyder, H. S. *Phys. Rev.* **1952**, *88*, 1190-1196.

[44] Good, M. L. **1953**, University of California Radiation Laboratory Report UCRL 4146, Berkely, CA.

[45] Denison, D. R. *J. Vac. Sci. Technol.* **1971**, *8*, 266-269.

[46] Bier, M. A.; Park, M.; Syka, J. E. P. **1995**, US Patent, 5420425 A.

[47] Hager, J. W. **2001**, US Patent, 6177668.

[48] Hager, J. W. *Rapid Commun. Mass Spectrom.* **2002**, *16*, 512-526.

[49] Londry, F. A.; Hager, J. W. *J. Am. Soc. Mass Spectrom.* **2003**, *14*, 1130-1147.

[50] Stephens, W. *Phys. Rev.* **1946**, *69*, 691.

[51] Wolff, M. M.; Stephens, W. E. *Rev. Sci. Instrum.* **1953**, *24*, 616-617.

[52] Wiley, W. C.; McLaren, I. H. *Rev. Sci. Instrum.* **1955**, *26*, 1150-1157.

[53] McLuckey, S. A.; Wells, J. M. *Chem. Rev.*, **2001**, *101*, 571-606.

[54] Vestal, M. L.; Juhasz, P.; Martin, S. A. *Rapid Commun. Mass Spectrom.* **1995**, *9*, 1044-1050.

[55] Brown, R. S.; Lennon, J. L. *Anal. Chem.* **1995**, *67*, 1998-2003.

[56] Whittal, R. M.; Li, L. *Anal. Chem.* **1995**, *67*, 1950-1954.

[57] Mamyrin, B. A.; Karataev, V. I.; Shmikk, D. V.; Zagulin, V. A. *Sov. Phys. JETP.* **1973**, *37*, 45.

[58] Short, R. T.; Todd, R. J. *J. Am. Soc. Mass Spectrom.* **1994**, *5*, 779-787.

[59] Poschenrieder, W. P. *Int. J. Mass Spectrom.* **1972**, *9*, 357-373.

[60] Sakurai, T.; Fujita, Y.; Matsuo, T.; Matsuda, H.; Katakuse, I.; Miseki, K. *Int. J. Mass Spectrom.* **1985**, *66*, 283-290.

[61] McLuckey, S. A.; Goeringer, D. E. *J. Mass Spectrom.* **1997**, *32*, 461-474.

[62] McLuckey, S. A. *J. Am. Soc. Mass Spectrom.* **1992**, *3*, 599-614.

[63] Syka, J. E. P.; Louris, J. N.; Kelley, P. E.; Stafford, G. C.; Reynolds, W. E. **1987**, US Patent 4736101.

[64] Jonscher, K. R.; Yates J. R. III. *Anal. Biochem.* **1997**, *244*, 1-15.

[65] Wells, J. M.; McLuckey, S. A. *Method. Enzymol.* **2005**, *402*, 148-185.

[66] Goeringer, D. E.; Viehland, L. A.; Danailov, D. M. *J. Am. Soc. Mass Spectrom.* **2006**, 889-902.

[67] Prentice, B. M.; Santini, R. E.; McLuckey, S. A. *Int. J. Mass Spectrom.* **2011**, *22*, 1486-1492.

[68] Webb, I. K.; Londry, F. A.; McLuckey, S. A. *Rapid Commun. Mass Spectrom.* **2011**, *25*, 2500-2510.

[69] Prentice, B. M.; McLuckey, S. A. *J. Am. Soc. Mass Spectrom.* **2012**, *23*, 736-744.

[70] Reilly, J. P. *Mass Spectrom. Rev.* **2009**, *28*, 425-447.

[71] Tecklenburg, R. E. Jr.; Miller, M. N.; Russell, D. H. *J. Am. Chem. Soc.* **1989**, *111*, 1161-1171.

[72] Wilson, J. J.; Brodbelt, J. S. *Anal. Chem.* **2007**, *79*, 7883-7892.

[73] Ly, T.; Julian, R. R. *Angew. Chem. Int. Edit.* **2009**, *48*, 7130-7137.

[74] Kelleher, N. L. *Anal. Chem.* **2004**, *A*, 196-203.

[75] Roepstorff, P.; Fohlman, J. *Biomed. Mass Spectrom.* **1984**, *11*, 601.

[76] Johnson, R. S.; Martin, S. A.; Biemann, K.; Stults, J. T.; Watson, J. T. *Anal. Chem.* **1987**, *59*, 2621-2625.

[77] Paizs, B.; Suhai, S. *Mass Spectrom. Rev.* **2005**, *24*, 508-548.

[78] Vaisar, T.; Urban, J. *J. Mass Spectrom.* **1996**, *31*, 1185-1187.

[79] Sun, Q.; Nelson, H.; Ly, T.; Stoltz, B. M.; Julian, R. R. *J. Proteome Res.* **2009**, *8*, 958-966.

[80] Johsson, A. P. *CMLS Cell. Mol. Life Sci.* **2001**, *58*, 868-884.

[81] Back, J. W.; de Jong, L.; Muijsers, A. O.; de Koster, C. G. *J. Mol. Biol.* **2003**, 303-313.

[82] Gatlin, C. L.; Tureček, F. *Anal. Chem.* **1994**, *66*, 712-718.

[83] Girod, M.; Dagany, X.; Antoine, R.; Dugourd, P. *Int. J. Mass Spectrom.* **2011**, *308*, 41-48.

[84] Badu-Tawiah, A. K.; Campbell, D. I.; Cooks, R. G. *J. Am. Soc. Mass Spectrom.* **2012**, *23*, 1077-1084.

[85] Espy, R. D.; Wleklinski, M.; Yan, X.; Cooks, R. G. *Trac-Trend. Anal. Chem.* **2014**, *57*, 135-146.

[86] Gibson, Q. H. *Methods Enymol.* **1969**, *16*, 187-228.

[87] Kolakowski, B. M.; Konermann, L. *Anal. Biochem.* **2001**, *292*, 107-114.

[88] Kolakowski, B. M.; Simmons, D. A.; Konermann, L. *Rapid Commun. Mass Spectrom.* **2000**, *14*, 772-776.

[89] Zechel, D. L.; Konermann, L.; Withers, S. G.; Douglas, D. J. *Biochem.* **1998**, *37*, 7664-7669.

[90] Konermann, L.; Rosell, F. I.; Mauk, A. G.; Douglas, D. J. *Biochem.* , **1997**, *36*, 6448-6454.

[91] Figeys, D.; Gygi, S. P.; McKinnon, G.; Aebersold R. *Anal. Chem.* **1998**, *70*, 3728-3734.

[92] Oleschuk, R. D.; Harrison, D. J. *Trac-Trend. Anal. Chem.* **2000**, *19*, 379-388.

[93] Fortier, M.-H.; Bonneil, E.; Goodley, P.; Thibault, P. *Anal. Chem.* **2005**, *77*, 1631-1640.

[94] Wang, C.; Oleschuk, R.; Ouchen, F.; Li, J.; Thibault, P.; Harrison, D. J. *Rapid Commun. Mass Spectrom.* **2000**, *14*, 1377-1383.

[95] Effenhauser, C. S.; Bruin, G. J. M.; Paulus, A. *Eletrophoresis.* **1997**, *18*, 2203-2213.

[96] Miladinović, S. M.; Fornelli, L.; Lu, Y.; Piech, K. M.; Girault, H. H.; Tsybin, Y. O. *Anal. Chem.* **2012**, *84*, 4647-4651.

[97] Mark, L. P.; Gill, M. C.; Maut, M.; Derrick, P. J. *Eur. J. Mass Spectrom.* **2012**, *18*, 439-446.

[98] Chen, H.; Venter, A.; Cooks, R. G. *Chem. Commun.* **2006**, 2042-2044.

[99] Li, M.; Hu, B.; Li, J.; Chen, R.; Zhang, X.; Chen, H. *Anal. Chem.* **2009**, *81*, 7724-7731.

[100] Chang, D.-Y.; Lee, C.-C.; Shiea, J. *Anal. Chem.* **2002**, *74*, 2465-2469.

[101] Shieh, I.-F.; Lee, C.-Y.; Shiea, J. *J. Proteome Res.* **2004**, *4*, 606-612.

[102] Kharlamova, A.; Prentice, B. M.; Huang, T.; McLuckey, S. A. *Int. J. Mass Spectrom.* **2011**, *300*, 158-166.

[103] Girod, M.; Antoine, R.; Dugourd, P.; Love, C.; Mordehai, A.; Stafford, G. *J. Am. Soc. Mass Spectrom.* **2012**, *23*, 1221-1231.

[104] Kostyukevich, Y.; Kononikhin, A.; Popov, I.; Nikolaev, E. *Anal. Chem.* **2013**, *85*, 5330-5334.

[105] Kharlamova, A.; Prentice, B. M.; Huang, T.; McLuckey, S. A. *Anal. Chem.* **2010**, *82*, 7422-7429.

[106] Kharlamova, A.; McLuckey, S. A. *Anal. Chem.* **2011**, *83*, 431-439.

[107] Kharlamova, A.; DeMuth, J. C.; McLuckey, S. A. *J. Am. Soc. Mass Spectrom.* **2011**, *23*, 88-101.

[108] Kharlamova, A.; Fisher, C. M.; McLuckey, S. A. *J. Mass Spectrom.* **2014**, *49*, 437-444.

[109] Kostyukevich, Y.; Kononikhin, A.; Popov, I.; Spasskiy, A.; Nikolaev, E. *J. Mass Spectrom.* **2015**, *50*, 49-55.

[110] Thomson, J. J. *Science.* **1913**, *37*, 360-364.

[111] Eyring, H.; Hirschfelder, J. O.; Taylor, H. S. *J. Chem. Phys.* **1936**, *4*, 479-491.

[112] Eberlin, M. N. *Mass Spectrom. Rev.* **1997**, *16*, 113-144.

[113] Kenttämaa, H. I.; Cooks, R. G. *J. Am. Chem. Soc.* **1989**, *111*, 4122-4123.

[114] Fetterolf, D. D.; Yost, R. A.; Eyler, J. R. *Org. Mass Spectrom.* **1984**, *19*, 104-105.

[115] Brodbelt, J. S. *Mass Spectrom. Rev.* **1997**, *16*, 91-110.

[116] Ogorzalek Loo, R. R.; Smith, R. D. *J. Am. Soc. Mass Spectrom.* **1994**, *5*, 207-220.

[117] Kaltashov, I. A.; Doroshenko, V. M.; Cotter, R. J. *Proteins.* **1997**, *28*, 53-58.

[118] McLuckey, S. A.; Glish, G. L.; Van Berkel, G. J. *Anal. Chem.* **1991**, *63*, 1971-1978.

[119] Thomson, J. J.; Rutherford, E. *Philos. Mag.* **1896**, *42*, 392-407.

[120] Rutherford, E. *Philos. Mag.* **1897**, *44*, 422-440.

[121] Prentice, B. M.; McLuckey, S. A. *Chem. Commun.* **2013**, *49*, 947-965.

[122] Mentinova, M.; McLuckey, S. A. *J. Am. Chem. Soc.* **2010**, *132*, 18248-18257.

[123] Mentinova, M.; Barefoot, N. Z.; McLuckey, S. A. *J. Am. Soc. Mass Spectrom.* **2011**, *23*, 282-289.

[124] Webb, I. K.; Mentinova, M.; McGee, W. M.; McLuckey, S. A. *J. Am. Soc. Mass Spectrom.* **2013**, *24*, 733-743.

[125] McGee, W. M.; Mentinova, M.; McLuckey, S. A. *J. Am. Chem. Soc.* **2012**, *134*, 11412-11414.

[126] Peng, Z.; McGee, W. M.; Bu, J.; Barefoot, N. Z.; McLuckey, S. A. *J. Am. Soc. Mass Spectrom.* **2015**, *26, 174-180.*

[127] Hassell, K. M.; Stutzman, J. R.; McLuckey, S. A. *Anal. Chem.* **2010**, *82*, 1594-1597.

[128] Stutzman, J. R.; Luongo, C. A.; McLuckey, S. A. *J. Mass Spectrom.* **2012**, *47*, 669-675.

[129] Prentice, B. M.; Gilbert, J. D.; Stutzman, J. R.; Forrest, W. P.; McLuckey, S. A. *J. Am. Soc. Mass Spectrom.* **2013**, *24*, 30-37.

[130] Gilbert, J. D.; Prentice, B. M.; McLuckey, S. A. *J. Am. Soc. Mass Spectrom.* **2015,** ASAP.

[131] Stutzman, J. R.; Blanksby, S. J.; McLuckey, S. A. *Anl. Chem.* **2013**, *85*, 3752-3757.

[132] Pilo, A. L.; McLuckey, S. A. *J. Am. Soc. Mass Spectrom.* **2014**, *25*, 1049-1057.

[133] Pilo, A. L.; Bu, J.; McLuckey, S. A. *J. Am. Soc. Mass Spectrom.* **2015**, accepted.

[134] Luongo, C. A.; Bu, J.; Burke, N. L.; Gilbert, J. D.; Prentice, B. M.; Cumming. S.; Reed, C. A.; McLuckey, S. A. *J. Am. Soc. Mass Spectrom.* **2015**, *26*, 404-414.

[135] Scalf, M.; Westphall, M. S.; Smith, L. M. *Anal. Chem.* **2000**, *72*, 52-60.

[136] Stephenson, Jr., J. L.; McLuckey, S. A. *J. Am. Chem. Soc.* **1996**, *118*, 7390-7397.

[137] Syka, J. E. P.; Coon, J. J.; Schroeder, M. J.; Shabanowitz, J.; Hunt, D. F. *Proc. Natl. Acad. Sci. U. S. A.* **2004**, *101*, 9528-9533.

[138] Zubarev, R. A.; Kelleher, N. L.; McLafferty, F. W. *J. Am. Chem. Soc.* **1998**, *120*, 3265-3266.

[139] McLuckey, S. A.; Stephenson, Jr., J. L. *Mass Spectrom. Rev.* **1998**, *17*, 369-407.

[140] Pitteri, S. J.; McLuckey, S. A. *Mass Spectrom. Rev.* **2005**, *24*, 931-958.

[141] Mather, R. E.; Todd, J. F. J. *Int. J. Mass Spectrom.* **1980**, *33*, 159-165.

[142] Xia, Y.; Wu, J.; Londry, F. A.; Hager, J. W.; McLuckey, S. A. *J. Am. Soc. Mass Spectrom.* **2005**, *16*, 71-81.

[143] Wu, J.; Hager, J. W.; Xia, Y.; Londry, F. A.; McLuckey, S. A. *Anal. Chem.* **2004**, *76*, 5006-5015.

[144] Liang, X.; Hager, J. W.; McLuckey, S. A. *Anal. Chem.* **2007**, *79*, 3363-3370.

[145] Emory, J. F.; Hassell, K. H.; Londry, F. A.; McLuckey, S. A. *Rapid Commun. Mass Spectrom.* **2009**, *23*, 409-418.

[146] Morgan, W. L.; Bates, D. R. *J. Phys. B: At., Mol. Opt. Phys.* **1992**, *25*, 5421-5430.

[147] Bates, D. R.; Morgan, W. L. *Phys. Rev. Lett.* **1990**, *64*, 2258-2260.

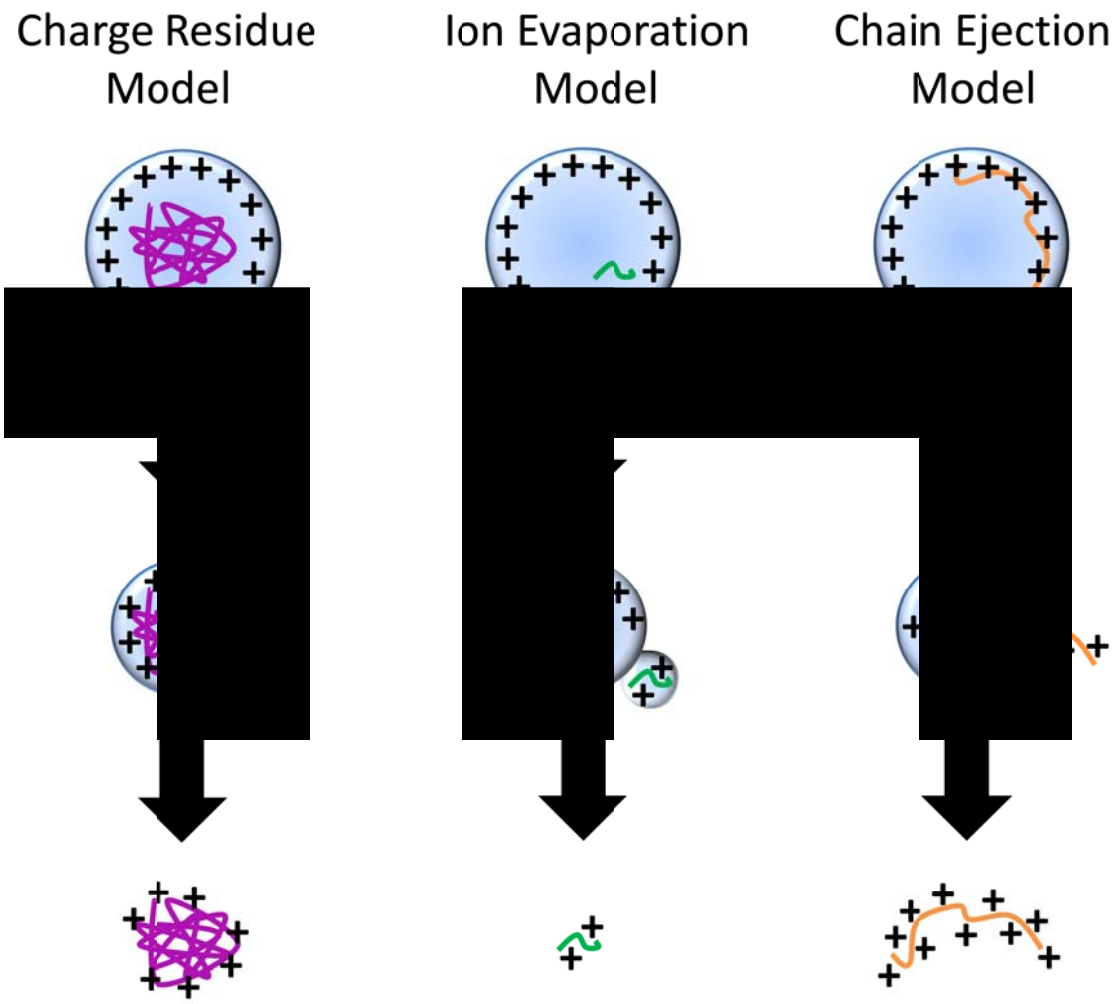

Figure 1.1 Electrospray ionization mechanims. Adapted with permission from reference 20. Copyright 2013 American Chemical Society.

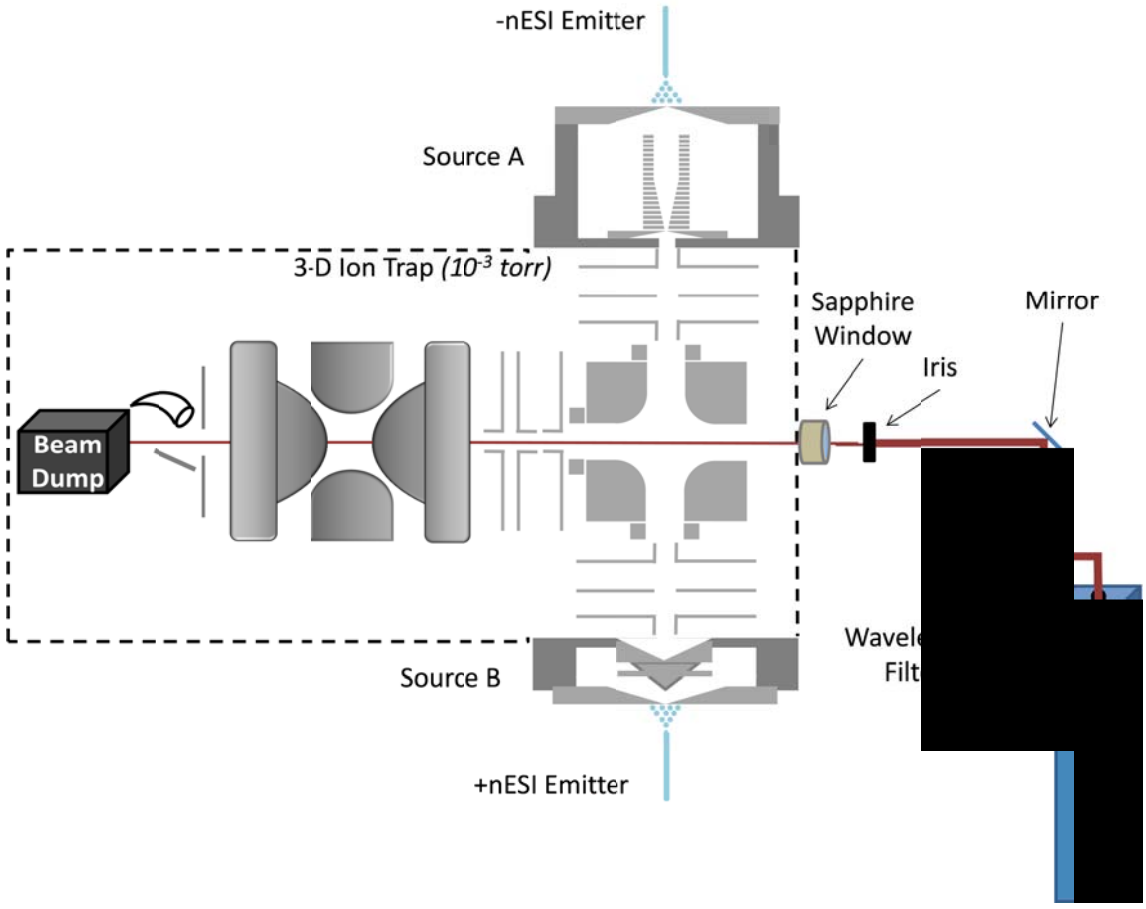

Figure 1.2 Instrument schematic for the dual source 3D ion trap used in this work. Reprinted with permission from reference 33. Copyright 2015 John Wiley and Sons.

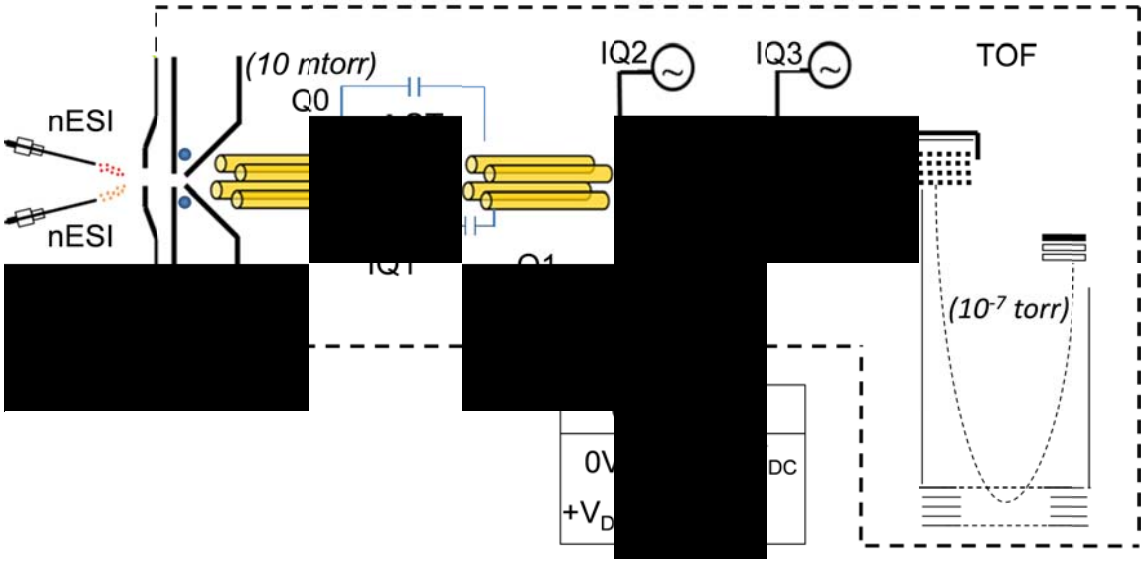

Figure 1.3 Instrument schematic for the QqTOF (QSTAR Pulsar XL, AB Sciex, ON, Canada) modified for ion trap CID and ion/ion reactions used in this work. Adapted with permission from reference 34. Copyright 2006 American Chemical Society.

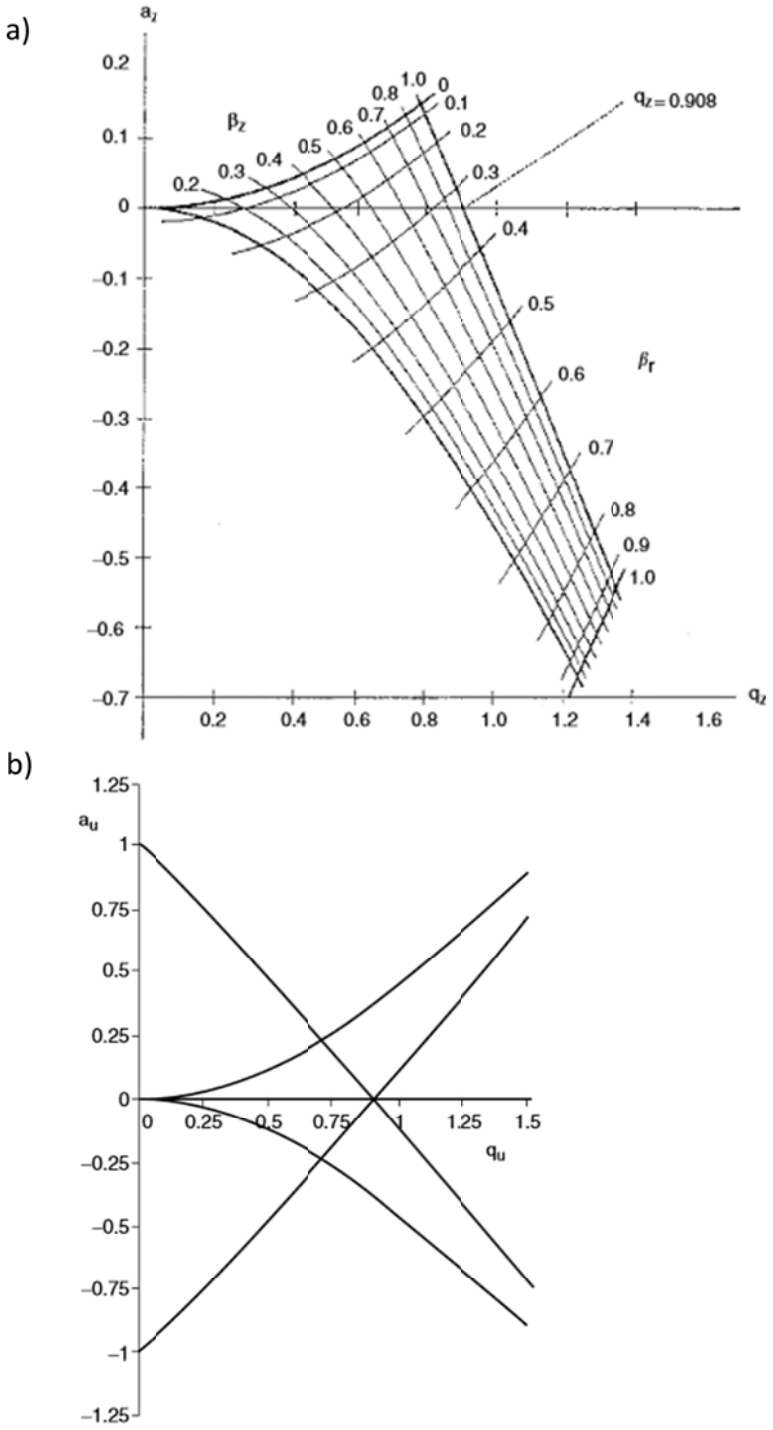

Figure 1.4 Mathieu Stability Diagram for the first stability region in a 3D ion trap (a) and linear ion trap (b). Reprinted with permission from reference 41. Copyright 2005 John Wiley and Sons.

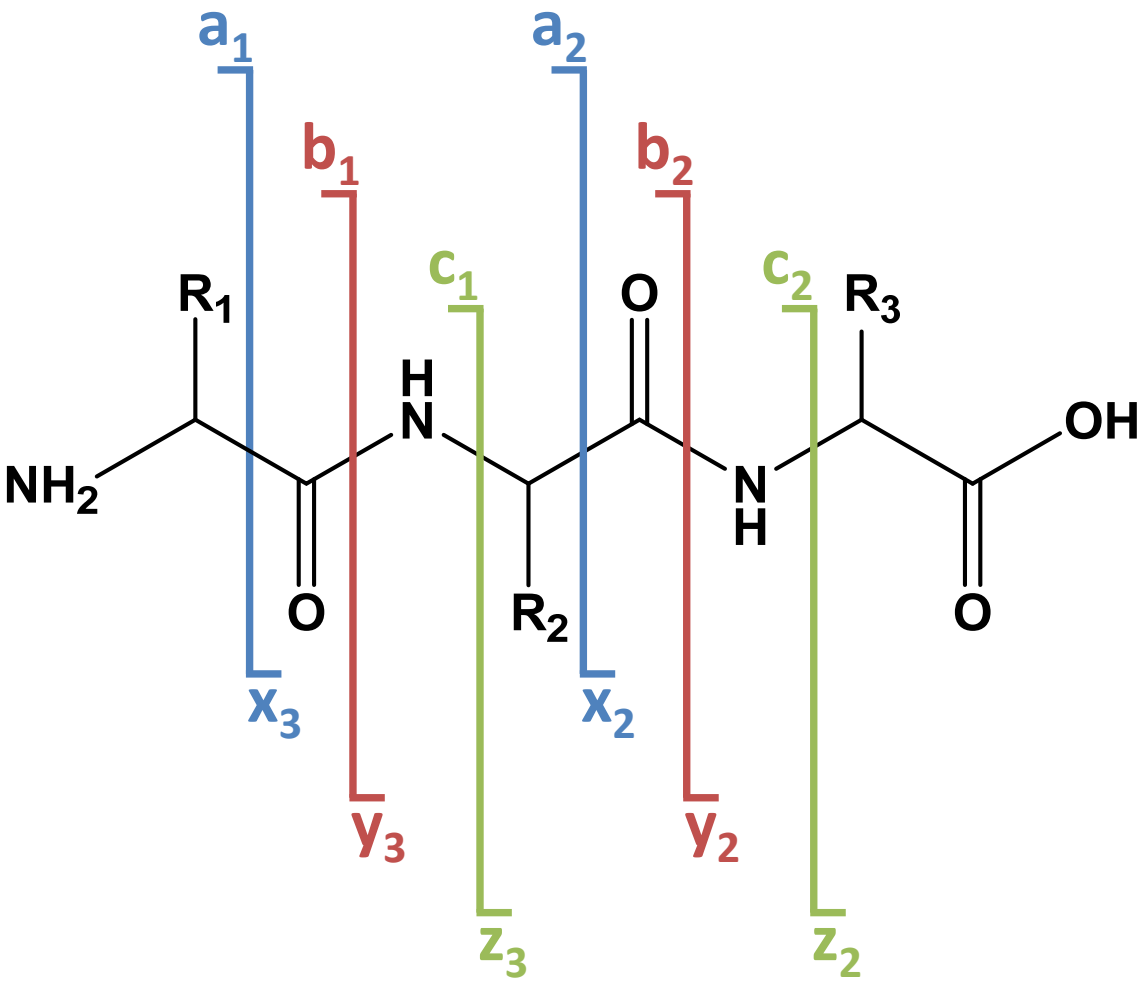

Figure 1.5 Peptide fragmentation nomenclature as proposed by references 75 and 76.

CHAPTER 2. AFFECTING PROTIEN CHARGE STATE DISTRIBUTIONS IN NANO-ELECTROSPRAY IONIZATION VIA IN-SPRAY SOLUTION MIXING USING THETA CAPILLARIES

Portions and figures of this chapter were published previously as reference 66, copyright 2014 American Chemical Society.

2.1 Introduction

Electrospray ionization (ESI)[1] has been instrumental in enabling the mass spectrometry of proteins due, in part, to the multiple charging of the analyte molecules, which brings the high mass molecule-ions into the operational mass-to-charge range of most mass spectrometers. The conformation of the protein in solution plays a role in determining the charge state distribution (CSD) observed in the mass spectrum. CSDs weighted to high relative charge states correlate with denatured/unfolded forms of a protein, while CSDs weighted to relatively low charge states tend to reflect more native/folded protein conformations.[2,3,4 5] The range and magnitudes of charge states can have important implications for mass spectrometry and tandem mass spectrometry experiments. For example, higher charge states are often preferred for protein sequencing studies, as dissociation thresholds tend to decrease with increasing protein charge.[6,7] Dissociation efficiencies, in particular, increase with charge for electron

transfer dissociation (ETD)[8] and electron capture dissociation (ECD).[9,10,11] Many solution additives have been shown to affect protein charge states including acids/bases or various solvents,[12,13,14] denaturing agents (e.g., urea, guanidine hydrochloride), 'supercharging' agents (e.g., tetramethylene sulfone (sulfolane) and *m*-nitrobenzyl alchohol (*m*-NBA)),[15,16] or derivatizing agents.[17] All of these methods require the addition of various agents to the bulk solution which can waste sample, cause deleterious effects on the ESI response, and/or prevent the observation of short-lived intermediates or non-covalent complexes.

To avoid manipulation of the bulk solution, various methods have been developed to alter protein charge states either in the gas-phase after the fully desolvated ions are formed or in the solution/droplet-phases between the ESI tip and the orifice of the mass spectrometer. Manipulation of protein charge states has been demonstrated in the gas phase via ion/molecule[18,19] and ion/ion[20,21,22,23] reactions. One method of mixing analyte solutions with reagents during ESI is to leak gaseous vapors into the interface of the mass spectrometer. For example, Kharlamova *et al.* introduced acidic and basic vapors via a leak-in set-up in which a test tube containing the reagent was placed in-line with the nitrogen curtain gas flow. The nitrogen gas entrained the reagent head-space vapors and introduced them to the interface region of a mass spectrometer where the vapors interacted with the electrospray droplets.[24,25,26] Similarly, reagent vapors have been introduced to electrospray droplets by placing a plate or a vial of the reagent below the spray region of the interface[27] and by mixing vapors with the nebulizing gas.[28] These methods have been used to manipulate protein

charge states,[24,25,26] decrease salt adducts on biomolecules,[29] and to perform on-the-fly hydrogen-deuterium exchange (HDX) studies.[27,30] However, these techniques are limited to the use of volatile reagents and may require instrument modifications for implementation.

Several other techniques have been developed to effect analyte and reagent mixing in the solution/droplet phase between the ESI tip and the orifice of the mass spectrometer, including extractive electrospray ionization (EESI),[31,32] fused droplet-electrospray ionization (FD-ESI),[33,34] and liquid sampling desorption electrospray ionization (DESI).[35] These techniques enable the mixing of nonvolatile reagents with analyte solutions without addition to the bulk solution. One common class of nonvolatile reagents used to manipulate protein charge states is supercharging agents. The nonvolatile characteristic of supercharging agents may play a key role in the mechanism for increasing protein charge states. While the mechanism associated with supercharging remains under study, it has been proposed that the nonvolatile reagent becomes concentrated in the ESI droplet during the evaporation process, thus increasing the surface tension of the droplets.[36] The increased surface tension of the droplet results in an increase in the droplets ability to accommodate charges according to the Rayleigh charge limit theory.[37] The role of protein conformation in solution is also debated regarding the supercharging mechanism.[38] Recently Miladinović *et al.* employed a dual-spraying microchip which contains two microchannels that cross on-top of each other at the tip of the chip without connecting. Protein and supercharging agent solutions were pumped separately through the two channels and ionization was

effected by applying a voltage to an electrode in contact with the protein solution. Mixing of the protein and supercharging agent solutions occurred at the tip of the microchip and in the spray plume. The authors reported the observation of slightly higher charge states as compared to mixing the analyte solution with additional solvent in the device.[39] Additionally Konermann *et al.* have developed a technique to perform time-resolved ESI to monitor the folding and unfolding kinetics of proteins such as myoglobin and cytochrome *c*.[40] This technique combines solution flows from two syringes into a single capillary. Sampling the solution mixture at different lengths of the capillary has been correlated with mixing time and the observation of short-lived protein intermediates has been reported.[41] These solution/droplet phase mixing techniques enable the use of nonvolatile reagents without adding the reagent to the bulk solution; however, they often require instrument modifications or additional equipment.

Nano-ESI (nESI) is often performed using a borosilicate capillary that has been heated and pulled to a tip. The sample is loaded into the capillary and is sprayed and ionized by applying a voltage to a conductive material that is in contact with the solution. Recently, Mark *et al.* used theta-shaped borosilicate glass capillaries, which are round capillaries containing a glass septum through the center of the capillary that effectively divides the capillary into two separate channels, for nESI. Electrical contact with the solution was made by hand painting or sputter coating the tips with titanium and/or gold. The authors demonstrated solution mixing via complexation of vancomycin and diacetyl-L-lysyl-D-alanyl-D-alanine when spraying the analytes from opposite sides of a

theta tip. The authors also demonstrated HDX between a solution of vancomycin and deuterated vancomycin when sprayed from opposite channels of the tip. The authors believe the solution interactions occur in the Taylor cone of the spray, thus limiting the available mixing time of the solutions.[42]

All of these techniques enable the interaction of the analyte and reagent in the electrospray tip, in the Taylor cone, and/or in the droplets as they evaporate and travel through the interface of the mass spectrometer. Thus, these techniques are well suited for observing short time-scale interactions. Short-lived and/or intermediately unfolded protein conformations can be observed under these conditions. This is particularly advantageous when analyzing non-covalent protein complexes. For example, myoglobin contains a non-covalently attached heme group which is readily lost upon denaturation/unfolding of the protein in solution.[43] However, the limited mixing time involved in most of these techniques makes it possible to observe higher charge states of myoglobin without the loss of the heme group.

In this chapter, the use of borosilicate theta capillaries, similar to those implemented by Mark *et al.*,[42] for protein charge state manipulation is reported. The capillaries are heated and pulled to a tip, much like conventional, single barreled nESI capillaries. Rather than painting or sputter coating the tip with a conductive material to effect ionization as described previously,[42] a platinum wire electrode is inserted into one channel of the theta tip to form an electrical contact with the analyte solution. With this configuration, a single wire electrode can be placed in either side of the theta tip, or a dual emitter can be used in which electrodes held at the same potential are placed into

both sides of the tip simultaneously. Regardless of electrode placement (each side individually or both sides simultaneously), the generated signal contains characteristics of both solutions loaded into the theta tip. Because the glass septum separates the solutions while they are in the capillary, the majority of solution mixing occurs in the Taylor cone and during droplet evolution and evaporation processes as the droplets travel through the interface of the mass spectrometer. Thus, the resulting spectrum includes species that exist on this short timescale (<1 millisecond).[44] The relatively short timescale is an interesting platform for studying protein denaturation as the extent of protein unfolding is dependent upon the kinetics of the conformational change, which is protein dependent. The denaturation and/or increased charging of several proteins (including myoglobin, cytochrome *c*, and carbonic anhydrase) on this timescale are reported.

2.2 Experimental

2.2.1 Materials

All samples were prepared in water purified by a Barnstead nanopure infinity ultrapure water system (Thermo Fisher Scientific, Waltham, MA). Cytochrome *c* from bovine heart, myoglobin from equine skeletal muscle, carbonic anhydrase II from bovine erythrocytes, oxalic acid, tetramethylene sulfone (sulfolane), and 3-nitrobenzyl alcohol (*m*-NBA) were purchased from Sigma Aldrich (St. Louis, MO). Protein solutions were used without further purification by diluting aqueous stock solutions to a final

concentration of 5-20μM in water. Sulfolane and *m*-NBA solutions were diluted to final concentrations of 1% and 0.5% respectively by volume in water. Acetic acid and formic acid were purchased from Malinckrodt Chemicals (Phillipsburg, NJ) and were diluted to final concentrations of 0.1% to 10% acid by volume in water or were used without further dilution (100% acid). Hydrochloric acid was purchased from J. T. Baker (Avantor, Center Valley, PA) and was diluted to a final concentration of 0.175M in water.

2.2.2 Apparatus and Procedures

All experiments were performed using a prototype version of a QqTOF tandem mass spectrometer (Q-Star Pulsar XL, AB Sciex, Concord, ON) modified to allow for ion trap CID and ion/ion reactions.[45] These features, however, were not employed in the experiments described in this chapter. Single-barreled borosilicate capillaries and borosilicate theta glass capillaries were purchased from Sutter Instrument Co. (Novato, CA). The single barreled borosilicate capillaries have an internal diameter of 0.86 mm. The theta glass capillaries have an internal diameter of ~1.17mm and contain a 0.165mm thick glass septum that runs the length of the capillary, dividing the capillary into two parallel channels. Both the single barreled and theta glass capillaries were pulled to a ~10μm tip on a Flaming/Brown micropipette puller (Sutter Instrument Co., Novato, CA). Each channel of the theta tip was loaded individually with separate solutions. The wire electrode was placed in one side of the theta tip at a time to effect ionization, or a dual wire electrode was fashioned to apply equal potentials to solutions in both sides of the theta tip simultaneously. All pH measurements of protein/acid

solution mixtures were made with an Orion perpHecT LogR meter, model 320 (Thermo Fisher Scientific; Waltham, MA).

2.3 Results and Discussion

Protein solutions were loaded into one side of the theta tip, while reagent solutions were added to the opposite side. Similar results can be obtained by placing the electrode in either side individually or in both sides of the theta tip simultaneously. An example is illustrated in Figure 2.1, which summarizes a series of experiments with myoglobin and acetic acid.

The intensity-weighted average charge state was calculated according to equation (2.1) in which N is the number of observed analyte charge states, q_i is the net charge of the i^{th} charge state, and W_i is the signal intensity of the i^{th} charge state.[15]

$$q_{av} = \frac{\sum_i^N q_i W_i}{\sum_i^N W_i} \qquad (2.1)$$

We note that spectra can be obtained by loading a single side of a theta tip and placing the electrode in the same side (data not shown); however, the resulting signal intensity and stability are often diminished compared to spraying the same solution from a regular, single-barreled tip. Protein solutions have been sprayed from a single side of a theta tip with no solution added to the opposite side to ensure that the native-like spectrum would be generated. As a control, the same theta tip was then loaded with acetic acid in the opposite side and sprayed to ensure that shifts in protein CSD are correlated to acid-protein mixing.

2.3.1 Shifting Protein CSD with Acid Solutions in Theta Tips

Holomyoglobin (pI = 6.8-7.2) is a 17.6 kDa protein that contains a non-covalently bound heme group. The tertiary structure of holomyoglobin is stabilized by hydrogen bonding and the interaction of the non-covalently bound heme group with a proximal histidine within a hydrophobic pocket.[43] The non-covalent complex can be observed under native electrospray conditions.[46,47,48] However, myoglobin rapidly denatures upon exposure to acidic environments via a short-lived intermediate of unfolded holomyoglobin prior to the loss of the heme group yielding apomyoglobin.[41] Holomyoglobin is observed when spraying myoglobin from water without added acid while the addition of 0.5% acetic acid results in denaturation of the protein such that only apo-myoglobin peaks are observed (see Figure 2.1b and Figure 2.1d, respectively). An unfolded holomyoglobin intermediate has been observable under conditions in which the time-scale for mixing of myoglobin with acid is limited (microsecond to millisecond timescale).[24,40] Theta tips isolate the solutions in each side until the tip of the capillary where the Taylor cone forms. Presumably, most of the solution mixing occurs in the Taylor cone and in the progeny droplets as they travel toward the orifice of the mass spectrometer, resulting in a short mixing time-scale (<1ms). The theta tip spectra support this conclusion as minor contributions from both apomyoglobin and denatured/unfolded holomyoglobin appear in Figure 2.1a, c, and e, where myoglobin is mixed with acetic acid by spraying from a theta tip. The average charge state of holomyoglobin sprayed from water in a regular tip is about +8.3 (Figure 2.1b) compared to +10.6 when mixed with 1% acetic acid in the theta tips (Figure 2.1a). When the

myoglobin and acetic acid solutions are mixed and sprayed from a regular tip, the average charge state of apomyoglobin is +19.0 (Figure 2.1d) compared to +14.0 when mixed via the theta tips (Figure 2.1a). The acid-induced denaturation of myoglobin in the theta tips is evidenced by the shift of the holomyoglobin CSD to a higher average charge state and by the presence of apomyoglobin peaks. Mixing via the theta tips enables observation of the short-lived unfolded myoglobin without the loss of heme.

The extent of protein CSD shift can be controlled by varying the concentration of the acid. Figure 2.2a, c, and e show the effect of spraying 1%, 10%, and 100% acetic acid solutions, respectively, opposite myoglobin in a theta tip. The average CSD of apo- and holomyoglobin increases with acetic acid concentration (Figure 2.2a, c, and e): +14.0a/+10.6h (1% acetic acid), +16.6a/+11.1h (10% acetic acid), +18.4a/+16.5h (100% acetic acid). As shown in Figure 2.2b, the addition of as little as 0.5% acetic acid to bulk myoglobin solution results in 100% apomyoglobin signal.

Similar experiments were performed using cytochrome *c* (pI = 10-10.5) and carbonic anhydrase (pI = 5.9) as shown in Figure 2.3 and Figure 2.4, respectively. Bovine cytochrome *c* is a 12.2 kDa protein containing 104 amino acids and a single heme that is covalently attached via two thioether linkages.[49] The unfolding intermediates and resulting charge state distributions of cytochrome *c* are well known, including the transition from a more folded, lower CSD (centered around the +8/+9 charge state) to a more unfolded/denatured, higher CSD (centered around the +17 to +19 charge state) upon decreasing the pH below 2 to 3.[50,51,52,53,54] The observed CSD of cytochrome *c* when sprayed out of water without added acid is +5 to +11 (q_{av} = +7.6, Figure 2.5a).

When cytochrome *c* is mixed with acetic acid upon spraying from a theta tip, the higher CSD (centered around the +15 charge state) becomes observable and increases in abundance as the acetic acid concentration is increased from 1% (Figure 2.3a) to 100% (Figure 2.3e). The shift in CSD obtained from mixing cytochrome *c* with acetic acid via the theta tips (q_{av} = +8.6 to +12.0, Figure 2.3a, c, e) is slightly less than that observed upon mixing acetic acid with cytochrome *c* in solution (q_{av} = +9.0 to +13.5, Figure 2.3b, d, f).

Bovine carbonic anhydrase was also sprayed opposite various concentrations of acetic acid in the theta tips (Figure 2.4). Carbonic anhydrase (pI = 5.9) is a 29 kDa protein that contains a divalent zinc ion coordinated to 3 histidine residues and a water molecule within the central cavity making up the active site of the enzyme.[55,56] It is well known that carbonic anhydrase undergoes two transitions in which a partially expanded/loosened intermediate is observable upon acid denaturation occurring within the pH ranges of 4.8-4.0 (transition I) and 3.4-2.5 (transition II).[57,58] The carbonic anhydrase CSD obtained from spraying the protein out of water without added acid from a regular tip (Figure 2.5b) ranged from +9 to +17 (q_{av} = +12.5). Upon mixing carbonic anhydrase with 1% (Figure 2.4a), 10% (Figure 2.4c), and 100% (Figure 2.4e) acetic acid via the theta tips, the resulting average charge state increased from +13.4, to +13.5, to +25.3, respectively. The two lower concentrations of acetic acid resulted in a bimodal distribution centered around the +15/+16 and the +8/+9 charge states, likely indicating the presence of two distinct conformations of the protein. With 100% acetic acid in the theta tip the CSD shifted to much higher charge states, centered around the

+26 charge state, suggesting an extended conformation. In comparison to the control spectra, in which the protein was mixed in solution with 0.5% (Figure 2.4b), 5% (Figure 2.4d), and 50% (Figure 2.4f) acetic acid and sprayed from a regular tip, only the higher CSD was observed with slight variations in the most abundant and average charge states, respectively: +23 (q_{av} = +25) , +27 (q_{av} = +27), +28 (q_{av} = +28.4). Additionally, a mixture of holo- and apo-carbonic anhydrase was observed when acetic acid was mixed with carbonic anhydrase via a theta tip (Figure 2.4a, c, and e), while only apo-carbonic anhydrase was observed for the solution-phase mixtures sprayed from a single-barreled capillary (Figure 2.4b, d, and f).

The short timescale and effective pH/acid concentration play a role in determining the species that will be observed in the mass spectrum. As the acid concentration increases, the protein denaturation rate is expected to increase, which is consistent with the observation of the more denatured protein species (higher charge states and apomyoglobin) when mixed with higher concentrations of acid. The extent of the observed shift in CSD is protein dependent as proteins have different denaturation kinetics under various pH conditions. Even at low concentrations of acetic acid (0.5%) mixed in solution with myoglobin (Figure 2.2b), almost exclusively apomyoglobin peaks are observed, indicating that a solution pH of 3.3 results in full denaturation at equilibrium. However, all myoglobin theta tip spectra indicate that the protein denaturation kinetics are sufficiently slow on the time-scale of the theta tip experiment that the intermediate (higher holomyoglobin charge states) is observable. This is consistent with stopped flow studies performed by Konermann *et al.* where they

reported lifetimes of 0.38 ± 0.06s for the unfolded holomyoglobin intermediate.[41] Similarly, the solution mixture of acetic acid with carbonic anhydrase sprayed from a regular tip shows only the higher CSD even at lower concentrations of acetic acid (0.5%, Figure 2.4b), while two CSDs are observable in the theta tip mixing spectra for 1% (Figure 2.4a) and 10% (Figure 2.4c) acetic acid concentrations. When 100% acetic acid is mixed with carbonic anhydrase via the theta tip (Figure 2.4e), only the higher CSD is observed. In contrast, spectra in which cytochrome *c* was mixed with lower concentrations of acetic acid in solution (Figure 2.3b and 2d) show two CSDs centered around the +15/+16 and the +9 charge state. The two distinct CSDs indicate that in the pH range of 2.4 to 2.9, there are multiple conformations of the protein present at equilibrium in solution. The kinetics of cytochrome *c* unfolding upon acid denaturation are not quite fast enough to reach equilibrium on the timescale of the theta tip experiment as evidenced by the lower relative abundance of the higher CSD as compared to the solution mixture at equilibrium (Figure 2.3a-d). However, the same two CSDs are still present. This provides evidence that there is no partially denatured intermediate observable via CSDs on the time-scale of this experiment (<1 ms). Konermann and Douglas also found only two CSDs for cytochrome *c* on the millisecond time-scale, which indicated the loss of tertiary structure (between pH 2-4), while they concluded that protein CSD was not a sensitive measurement for the known change in secondary structure for cytochrome *c*.[50,59]

It is important to note that the relative contribution of each solution in the theta tips to the Taylor cone upon spraying will also play a significant role in the full extent of

CSD shifting observed. Every theta tip used for these experiments was pulled individually such that the tip geometry varies from tip to tip, which may have an impact on the ability of each side of the tip to spray evenly. Additionally, mixing within the theta tip capillary cannot be completely ruled out. In rare instances, the relative contribution of higher and lower CSDs to the overall spectrum would change over time such that the first few spectra would show dominant signal of the more denatured species while over time the more native species would start to dominate the signal. After a short period of time (several seconds to a minute usually) the spectrum would reach a steady-state in which the relative contribution of higher and lower charge states was constant. This observation was most dramatic when using 100% acetic acid on one side of the theta tip with the protein in water on the opposite side. Presumably, this effect is due to diffusion at the solution contact point at the end of the theta tip prior to nESI. All spectra presented here were taken under conditions in which the relative signals in the spectra were not changing over time.

As indicated above (see Figure 2.3e), a dramatic shift in the CSD of cytochrome *c* in the theta tip experiments was noted only with the 100% acetic acid experiment. Thus, it may be useful to spray proteins like cytochrome *c* opposite stronger acids to increase the rate of denaturation of the protein. Cytochrome *c* was sprayed opposite formic acid (pKa = 3.75, vapor pressure (vp) = 35 torr), oxalic acid (pKa = 1.25, vp = 0.001 torr), and HCl (pKa = -8, vp = 120 torr) in the theta tips (Figure 2.6a, c, and e, respectively). The solution mixtures of each acid with cytochrome *c* sprayed from regular tips are given in Figure 2.6b, d, and f for formic acid, oxalic acid, and HCl respectively. Formic acid and

HCl were each sprayed with concentrations of 0.875M for comparison with 1% acetic acid (pKa = 4.76, vp = 11 torr) data (1% acetic acid ≈ 0.875M). Oxalic acid was sprayed at a much lower concentration as comparable concentrations would clog the theta tips due to its low vapor pressure. There is an overall positive correlation between the acid strength and the average charge state observed in the spectra generated from mixing cytochrome *c* with the acids via the theta tips; acetic acid q_{av} = +8.6 (Figure 2.3a), formic acid q_{av} = +8.3 (Figure 2.6a), oxalic acid q_{av} = +9.7 (Figure 2.6c), and HCl q_{av} = +10.2 (Figure 2.6e). There are two CSDs for the solution mixture of each acid (Figure 2.3b, and Figure 2.6b, d, and f) and for the theta tip experiments with formic (Figure 2.6a) and oxalic acid (Figure 2.6c). The lower cytochrome *c* CSD observed with HCl mixed both in solution (Figure 2.6f) and via spraying from a theta tip (Figure 2.6e) is centered around the +7 charge state, as opposed to being centered around the +8 or +10 charge state observed with the other acids. The presence of the +7 charge state has previously been attributed to the A-state of the protein in which the protein re-folds at low pH into a molten globule structure. The A-state has been observed in solution at equilibrium and on the microsecond timescale.[24,60,61,62,63,64] Goto et al. and Mirza and Chait have found that the acid anion plays an important role in the refolding of denatured proteins upon further decrease in pH as the addition of acid increases the anion concentration sufficiently to counteract the increased repulsive forces of the positive charges at high acid concentration, enabling the protein to refold. The counter-ion effect may underlie the observation of the lower CSD (centered around the +7 charge state) with HCl at a pH of 1.0 (Figure 2.6f) while it is not observed with acetic acid at a pH of 0.8 (Figure 2.3f).

The theta tips are also advantageous for use with non-volatile acids, which cannot be used with various leak-in/vapor techniques. Oxalic acid is a non-volatile acid that can be mixed with protein solutions to shift the CSD to higher charge states via spraying from a theta tip (Figure 2.6c). The cytochrome *c* CSD shifted from +5 to +12 (q_{av} = +7.6, Figure 2.5a) when sprayed from water in a single-barreled tip to two distinct CSDs centered around the +15 and +9 charge states when mixed with oxalic acid in the theta tip (Figure 2.6c). The shift in protein CSD indicates solution mixing despite the nonvolatile characteristic of oxalic acid. A disadvantage of nonvolatile acids mixed in solution is the resulting adducts, which decrease the signal intensity of the protonated molecule. However, protein adduction was minimized by mixing the protein and acid solutions in the theta tips as compared to mixing in solution. The greatest difference in protein adducts was observed with oxalic acid and HCl (Figure 2.6c-f). For example, many oxalic acid adducts were observed when mixed with cytochrome *c* in solution (Figure 2.6d). The degree of adduction is much less with the short time-scale solution mixing effected with the theta tips as opposed to spraying solution mixtures from a single barreled tip. Thus, the theta tips provide a simple, inexpensive method for shifting protein CSD with various acids and concentrations, including nonvolatile acids, while minimizing protein adducts.

2.3.2 Shifting Protein CSD with Supercharging Agents in Theta Tips

As demonstrated above with oxalic acid, one advantage of using the theta tips to effect analyte and reagent mixing on a short time-scale is their compatibility with

nonvolatile reagents. Supercharging agents are a major class of nonvolatile reagents that are used to increase charge states of peptides and proteins. Two of the most commonly used supercharging agents are sulfolane and *m*-NBA. To demonstrate the use of theta tips with supercharging agents, cytochrome *c* (Figure 2.7) and myoglobin (Figure 2.8) were each mixed with sulfolane and *m*-NBA via spraying from a theta tip and the generated spectra are compared to the respective solution mixture controls.

Cytochrome *c* was sprayed opposite 1% sulfolane (Figure 2.7a) and 0.5% *m*-NBA (Figure 2.7c) in a theta tip. The cytochrome *c* CSD shifted from q_{av} = +7.6 sprayed from water in a regular tip (Figure 2.5a) to q_{av} = +8.7 and +8.2 with sulfolane and *m*-NBA, respectively, sprayed from theta tips. The average cytochrome *c* charge states obtained via mixing the same sulfolane and *m*-NBA solutions with the protein in solution and spraying from a regular tip were +9.2 and +9.8 respectively. The overall appearances of the theta tip and regular tip spectra are quite similar, in that the CSD was shifted to a slightly higher CSD, but only one distribution is observed for cytochrome *c* for both supercharging agents, unlike the two distinct distributions observed with the acids above.

Similarly, myoglobin was sprayed opposite sulfolane (Figure 2.8a) and *m*-NBA (Figure 2.8c) in a theta tip and resulting spectra were compared to the solution mixtures sprayed from a regular tip (Figure 2.8b and d). As reported previously,[16,65] the addition of sulfolane and *m*-NBA to solutions of myoglobin results in the observation of apo- and holomyoglobin signals, which are also observed in the control spectra and the theta tip spectra reported herein (Figure 2.8). The percentage of apomyoglobin peaks increases

from 9% to 33% with sulfolane and to 45% with *m*-NBA, which is consistent with previous observations in which greater shifts in CSD and denaturation were observed with *m*-NBA than with sulfolane.[65] Similar to the results described above with cytochrome *c*, the overall appearance of the spectra for mixing sulfolane with myoglobin via the theta tips is similar to the solution phase mixture sprayed from a regular tip.

As previously mentioned, the mechanism by which supercharging agents increase the charge state of proteins is still unclear. Lomeli *et al.* have found that *m*-NBA concentrations below 1.0% do not denature myoglobin in bulk solution.[16] Additionally, Sterling *et al.* have determined that the addition of sulfolane from 0.0-7.5% sulfolane destabilizes the native conformation of myoglobin in solution, however no loss of helicity was observed at room temperature.[65] The lack of denaturation in bulk solution indicates that the denaturation of the proteins likely occurs during the electrospray process in the droplet. The theta tip results are consistent with this conclusion as the theta tip spectra are similar to the bulk solution mixture spectra, indicating that the equilibrium state of the protein in the bulk solution is not significantly affected by the presence of the supercharging agent. The time-scale of protein denaturation using the supercharging agents appears to be similar in both the theta tip (limited to the microsecond mixing timescale) and regular tip spectra, suggesting that the processes that underlie supercharging occur during the electrospray process.

2.4 Conclusions

The use of pulled borosilicate theta glass capillaries as nESI emitters to effect microsecond timescale mixing of protein and denaturant solutions results in shifts in protein CSD without requiring modification of the bulk solution. The extent of protein CSD shift is determined by acid identity, acid concentration, and the kinetics of unfolding of the protein. Due to the short time-scale of mixing, short-lived intermediate species such as the higher CSD of holomyoglobin can be observed. Theta tips also allow for the use of nonvolatile acids and supercharging agents which are not compatible with other vapor leak-in techniques. No instrument modifications are necessary, which should make this approach widely accessible to the analytical mass spectrometry community.

2.5 References

[1] Fenn, J. B.; Mann, M.; Meng, C. K.; Wong, S. F.; Whitehouse, C. M. *Science* **1989**, *246*, 64-71.

[2] Chowdhury, S. K.; Katta, V.; Chait, B.T. *J. Am. Chem. Soc.* **1990**, *112*, 9012-9013.

[3] Kaltashov, I.A.; Eyles, S. J. *Mass Spectrom. Rev.* **2002**, *21*, 37-71.

[4] Fenn, J. B. *J. Am. Soc. Mass Spectrom.* **1993**, *4*, 524-535.

[5] Fenn, J. B. *J. Am. Soc. Mass Spectrom.* **1993**, *4*, 524-535.

[6] Reid, G. E.; Wu, J.; Chrisman, P. A.; Wells, M.; McLuckey, S. A. *Anal. Chem.* **2001**, *73*, 3274-3281.

[7] Jockusch, R. A.; Schnier, P. D.; Price, W. D.; Strittmatter, E. F.; Demirev, P. A.; Williams, E. R. *Anal. Chem.* **1997**, *69*, 1119-1126.

[8] Syka, J. E.; Coon, J. J.; Schroeder, M. J.; Shabanaowitz, J.; Hunt, D. F. *Proc. Natl. Acad. Sci.USA* **2004**, *101*, 9528-9533.

[9] Zubarev, R. A.; Kelleher, N. L.: McLafferty, F. W. *J. Am. Chem. Soc.* **1998**, *120*, 3265-3266.

[10] Iavarone, A.; Paech, K.; Williams, E. R. *Anal. Chem.* **2004**, *76*, 2231-2238.

[11] Zubarev, R. A.; Horn, D. M.; Fridriksson, E. K.; Kelleher, N. L.; Kruger, N. A.; Lewis, M. A.; Carpenter, B. K.; McLafferty, F. W. *Anal. Chem.* **2000**, *72*, 563-573.

[12] Loo, J. A.; Ogorzalek Loo, R. R.; Udseth, H. R.; Edmonds, C. G.; Smith, R. D. *Rapid Commun. Mass Spectrom.* **1991**, *5*, 101-105.

[13] Iavarone, A. T.; Jurchen, J. C.; Williams, E. R. *J. Am. Soc. Mass Spectrom.* **2000**, *11*, 976-985.

[14] Le Blanc, J. C. Y.; Wang, J.: Guevremont, R. Siu, K. W. M. *Org. Mass Spectrom.* **1994**, *29*, 587-593.

[15] Iavarone, A. T.; Jurchen, J. C.; Williams, E. R. *Anal. Chem.***2001**, *73*, 1455-1460.

[16] Lomeli, S. H.; Peng, I. X.; Yin, S.; Ogorzalek Loo, R. R.; Loo, J. A. *J. Am. Soc. Mass Spectrom.* **2010**, *21*, 127-131.

[17] Krusemark, G. J.; Frey, B. L.; Belshaw, P. J.; Smith, L. M. *J. Am. Soc. Mass Spectrom.* **2009**, *20*, 1617-1625.

[18] McLuckey, S. A.; Van Berkel, G. J.; Glish, G. L. *J. Am. Chem. Soc.* **1990**, *112*, 5668-5670.

[19] Ogorzalek Loo, R. R.; Winger, B. E.; Smith, R. D. *J. Am. Soc. Mass Spectrom.* **1994**, *5*, 1064-1071.

[20] Stephenson, J. L., Jr.; McLuckey, S. A. *J. Am. Chem. Soc.* **1996**, *118*, 7390-7397.

[21] Scalf, M.; Westphall, M. S.; Krause, J.; Kaufman, S. L.; Smith, L. M. *Science* **1999**, *283*, 194-197.

[22] He, M.; McLuckey, S. A. *J. Am. Chem. Soc.* **2003**, *125*, 7756-7757.

[23] He, M.; McLuckey, S. A. *Anal. Chem.* **2004**, *76*, 4189-4192.

[24] Kharlamova A.; Prentice, B. M.; Huang, T.-Y.; McLuckey, S. A. *Anal. Chem.* **2010**, *82*, 7422-7429.

[25] Kharlamova, A.; McLuckey, S. A. *Anal. Chem.* **2011**, *83*, 431-439.

[26] Kharlamova, A.; DeMuth, J. C.; McLuckey, S. A. *J. Am. Soc. Mass Spectrom.* **2011**, *23*, 88-101.

[27] Kostyukevich, Y.; Kononikhin A.; Popov, I.; Nikolaev, E. *Anal. Chem.* **2013**, *85*, 5330-5334.

[28] Girod, M.; Antoine, R.; Dugourd, P.; Love, C.; Mordehai, A.; Stafford, G. *J. Am. Soc. Mass Spectrom.* **2012**, *23*, 1221-1231.

[29] Kharlamova, A.; Prentice, B. M.; Huang, T.-Y.; McLuckey, S. A. *Int. J. Mass Spectrom.* **2011**, *300*, 158-166.

[30] Takáts, Z.; Schlosser, G.; Vékey, K. Int. J. Mass Spectrom. **2003**, *228*, 729-741.

[31] Chen, H.; Touboul, D.; Jecklin, M. C.; Zheng, J.; Luo, M.; Zenobi, R. *Eur. J. Mass Spectrom.* **2007**, *13*, 273-279.

[32] Chen, H.; Venter, A.; Cooks, R. G. *Chem. Commun.* **2006**, *19*, 2042-2044.

[33] Chang, D.-Y.; Lee, C.-C.; Shiea, J. *Anal. Chem.* **2002**, *74*, 2465-2469.

[34] Shieh, I-F.; Lee C.-Y.; Shiea, J. *J. Proteome Res.* **2005**, *4*, 606-612.

[35] Miao, Z.; Wu, S.; Chen, H. *J. Am. Soc. Mass Spectrom.* **2010**, *21*, 1730-1736.

[36] Iavarone, A. T.; Williams, E. R. *J. Am. Chem. Soc.* **2003**, *125*, 2319-2327.

[37] Lord Rayleigh *Philos. Mag.* **1882**, *14*, 184-186.

[38] Lomeli, S. H.; Yin, S.; Ogorzalek Loo, R. R.; Loo, J. A. *J. Am. Soc. Mass Spectrom.* **2009**, *20*, 593-596.

[39] Miladinović, S. M.; Fornelli, L.; Lu, Y.; Piech, K. M.; Girault, H. H.; Tsybin, Y. O. *Anal. Chem.* **2012**, *84*, 4647-4651.

[40] Konermann, L.; Collings, B. A.; Douglas, D. J. *Biochemistry* **1997**, *36*, 5554-5559.

[41] Konermann, L.; Rosell, F. I.; Mauk, A.G.; Douglas, D. J. *Biochemistry* **1997**, *36*, 6448-6454.

[42] Mark, L. P.; Gill, M. C.; Mahut, M.; Derrick, P. J. *Eur. J. Mass Spectrom.* **2012**, *18*, 439-446.

[43] Evans, S. V.; Brayer G. D. *J. Mol. Biol.* **1990**, *23*, 885-897.

[44] Schneider, B. B.; Baranov, V. I.; Javaheri, H.; Covey, T. R. *J. Am. Soc. Mass Spectrom.* **2003**, *14*, 1236-1246.

[45] Xia, Y.; Chrisman, P.A.; Erickson, D. E.; Liu, J.; Liang, X.; Londry, F. A.; Yang, M. J.; McLuckey, S. A. *Anal. Chem.* **2006**, *78*, 4146-4154.

[46] Katta, V.; Chait, B. T.; *J. Am. Chem. Soc.* **1991**, *113*, 8534-8535.

[47] Li, Y.-T.; Hsich, Y.-L.; Henion, J. D. *J. Am. Soc. Mass Spectrom.* **1993**, *4*, 631-637.

[48] Loo, J. A. *Mass Spectrom. Rev.***1997**, *16*, 1-23.

[49] Margoliash, E.; Schejter, A. *Advan. Protein Chem.* **1966**, *21*, 113-286.

[50] Konermann, L.; Douglas, D. J. *Biochemistry* **1997**, *36*, 12296-12302.

[51] Grandori, R.; Matecko, I.; Müller, N. *J. Mass Spectrom.* **2002**, *37*, 191-196.

[52] Goto, Y.; Hagihara, Y.; Hamada, D.; Hoshino, M.; Nishii, I. *Biochemistry* **1993**, *32*, 11878-11885.

[53] Grandori, R. *Protein Sci.* **2002**, *11*, 453-458.

[54] Bai, Y. Sosnick, T. R.; Mayne, L.; Englander, S. W. *Science* **1995**, *269*, 192-197.

[55] Lindskog, S. *Pharmacol. Ther.***1997**, *74*, 1-20.

[56] Saito, R.; Sato, T.; Ikai, A.; Tanaka, N. *Acta. Cryst.* **2004**, *D60*, 792-795.

[57] Wong, K.-P.; Hamlin, L. M. *Biochemistry*, **1974**, *13*, 2678-2683.

[58] Wong, K.-P.; Tanford, C. *J. Biol. Chem.*, **1973**, *248*, 8518-8523.

[59] Ikai, A.; Fish, W. W.; Tanford, C. *J. Mol. Biol.* **1973**, *73*, 165-184.

[60] Fink, A. L.; Calciano, L. J.; Goto, Y.; Kurotsu, T.; Palleros, D. R. *Biochemistry*, **1994**, *33*, 12504-12511.

[61] Goto, Y.; Calciano, L. J.; Fink, A. L. *Proc. Natl. Acad. Sci. USA* **1990**, *87*, 573-577.

[62] Bychkova, V. E.; Dujsekina, A. E.; Lenin, S. I.; Tiktopulo, E. I.; Uversky, V. N.; Ptitsyn, O. B. *Biochemistry* **1996**, *35*, 6058-6063.

[63] Mirza, U. A.; Chait, B. T. *Anal. Chem.* **1994**, *66*, 2898-2904.

[64] Jeng, M.-F.; Englander, S. W. *J. Mol. Biol.* **1991**, *221*, 1045-1061.

[65] Sterling, H. J.; Daly, M. P.; Geld, G. K.; Thoren, K. L.; Kintzer, A. F.; Krantz, B. A.;

[66] Fisher, C. M.; Kharlamova, A.; McLuckey, S. A. *Anal. Chem.* **2014**, *86*, 4581-4588.

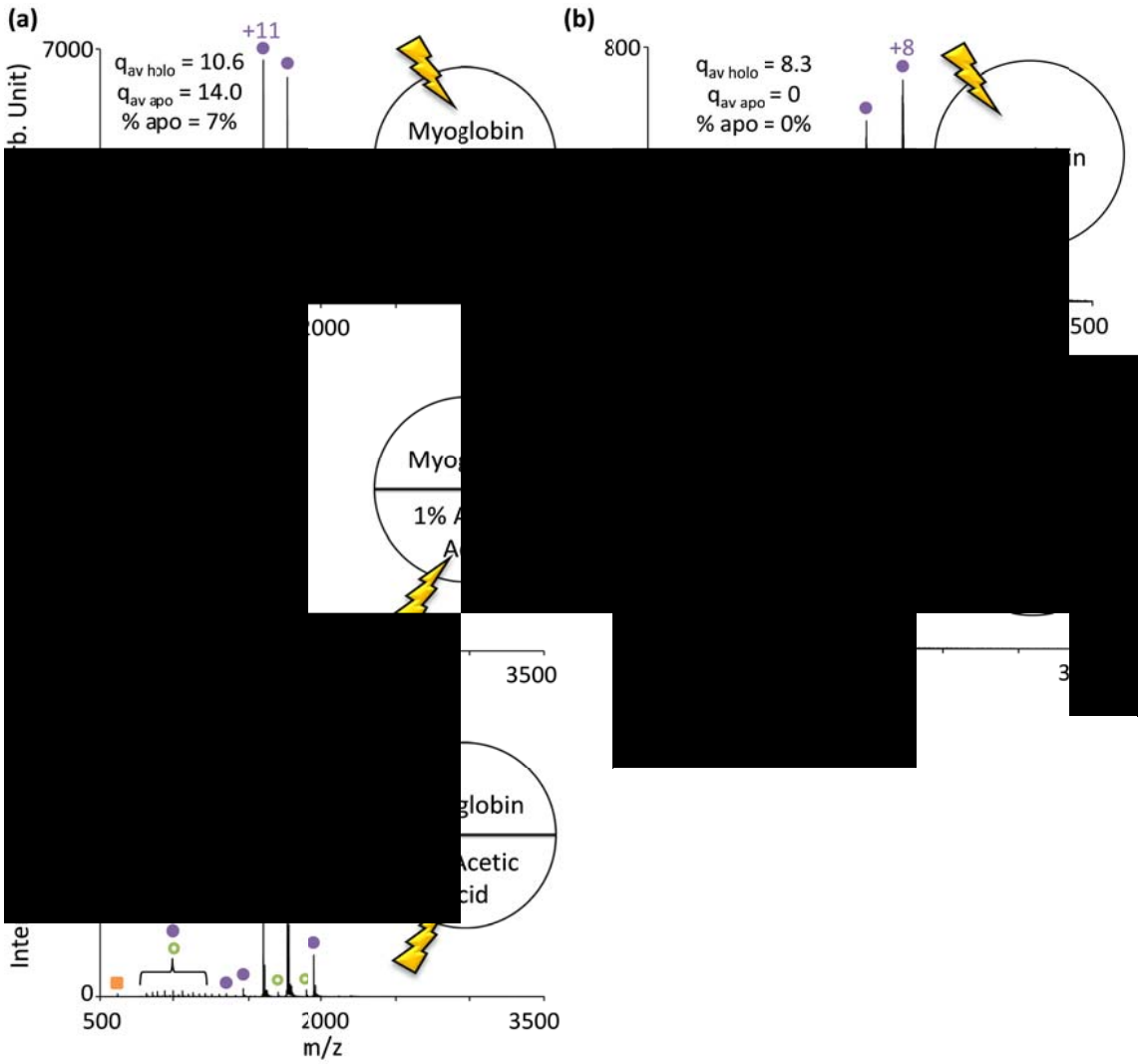

Figure 2.1 Positive nESI spectra of myoglobin and 1% acetic acid sprayed from opposite sides of a theta tip with an emitter in the (a) myoglobin side, (c) acetic acid side, and (e) with a dual emitter in both sides simultaneously. For comparison (b) myoglobin in water without acid and (d) myoglobin with 0.5% acetic acid (pH 2.9) mixed in solution were sprayed from regular tips. (●) indicates holomyoglobin charge states, (o) indicates apomyoglobin charge states, and (■) indicates heme. Lightning bolts indicate emitter location.

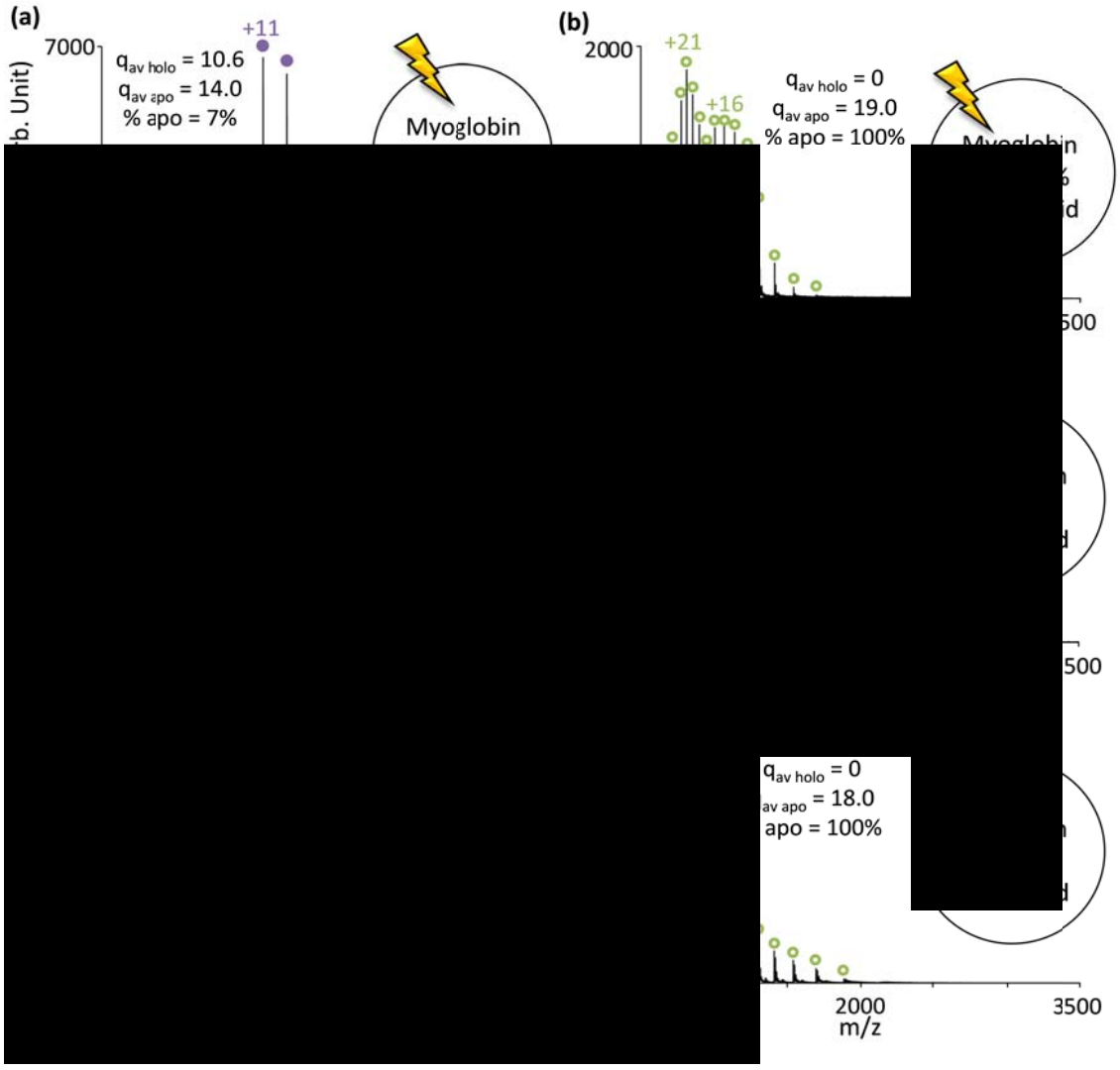

Figure 2.2 Myoglobin sprayed opposite (a) 1%, (c) 10%, and (e) 100% acetic acid in the theta tips. For comparison, myoglobin was mixed with equi-volume amounts of (b) 1%, (d) 10%, and (f) 100% acetic acid to yield final concentrations of 0.5% (pH 2.9), 5% (pH 2.2), and 50% (pH 0.8) acetic acid, respectively, and sprayed from a regular tip. Magenta dots (●) indicate holomyoglobin charge states, open circles (o) indicates apomyoglobin charge states, and yellow squares (■) indicate heme. Lightning bolts indicate emitter location.

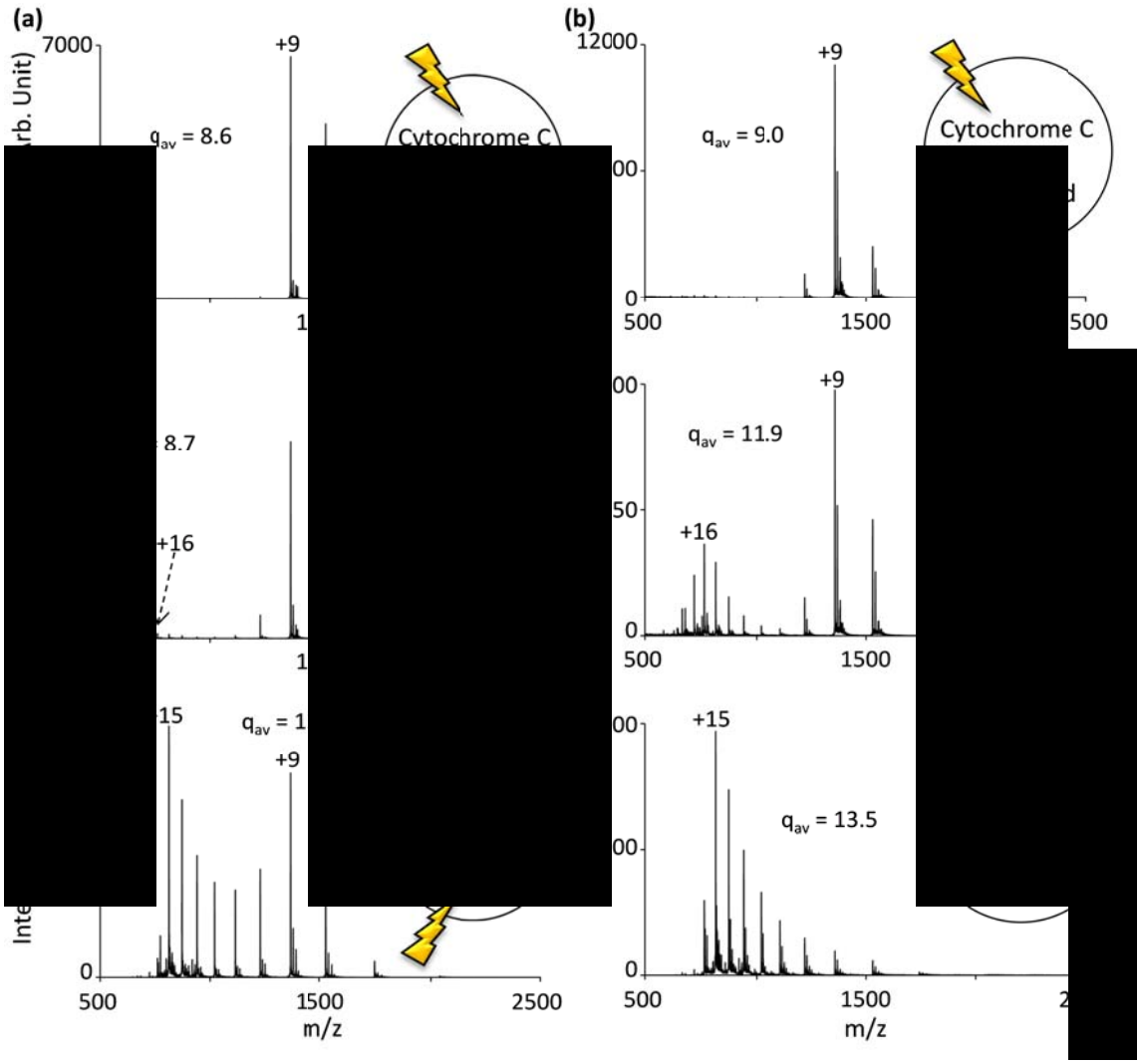

Figure 2.3 Cytochrome *c* sprayed opposite (a) 1%, (c) 5%, and (e) 100% acetic acid from a theta tip. Cytochrome *c* was mixed in solution with (b) 0.5%, pH 2.9; (d) 2.5%, pH 2.4; and (f) 50%, pH 0.8) acetic acid and sprayed from a regular tip for comparison.

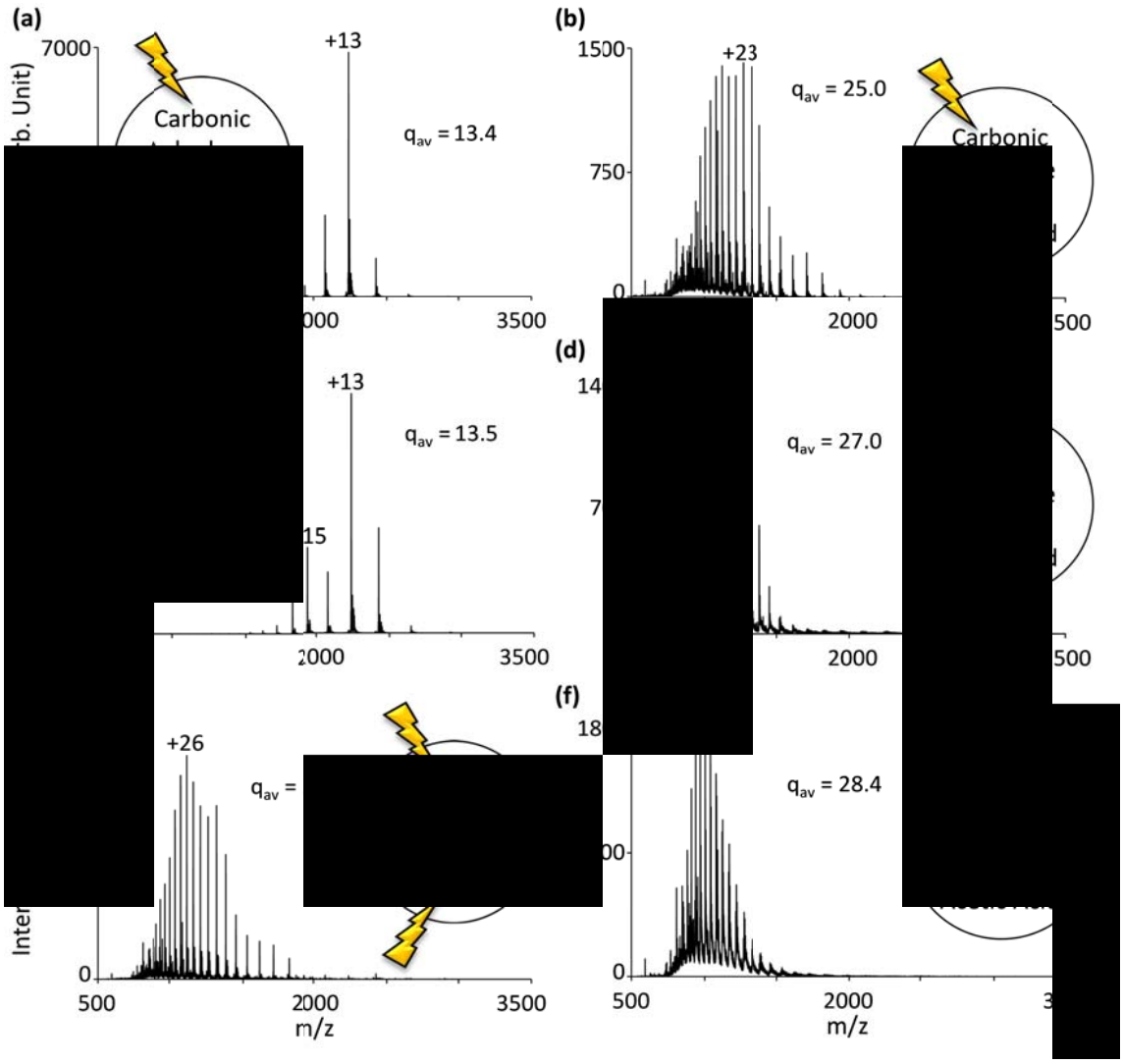

Figure 2.4 Carbonic anhydrase was sprayed opposite (a) 1%, (c) 10%, and (e) 100% acetic acid from a theta tip. For comparison, carbonic anhydrase was mixed in solution with (b) 0.5%, pH 2.9; (d) 5%, pH 2.2; and (f) 50%, pH 0.8 acetic acid and sprayed from a regular tip.

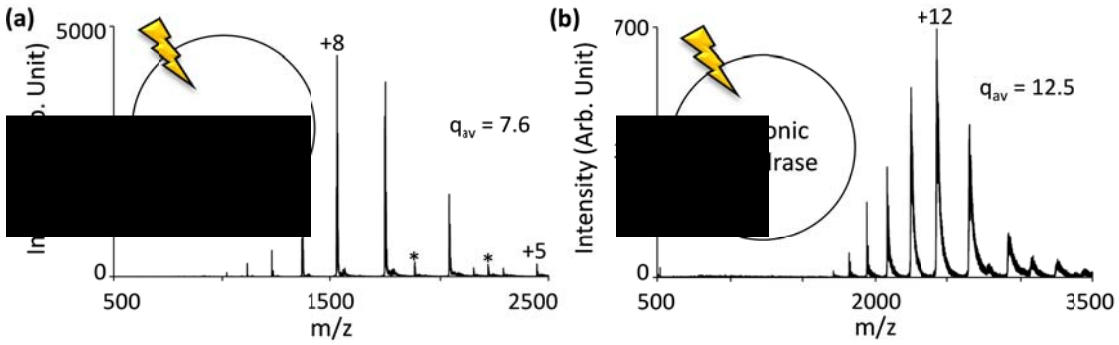

Figure 2.5 Control spectra of cytochrome c (a) and carbonic anhydrase (b) sprayed out of water from a single-barreled capillary tip.

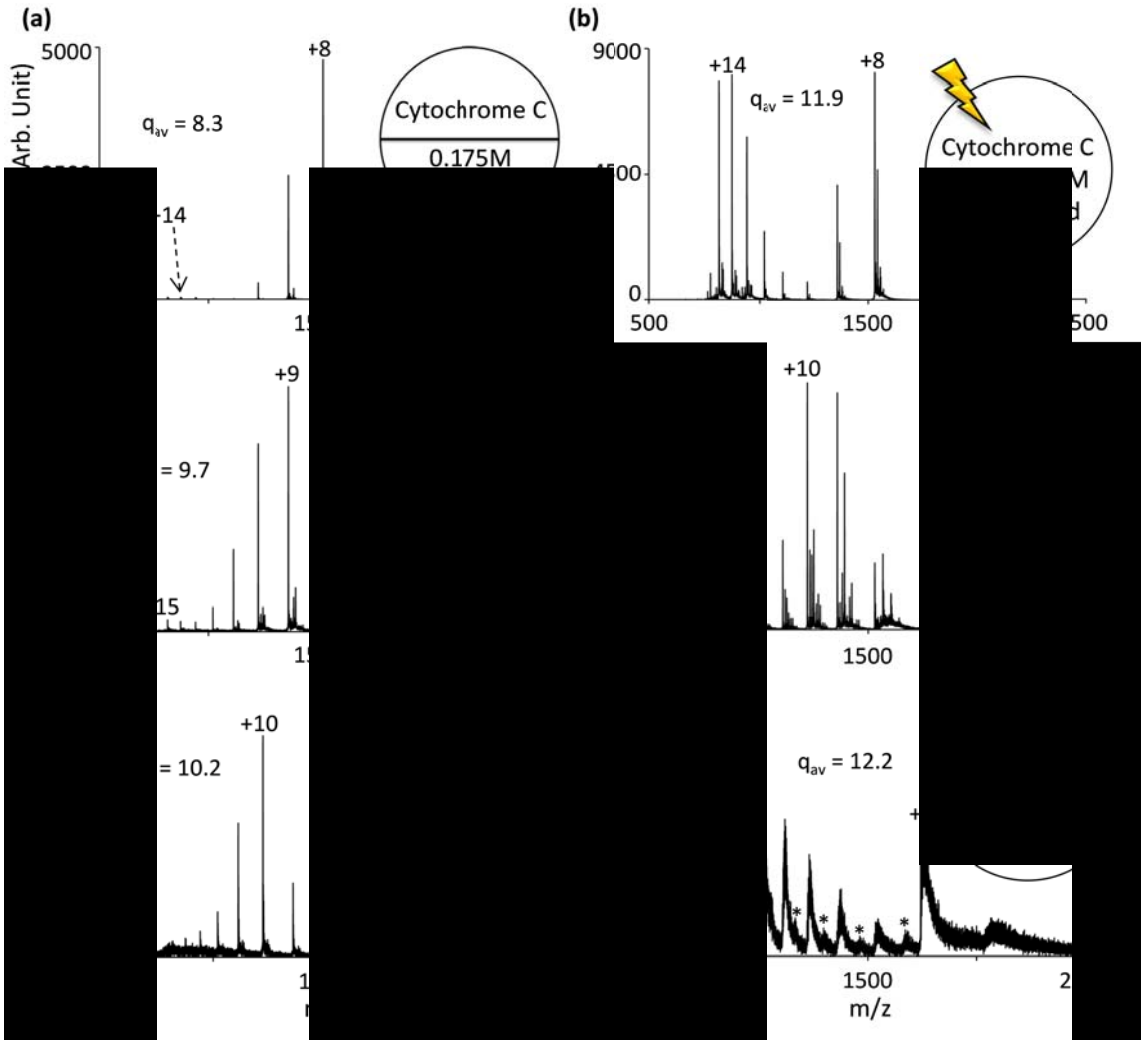

Figure 2.6 Cytochrome *c* sprayed opposite (a) 0.175M formic acid, (c) 4.4mM oxalic acid, and (e) 0.175M HCl in the theta tips. Cytochrome *c* was also mixed in solution with (b) 0.0875M formic acid, pH 2.3; (d) 2.2mM oxalic acid, pH 2.6; and (f) 0.0875M HCl, pH 1.0 and sprayed from a regular tip. The (*) indicates cytochrome *c* dimer charge states.

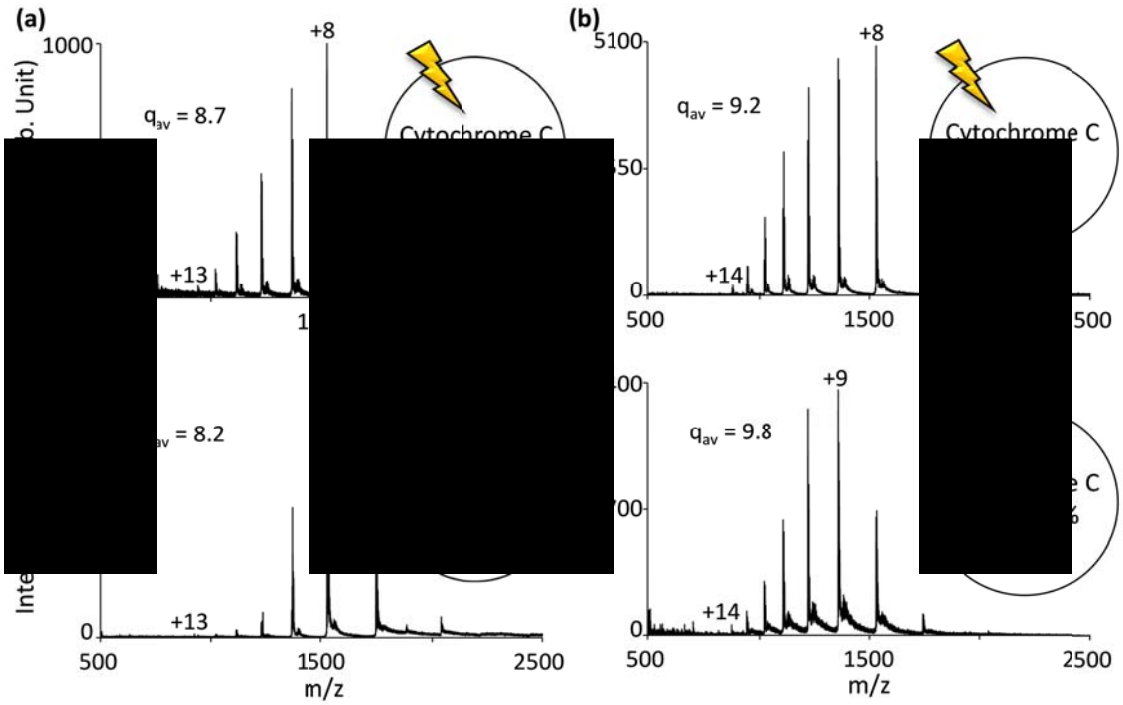

Figure 2.7 Cytochrome *c* sprayed opposite (a) 1% sulfolane and (c) 0.5% *m*-NBA in a theta tip. Solution mixtures of cytochrome *c* with (b) 0.5% sulfolane and (d) 0.25% *m*-NBA were sprayed from regular tips for comparison.

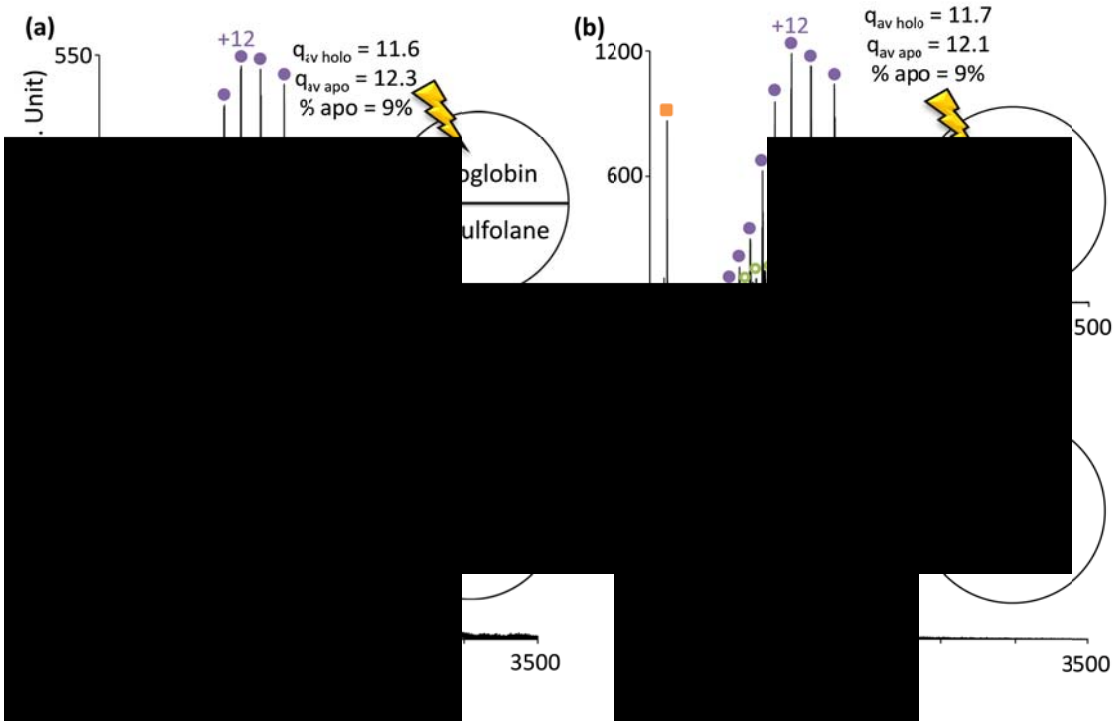

Figure 2.8 Myoglobin sprayed opposite (a) 1% sulfolane and (c) 0.5% *m*-NBA in a theta tip. Solution mixtures of myoglobin with (b) 0.5% sulfolane and (d) 0.25% *m*-NBA were sprayed from regular tips for comparison.

CHAPTER 3. ELECTROOSMOTICALLY-CONTROLLED SOLUTION MIXING IN BOROSILICATE THETA GLASS NESI EMITTERS

3.1 Introduction

Mass spectrometry is a useful tool for studying varieties of organic, inorganic, and biological molecules. Particularly with the development of electrospray ionization (ESI),[1,2] the analysis of large biomolecules has become possible due to the generation of multiply charged analyte ions that fall into a mass-to-charge (*m/z*) range that is accessible by a wide variety of mass analyzers. The advent of nano-ESI (nESI) has further improved this technique with its improved ionization efficiency and the requirement for lower sample volumes and analyte concentrations.[3,4] Mass spectrometry is also attractive as an analytical tool due to its speed, linear dynamic range, and high specificity via accurate mass measurement. These figures of merit have motivated the application of mass spectrometry to various fields including the study of reaction mechanisms, intermediates, products, and kinetics in the solution-phase and in the gas-phase.[5,6,7] In order to study reaction products, intermediates, and kinetics in solution on short timescales, such as the microseconds to seconds timescale, using ESI-MS, there must be means for mixing reactants just prior to entering the mass spectrometer.

There are a variety of techniques that can be used to mix reactants in line with a mass spectrometer. For example, there are vapor introduction techniques that result in the interaction of analytes in electrospray droplets with gaseous reactants in the atmosphere/vacuum interface of mass spectrometers. The vapors are introduced with countercurrent[8] or nebulizing gas flows,[9] or via evaporation from a vial placed outside the orifice of the mass spectrometer.[10] These techniques have been used for protein unfolding and refolding,[9,11,12,13] hydrogen/deuterium exchange (HDX),[10,14,15,16] and salt reduction on biomolecules.[8,17] While these results enable the study of reactions that occur on the sub-millisecond timescale, they are limited to volatile reagents and can provide only a limited range of reaction times (i.e. limited to the lifetime of the droplet within the interface of the mass spectrometer).

In addition to vapor introduction techniques, reactants can be mixed just prior to the mass spectrometer in the droplet and solution phases. For example, fused droplet ESI (FD-ESI) and extractive electrospray ionization (EESI) have been used to mix reagent and analyte droplets in front of the mass spectrometer.[18] FD-ESI has been used to improve biomolecule detection by circumventing interferences caused by high salt, buffer, or detergent concentrations[19,20] and EESI has been used to minimize sample preparation for the analysis of complex mixtures.[21,22] Reactive desorption electrospray ionization (rDESI) has also been used to mix an electrospray droplet with an analyte deposited on a surface in front of the mass spectrometer. This technique has been used for many applications to enhance the ionization efficiency and selectivity of analytes in complex mixtures without sample preparation.[23,24] While these techniques do not

necessarily require volatile reagents, the reaction times are limited to the droplet lifetime.

Stopped-flow techniques have the capability to analyze reactions with non-volatile reagents while providing flexibility in analyzing reactions on various, well-controlled timescales, enabling solution phase kinetic studies by mass spectrometry.[25] These techniques often involve a Y-shaped capillary system in which two solutions are individually pumped through separate capillaries into a junction where the two solutions flow together into a single capillary. The length of the single capillary containing the mixed solutions can be varied to sample the reaction at various time-points given a known solution flow rate.[26] Stopped-flow solution mixing techniques have proven useful for measuring reaction kinetics of various reactions including protein unfolding and refolding[25, 27, 28] as well as enzyme catalyzed reaction kinetics and intermediates[29,30,31] when coupled to mass spectrometry. One study combined a stopped-flow mixer with a DESI experiment, which provided a method for resolving reaction kinetics down to the sub-millisecond timescale.[32]

One of the main concerns with stopped-flow techniques involves solution mixing at the junction of the two solutions. Simply joining the flows at a junction point often results in poor mixing, depending on the turbulence of the solutions at the junction point. Without turbulence, the mixing of the two solutions is often dependent upon lateral diffusion, which is relatively slow for channels with diameters on the order of or greater than 10s to 100s of micrometers.[33] Various “mixers” have been developed to provide more turbulent mixing of the two solutions. One mixer developed by He and

Reginier *et al.* utilizes a system of intersecting channels with diameters ranging from 5 to 30 μm to improve the mixing of two solutions in a microfluidic stopped flow device.[34] While mixers can decrease the mixing timescale from seconds to milliseconds, the complex fabrication process may make them more expensive to purchase commercially and/or are more difficult for individuals to fabricate themselves. Additionally, coupling microfluidic stopped-flow devices to mass spectrometers can be challenging due to the necessity of matching flow rates from the mixing device to the duty cycle of the mass spectrometer to minimize sample loss.[35]

Recently, borosilicate theta capillaries have been used as nESI emitters to rapidly mix analyte solutions on the sub-millisecond timescale.[36,37,38,39] The theta capillaries are similar to the single-barreled capillaries often used for nESI; however, they contain a borosilicate septum that runs the length of the tube, dividing it into two individual channels. The capillaries can be pulled to a tip using a conventional tip puller and the septum has been shown to extend to the end of the tip.[36] Individual solutions can be loaded into the separate channels where they remain isolated up to the very end of the tip. Ionization of the solutions was originally shown by coating the tips with a conductive material, which was held at ground while an attractive potential was applied to the interface of the mass spectrometer.[36] More recently, ionization has been achieved by applying a voltage to the solution via a single wire placed in one channel of the capillary at a time[37] or using a dual emitter which applies a potential to two wires that are each placed into one of the channels simultaneously.[37,38,39]

The use of theta tips for the rapid mixing of analyte solutions is attractive because they are compatible with non-volatile reagents and are relatively simple to use, requiring no instrument modifications. Since they can be pulled using the same commercially available tip pullers that are used to generate nESI tips from single-barreled borosilicate capillaries, they are easily accessible. The utility of sub-millisecond timescale mixing using theta tips has been demonstrated in studies of protein unfolding[37,39] and refolding,[39] HDX,[36] supercharging,[37] and complex formation on the sub-millisecond timescale.[36,38] While it has been speculated that the tip diameter and the tip-orifice distance can be varied to access various reaction times,[38,39] these experiments are hindered by ion signal losses and decreased ionization efficiencies at non-optimal conditions. A new method for controlling the mixing/reaction time of two solutions just prior to introduction into a mass spectrometer is described using electroosmotic solution flow in theta glass nESI emitters.

3.2 Experimental

3.2.1 Chemicals

Myoglobin from equine skeletal muscle, hexadimethrine bromide (polybrene) and sulforhodamine B (acid form, laser grade, dye content 95%) were purchased from Sigma Aldrich (ST. Louis, MO). Rhodamine 610 chloride (rhodamine B) was purchased from Exciton (Dayton, OH). Glacial acetic acid was purchased from Malinckrodt Chemicals (Phillipsburg, NJ). All solutions were prepared using water purified by a Barnstead

nanopure infinity ultrapure water system (Thermo Fisher Scientific, Waltham, MA) at 15 MΩ. All proteins and other chemicals were used without further purification. Aqueous stock solutions of myoglobin were diluted to a final concentration of 5-20 µM in water. Aqueous stock solutions of Rhodamine B and sulforhodamine B were each diluted to a final concentration of ~90 µM. The aqueous polybrene solution was diluted to a final concentration of 5% w/v. The aqueous polybrene and rhodamine B solution mixture was diluted to a final concentration of 5% w/v polybrene and 90 µM rhodamine B.

3.2.2 Capillaries and Holder for nESI

Single-barreled borosilicate capillaries (1.50 mm O.D., 0.86 mm I.D., 10 cm length) and borosilicate theta glass capillaries (1.17 mm I.D., 10 cm length) were purchased from Sutter Instrument Co. (Novato, CA). The theta capillaries are very similar to the single-barreled capillaries except that they contain a 0.165 mm thick glass septum that runs the length of the capillary, dividing it into two channels. A Flaming/Brown micropipette puller from Sutter Instrument Co. (Novato, CA) was used to pull both the single-barreled and theta capillaries to tips with an O.D. of about 5-10 µm. The two solutions were loaded into each channel of the theta tip individually using Seque\Pro pipette tips from Bio-Rad Laboratories (Hercules, CA).

A theta glass holder containing two polytetrafluoroethylene (PTFE)-coated silver wire electrodes was purchased from Warner Instruments, LLC (Hamden, CT). The silver wires were removed from the holder to avoid silver redox reactions and replaced with PTFE insulated platinum wire with a 125 µm bare diameter and 200 µm coated diameter

(ADInstruments, Colorado Springs, CO). Each wire was inserted into the separate channels of the theta tip where they were in contact with the solutions previously loaded into each side. The wires were cut to an appropriate length such that they extend as far toward the end of the tip as possible.

3.2.3 Fluorescence Microscopy

An Olympus BX-51 optical microscope (Center Valley, PA) was used with a mercury excitation lamp for fluorescence excitation. An excitation filter was used to excite rhodamine B and sulforhodamine B solutions at wavelengths of 510-550 nm. An emission filter was used to detect rhodamine B and sulforhodamine B fluorescence at 590 nm. The microscope was also equipped with an Olympus DP71 camera (Center Valley, PA) which was used to record fluorescent images and videos. High voltage power supplies from ORTEC (model 556, Oak Ridge, TN) were used to supply voltages to the individual wires.

3.2.4 Mass Spectrometry

All mass spectra were collected using a QqTOF tandem mass spectrometer (Q-Star Pulsar XL, AB Sciex, Concord, ON, Canada), previously modified to allow for ion trap collision induced dissociation (CID) and ion/ion reactions; [40] although, these modifications were not utilized for the experiments described here. The potentials applied to the wire electrodes were supplied by the instrument supply (controlled by the Q-Star software) as well as additional high-voltage ORTEC power supplies. The

power supplies were fed into a high-voltage switchbox developed in house by the Jonathan Amy Facility for Chemical Instrumentation (JAFCI) at Purdue. A TTL trigger provided in the instrument software was used to trigger the switch box during the electroosmosis step of the scan function. These supplies were sufficient for performing the one-way electroosmosis experiments (Figure 3.1a). In order to generate and trigger the square wave used for the square wave electroosmosis experiments (Figure 3.1b), an additional TTL trigger from the instrument software was used to initiate a waveform generator (Agilent 33220A, Santa Clara, CA) which provided a square wave trigger to a DEI pulser (Directed Energy, Inc., PVX-4140, Fort Collins, CO). A potential versus time diagram showing the voltages applied to each wire electrode during a typical scan function for one-way electroosmosis and square wave electroosmosis experiments are depicted in Figure 3.1a and b, respectively. The relative voltages applied to each electrode are differentiated by the purple solid line and the orange dotted line. The wait step was not used for the square wave electroosmosis step, indicated by the gray box in Figure 3.1b. The ionization step is relatively short such that only ions from the mixed volume are sampled. The dump spray step is used to provide extra time to remove solution volume from the tip without collecting the ions that are generated (the low mass cut off in Q1 is set low to keep the ions from being transmitted to Q2 where the ions generated during the ionization step are stored) such that overall a larger volume of solution is sprayed from the tip than is mixed during the electroosmosis step. This ensures there will be no carry-over of mixed volume between subsequent scans and experiments. The mixed volume is determined by the electroosmosis flow rate as well as

the duration of the electroosmosis step. The flow rate of electroosmosis for the myoglobin and 1% acetic acid system, for example, was found to be roughly twice that of the spray flow rate when the voltage difference between the two wires was 200 V and the spray potential was +1.0-1.5 kV. The length of the dump spray step was made sufficiently long to remove all mixed solution by confirming that a subsequent experiment without electroosmosis yielded the original non-mixed mass spectrum.

3.3 Results and Discussion

3.3.1 Mixing Solutions in Theta Tips Using Electroosmosis

Electroosmosis is the process by which bulk solution flow is generated in glass capillaries or channels. It is caused by the negatively charged silicate groups on the surface of the capillary that give rise to the formation of an electrical bilayer in which positive ions in solution are attracted to the oppositely charged capillary surface. The formation of this bilayer results in electroosmotic flow of the bulk solution from the more positive terminal toward the more negative terminal. Electroosmosis can be used to move solution from one side of a theta tip to the opposite side of the theta tip by applying different voltages to the wire electrodes in contact with the solution in each side of the tip. To demonstrate this phenomenon, rhodamine B was used to monitor bulk solution flow in a theta tip. A theta tip was loaded with water in one side and with an aqueous solution of rhodamine B in the opposite side of the tip (Figure 3.2). Most of the rhodamine B in a solution of pH 6-7 exists as a zwitterion that is net neutral, thus

this dye can be used to trace the flow of the bulk solution due to electroosmosis (as a neutral it will not have electrophoretic mobility). Electroosmosis was effected by applying +300 V to the water side of the theta tip and +500 V to the opposite side containing the rhodamine B solution. A fluorescent microscope was used to monitor the location of the rhodamine B dye during electroosmosis, which indicates the flow of bulk solution from one side to another. Images were taken prior to electroosmosis (Figure 3.2a) and after 10 s (Figure 3.2b) and after 30 s (Figure 3.2c) of applying the voltages for electroosmosis. Figure 3.2a shows that rhodamine B fluorescence (bright orange/yellow color) is detected only in the right side of the theta tip prior to applying voltages. The red color in the left side of the tip is attributed to light reflections off the glass capillary. Upon applying a voltage difference of 200 V between the two wire electrodes, the bulk solution flows from the right side of the tip, which is held at the higher positive voltage, toward the left side of the tip, which is held at the lower positive voltage (Figure 3.2b, and c). The direction of solution flow is consistent with electroosmotic flow.

As mentioned above, the rhodamine B dye is mostly net neutral under the pH conditions used for the experiment (pH 6-7) and thus will be carried with the bulk solution flow. However, analytes that have a net charge in solution will have both electroosmotic and electrophoretic mobilities in the electric field, thus their observed motions are a combination of their electrophoretic and electroosmotic mobilities. For example, positively charged analytes will flow from the more positive terminal to the more negative terminal due to their electrophoretic mobility, which is the same direction of the bulk solution flow, thus their total velocity will be greater than the

electroosmotic velocity of the bulk solution. Conversely, negatively charged analytes will have electrophoretic mobilities in the opposite direction of the bulk solution flow (i.e. from the more negative terminal toward the more positive terminal). Depending on experimental variables (i.e. electrolyte strength, voltage gradient, solution pH, analyte charge, etc.) the electroosmotic mobility may be greater than the electrophoretic mobility. Thus, negatively charged ions will still travel in the same direction as the bulk solution, although at a lower velocity than the electroosmotic flow.

To demonstrate the competition between electrophoretic and electroosmotic mobilites of a charged analyte, sulforhodamine B, a net singly negatively charged dye in solution at a pH of 6-7, was used as a tracer dye (Figure 3.3). Similar to the experiment shown in Figure 3.2, a theta tip was loaded with water in the left side of the capillary and an aqueous solution of sulforhodamine B in the right side of the capillary. The fluorescent image in Figure 3.3a shows that fluorescence from the sulforhodamine B is only observed in the right side of the tip (bright orange/yellow color) prior to applying voltages to the wire electrodes. A +500 V potential was applied to the wire inserted in the water side (left), while a +300 V potential was applied to the wire inserted in the aqueous sulforhodamine B solution (right). Fluorescent images were taken after 10 s (Figure 3.3b) and after 30 s (Figure 3.3c) of applying the respective voltages to the wires. Electroosmotic flow of solution from the more positive terminal (water at +500 V, left) to the more negative terminal (aqueous sulforhodamine B at +300 V, right) is observed as indicated by the absence of fluorescence in the right side of the tip. If the electrophoretic velocity of the negatively charged dye was greater than the

electroosmotic velocity, then the fluorescent tracer dye would have been expected to move from the right side (+300 V) toward the left side (+500 V) of the tip. This result indicates that under these experimental conditions (~760 V/cm, pH 6-7) the electroosmotic flow velocity of the bulk solution is greater than the electrophoretic velocity of the sulforhodamine B analyte.

The polarity of the electrical bilayer that is responsible for electroosmotic flow can be reversed by coating a positively charged surfactant or polymer on the surface of the capillary. Reversing the polarity of the bilayer results in a reversed electroosmotic flow direction (i.e. from the more negative terminal to the more positive terminal). A common capillary coating or solution additive for this effect is polybrene (hexadimethrine bromide), a polymer containing positively charged quaternary ammoniums.[41,42] Polybrene was used to demonstrate reversed electroosmotic flow in the theta tips by adding it into water and into an aqueous solution of rhodamine B which were individually loaded into the left and right side of a theta tip, respectively (Figure 3.4a). As shown in Figure 3.4a, the rhodamine B is only present in the right side of the theta tip (red color) before applying voltages to the wires in the tip. A +500 V potential was applied to the wire in the aqueous polybrene solution (left), while a +300 V potential was applied to the wire in the aqueous polybrene and rhodamine B solution (right) and a video of the electroosmotic flow in real time was recorded (Video S-1). Images after 10 s and after 30 s of electroosmosis are provided in Figure 3.4b and c, respectively. The neutral dye is indicative of the flow of the bulk solution which moves

from the right side of the tip (+300 V) to the left side of the tip (+500 V), which is consistent with reversed electroosmotic flow.

3.3.2 Controlling Acid Denaturation of Myoglobin with Electroosmosis

The fluorescent tracer dye experiments are consistent with electroosmotic flow of solution from a more positive potential to a less positive potential (or the reversed direction with polybrene), resulting in the movement of solution from one side of a theta tip to the opposite side. This phenomenon can be exploited to provide a method for controlling the mixing times of solutions loaded into individual channels of a theta tip just prior to analysis by mass spectrometry. This experiment is carried out using a scan function similar to that shown in Figure 3.1a, in which the first step triggers the different voltages (ΔV = 100 V to 300 V) on the two wire electrodes followed by a 'wait' step in which both wire electrodes are held at the same potential that is lower than that required for a spray (i.e. 0 V to +500 V). The ionization step raises the voltage on both wires to a voltage sufficient for spray (i.e. +1 kV to +1.5 kV). One of the variables that affect the electroosmotic flow rate is the voltage gradient between the two electrodes, which is controlled by varying the voltage difference between the two wires in the theta tips. A larger ΔV is expected to result in the transfer of a larger volume from one side of the tip to the other (given a fixed time).

The acid denaturation of myoglobin was chosen as a system to demonstrate the use of electroosmosis to vary solution mixing and reaction time in the theta tips just prior to mass analysis. Myoglobin is a ~17.6 kDa protein with a tertiary structure

stabilized by hydrogen bonding and a heme group, which forms a non-covalent interaction with a proximal histidine within a hydrophobic pocket.[43] The acid-induced unfolding of holomyoglobin has been found to proceed first with the unfolding of holomyoglobin (containing the heme) followed by loss of the heme group to generate apomyoglobin. In addition, it is well established that more denatured/unfolded proteins exhibit higher charge state distributions (CSDs), while more native-like forms of proteins tend to appear at lower charge states due to Coulombic repulsion.[44,45,46] Thus, the denaturation of myoglobin is indicated by both a higher CSD as well as a mass shift equivalent to the loss of the heme group. The lifetime of the unfolded holomyoglobin intermediate has been found to be ~380 ms using time-resolved ESI-MS,[26] and has previously been observed by spraying myoglobin opposite acetic acid in theta tips.[37] Thus, the acid-induced unfolding of myoglobin is a good system for demonstrating the utility of electroosmosis in the theta tips on the millisecond timescale. When myoglobin is dissolved in water at a neutral pH (6-7) and is sprayed from a regular tip, the noncovalent myoglobin-heme complex can be preserved during the electrospray process.[47,48,49] This result is reproduced in Figure 3.5f. Myoglobin unfolds on the millisecond timescale and is very sensitive to acid concentration. Adding even a small concentration of acid (e.g. 0.5% acetic acid) to myoglobin in solution results in unfolding and loss of heme from the complex at equilibrium, as shown in Figure 3.5d. As previously described, the mixing of solutions sprayed from opposite sides of a theta tip occurs in the Taylor cone and subsequent droplets on the sub-millisecond timescale, which is shorter than the lifetime of the unfolded holomyoglobin intermediate.

Therefore, spraying myoglobin opposite 1% acetic acid (Figure 3.5b) results in less denaturation of myoglobin compared to mixing myoglobin and acid in solution (Figure 3.5d), as evidenced by the presence of only 3.1% apomyoglobin signal vs. 100% apomyoglobin signal relative to holomyoglobin signal, respectively.

Electroosmosis can be used to control the amount of mixing of myoglobin and 1% acetic acid solutions and thus can be used to control the extent of myoglobin denaturation (as indicated by the percentage of apomyoglobin relative to holomyoglobin signal in the spectrum) by varying the voltage gradient (i.e. the voltage difference, ΔV) between the two wire electrodes or by varying the duration of the electroosmosis step in the scan function. Figure 3.5 shows the utility of varying the ΔV between the wire electrodes in the theta tips during the electroosmosis step to control the amount of myoglobin denaturation on the millisecond timescale just prior to mass analysis (Figure 3.5a, c, and e). The duration of the electroosmosis and wait steps were kept constant at 50 ms each, while the voltage difference between the wires was varied between 100 V (Figure 3.5a), 200 V (Figure 3.5c), and 300 V (Figure 3.5e). In each of these spectra, the wire in the myoglobin side was held at +500 V during the electroosmosis and wait steps. The potential on the wire in the 1% acetic acid side was decreased to +400 V, +300 V, or +200V (Figure 3.5a, c, and e, respectively) during the electroosmosis step. In all cases, both wires were held at +500 V during the wait step such that there would be no volume transfer from one side of the tip to the other but that the voltage would be sufficiently lower than that necessary to initiate a stable nESI spray.

The total mixing volume can be varied by changing the voltage gradient between the two wires as shown in Figure 3.5, or by varying the duration of the electroosmosis step in the scan function shown in Figure 3.1. Figure 3.6a and c show the effect of varying the duration of the electroosmosis step on the amount of apo- vs. holomyoglobin present in the spectrum. To demonstrate the flexibility of voltages that can be used, both Figure 3.6a and c were taken with 0 V applied to the wire in the myoglobin solution and -100 V applied to the wire in the acetic acid solution during the electroosmosis step (ΔV = 100 V). A ~63% increase in apomyoglobin signal was observed when the duration of the electroosmosis step was increased from 50 ms (Figure 3.6a) to 100 ms (Figure 3.6c).

Unlike varying the voltage difference between the two wires (Figure 3.5), which effectively changes the volume of solution moved from one side of the tip to the other independent of time, varying the duration of the electroosmosis step (Figure 3.6a and c) changes both the volume of solution that is moved as well as the timescale for the interaction between the two solutions. The wait step was originally incorporated into the scan function to test the effect of interaction time independently of the volume of solution mixed. However, varying the wait time does not appreciably change the ratio of apo- and holomyoglobin observed in the spectrum when compared to the same experiment without a wait step. The millisecond timescale used for the wait step should be sufficient to result in an increase in the amount of apomyoglobin observed in the spectrum based on the lifetime of the unfolded holomyoglobin intermediate (i.e., 380 ms).[26] However, this assumes turbulent or complete mixing of the two solutions. If

electroosmotic flow of solution from one side of the tip to the opposite side of the theta tip is not turbulent, then incomplete mixing would be expected and the additional mixing/reaction occurring during the wait step would be diffusion limited, which is negligible (~9-11 x 10^{-7} cm^2/s for myoglobin in water)[50] on the millisecond timescale.

We note that all electroosmosis experiments were carried out with the wire in the myoglobin side held at the higher voltage relative to the wire in the 1% acetic acid side. Experiments were attempted in which the 1% acetic acid was held at the higher voltage; however, very poor myoglobin signal was observed upon spraying the mixed solutions. This observation has been attributed to incomplete mixing of the two solutions inside the theta tip. It is well known in the capillary electrophoresis and microfluidics communities that the bulk solution profile during electroosmosis is a plug flow, which often results in diffusion limited mixing at the interface of the two solutions.[33, 51] On the millisecond timescale, diffusion is relatively slow. When electroosmosis is performed in which solution is moved from one side of a theta tip to the other (i.e. one-way electroosmosis), the resulting mass spectrum will be a mixture of the diffusion limited, partially mixed volume from one side of the theta tip and the unmixed solution from the opposite side of the theta tip. Since experiments were performed with myoglobin at the higher electroosmosis voltage, it is not surprising that the lower charge states of holomyoglobin are observed in all one-way electroosmosis spectra (Figure 3.5a, c, and e; Figure 3.6a and c), since the unmixed myoglobin side will always contribute “native” myoglobin to the mixture in the Taylor cone.

One method commonly employed in the microfluidics community to improve mixing of solutions in microchannels is to design the channels to curve and turn to introduce turbulence.[51] For example, Kane *et al.* made a microfluidic channel with a serpentine structure, which goes through a series of 180^{o} turns to improve solution mixing to study protein folding.[52] A theta tip can be viewed as two channels that run parallel to each other. Moving solution from one side of the tip to the other side is similar to moving solution through a 180^{o} bent channel. Therefore it should be possible to improve solution mixing by moving solution back and forth between the two sides of the theta tip using electroosmosis. For this experiment, electroosmosis is still effected by applying a voltage difference between the two wires inserted into the two channels; however, the wire that is held at the higher relative potential (e.g. +100 V) is then switched to an equally lower potential (e.g. -100 V) relative to the opposite emitter (e.g. 0 V). Figure 3.1b shows the relative voltages applied to each wire electrode throughout the scan function during the square wave electroosmosis experiments.

Applying a square wave to one of the wires improves the mixing of the two solutions as evidenced by Figure 3.6. The duration of the one-way electroosmosis and wait steps in Figure 3.6a (50 ms each) and Figure 3.6c (100 ms each) are equivalent to one full period of a 10 Hz (Figure 3.6b) and 5 Hz (Figure 3.6d) square wave respectively. The amount of apomyoglobin signal increased from ~36% to ~91% when solution is moved in only one direction (Figure 3.6a) compared to moving solution back and forth between the two sides once using a 10 Hz square wave (Figure 3.6b). Similarly, when comparing one-way electroosmosis (Figure 3.6c) to electroosmosis with a 5 Hz square

wave (Figure 3.6d), the amount of apomyoglobin signal relative to holomyoglobin signal increased from ~82% to ~92%. When additional cycles of the square wave were used during the electroosmosis step, very little change in the amount of apo- vs. holomyoglobin was observed (Figure 3.7). Nearly all of the myoglobin species in solution are denatured to apomyoglobin after one square wave cycle, suggesting near complete solution mixing is achieved after as little as one square wave cycle.

3.4 Conclusions

Electroosmotically-controlled solution mixing within a borosilicate theta glass nESI emitter has been demonstrated. Electroosmosis is effected by applying different voltages to the wire electrodes inserted into each channel of the theta tip. Fluorescence microscopy was used to image the flow of rhodamine B tracer dyes from one channel of the theta tip to the opposite channel of the theta tip. This was demonstrated with a neutral dye as well as a negatively charged dye. Additionally, the electroosmosis flow direction was reversed by adding a positively charged surfactant, polybrene to the analyte solutions in each side of the theta tip. The utility of electroosmotically-controlled solution mixing in the theta tips was demonstrated using acid denaturation of myoglobin as a model system. Increasing the potential difference between each wire electrode (at a fixed time) or increasing the duration of the electroosmosis step increases the volume of solution transferred from one side of the tip to the opposite side of the tip, evidenced by an increase in the amount of apomyoglobin signal relative to holomyoglobin signal observed in the mass spectrum. A limitation to this method is

that mixing relies on diffusion to some extent, which is slow on the millisecond timescale. To address this limitation, a square wave potential was applied to one of the wire electrodes during the electroosmosis step which switches between a higher and a lower potential relative to the opposite wire electrode to effectively move solution back and forth between the two sides of the theta tip. This technique appears to induce nearly complete mixing of the two solutions with only 1 cycle of the square wave. The experiments described in this chapter demonstrate that electroosmosis can be effected in borosilicate theta tips to expand the use of theta nESI emitters to the analysis of reactions occurring on the millisecond timescale, as opposed to previous studies in which interaction times were limited to the microsecond timescale.

3.5 References

[1] Yamashita, M.; Fenn, J. B. *J. Phys. Chem.*, **1984**, *88*, 4451-4459.

[2] Fenn, J. B.; Mann, M.; Meng, C. K.; Wong, S. F.; Whitehouse, C. M. *Science* **1989**, *246*, 64-71.

[3] Wilm, M. S.; Mann, M. *Int. J. Mass Spectrom.* **1994**, *136*, 167-180.

[4] Wilm, M.; Mann, M. *Anal. Chem.***1996**, *68*, 1-8.

[5] Detlef, S. *Accounts Chem. Res.* **2012**, *45*, 1521-1532.

[6] Zechel, D. L.; Konermann, L.; Withers, S. G.; Douglas, D. J. *Biochem.* **1998**, *37*, 7664-7669.

[7] Santos, L. S.; Pavam, C. H.; Almeida, W. P.; Coelho, F.; Eberlin, M. N. *Angew. Chem. Int. Edit.* **2004**, *43*, 4330-4333.

[8] Kharlamova A.; Prentice, B. M.; Huang, T.-Y.; McLuckey, S. A. *Anal. Chem.* **2010**, *82*, 7422-7429.

[9] Girod, M.; Antoine, R.; Dugourd, P.; Love, C.; Mordehai, A.; Stafford, G. *J. Am. Soc. Mass Spectrom.* **2012**, *23*, 1221-1231.

[10] Kostyukevich, Y.; Kononikhin A.; Popov, I.; Nikolaev, E. *Anal. Chem.* **2013**, *85*, 5330-5334.

[11] Kharlamova, A.; McLuckey, S. A. *Anal. Chem.* **2011**, *83*, 431-439.

[12] Kharlamova, A.; DeMuth, J. C.; McLuckey, S. A. *J. Am. Soc. Mass Spectrom.* **2011**, *23*, 88-101.

[13] Kharlamova, A.; Prentice, B. M.; Huang, T.-Y.; McLuckey, S. A. *Int. J. Mass Spectrom.* **2011**, *300*, 158-166.

[14] Kharlamova, A.; Fisher, C. M.; McLuckey, S. A. *J. Mass Spectrom.* **2014**, *49*, 437-444.

[15] Takáts, Z.; Schlosser, G.; Vékey, K. Int. J. Mass Spectrom. **2003**, *228*, 729-741.

[16] Kostyukevich, Y.; Kononikhin, A.; Popov, I.; Nikolaev, E. *J. Mass Spectrom.* **2014**, *49*, 989-994.

[17] DeMuth, J. C.; McLuckey, S. A. *Anal. Chem.* **2014**, Article ASAP (DOI: 10.1021/ac503856v).

[18] Law, W. S.; Wang, R.; Hu, B.; Berchtold, C.; Meier, L.; Chen, H.; Zenobi, R. *Anal. Chem.* **2010**, *82*, 4494-4500.

[19] Chang, D.-Y.; Lee, C.-C.; Shiea, J. *Anal. Chem.* **2002**, *74*, 2465-2469.

[20] Shieh, I.-F.; Lee, C.-Y.; Shiea, J. *J. Proteome Res.* **2005**, *4*, 606-612.

[21] Chen, H.; Venter, A.; Cooks, R. G. *Chem. Commun.* **2006**, *19*, 2042-2044.

[22] Chen, H.; Yang, S.; Wortmann, A.; Zenobi, R. *Angew. Chem.* **2007**, *119*, 7735-7738.

[23] Huang, G.; Chen, H.; Zhang, X.; Cooks, R. G.; Ouyang, Z. *Anal. Chem.* **2007**, *79*, 8327-8332.

[24] Song, Y.; Cooks, R. G. *J. Mass Spectrom.* **2007**, *42*, 1086-1092.

[25] Kolakowski, B. M.; Simmons, D. A.; Konermann, L. *Rapid Commun. Mass Spectrom.* **2000**, *14*, 772-776.

[26] Konermann, L.; Rosell, F. I.; Mauk, A. G.; Douglas, D. J. *Biochem.* **1997**, *36*, 6448-6454.

[27] Wilson, D. J.; Konermann, L. *Anal. Chem.* **2003**, *75*, 6408-6414.

[28] Sogbein, O. O.; Simmons, D. A.; Konermann, L. *J. Am. Soc. Mass Spectrom.* **2000**, *11*, 312-319.

[29] Zechel, D. L.; Konermann, L.; Withers, S. G.; Douglas, D. J. *Biochem.* **1998**, *37*, 7664-7669.

[30] Li, Zhili; Sau, A. K.; Shen, S.; Whitehouse, C.; Baasov, T.; Anderson, K. S. *J. Am. Chem. Soc.* **2003**, *125*, 9938-9939.

[31] Wilson, D. J.; Kondermann, L. *Anal. Chem.* **2004**, *76*, 2537-2543.

[32] Miao, Z.; Chen, H.; Liu, P.; Liu, Y. *Anal. Chem.* **2011**, *83*, 3994-3997.

[33] Burke, B. J.; Regnier, F. E. *Anal. Chem.* **2003**, *75*, 1786-1791.

[34] He, B.; Burke, B. J. Zhang, X.; Zhang, R.; Regnier, F. E. *Anal. Chem.* **2001**, *73*, 1942-1947.

[35] Sung, W.-C.; Makamba, H.; Chen, S.-H. *Electrophoresis.* **2005**, *26*, 1783-1791.

[36] Mark, L. P.; Gill, M. C.; Mahut, M.; Derrick, P. J. *Eur. J. Mass Spectrom.* **2012**, *18*, 439-446.

[37] Fisher, C. M.; Kharlamova, A.; McLuckey, S. A. *Anal. Chem.* **2014**, *86*, 4581-4588.

[38] Mortensen, D. N.; Williams, E. R. *Anal. Chem.* **2014**, *86*, 9315-9321.

[39] Mortensen, D. N.; Williams, E. R. *Anal. Chem.* **2014**, Articles ASAP (DOI: 10.1021/ac503981c)

[40] Xia, Y.; Chrisman, P. A.; Erickson, D. E.; Liu, J.; Liang, X.; Londry, F. A.; Yang, M. J.; McLuckey, S. A. *Anal. Chem.* **2006**, *78*, 4146-4154.

[41] Córdova, E.; Gao, J.; Whitesides, G. M. *Anal. Chem.* **1997**, *69*, 1370-1379.

[42] Znaleziona, J.; Petr, J.; Knob, R.; Maier, V.; Ševčík, J. *Chromatographia*. **2008**, *67*, S5-S12.

[43] Evans, S. V.; Brayer G. D. *J. Mol. Biol.* **1990**, *23*, 885-897.

[44] Chowdhury, S. K.; Katta, V.; Chait, B.T. *J. Am. Chem. Soc.* **1990**, *112*, 9012-9013.

[45] Kaltashov, I.A.; Eyles, S. J. *Mass Spectrom. Rev.* **2002**, *21*, 37-71.

[46] Fenn, J. B. *J. Am. Soc. Mass Spectrom.* **1993**, *4*, 524-535.

[47] Katta, V.; Chait, B. T.; *J. Am. Chem. Soc.* **1991**, *113*, 8534-8535.

[48] Li, Y.-T.; Hsich, Y.-L.; Henion, J. D. *J. Am. Soc. Mass Spectrom.* **1993**, *4*, 631-637.

[49] Loo, J. A. *Mass Spectrom. Rev.***1997**, *16*, 1-23.

[50] Tyn, M. T.; Gusek, T. W. *Biotechnol. Bioeng.* **1990**, *35*, 327-338.

[51] Stone, H. A.; Stroock, A. D.; Ajdari, A. *Annu. Rev. Fluid Mech.* **2004**, *36*, 381-411.

[52] Kane, A. S.; Hoffmann, A.; Baumgärtel, P.; Seckler, R.; Reichardt, G.; Horsley, D. A.; Schuler, B.; Bakajin, O. *Anal. Chem.* **2008**, *80*, 9534-9541.

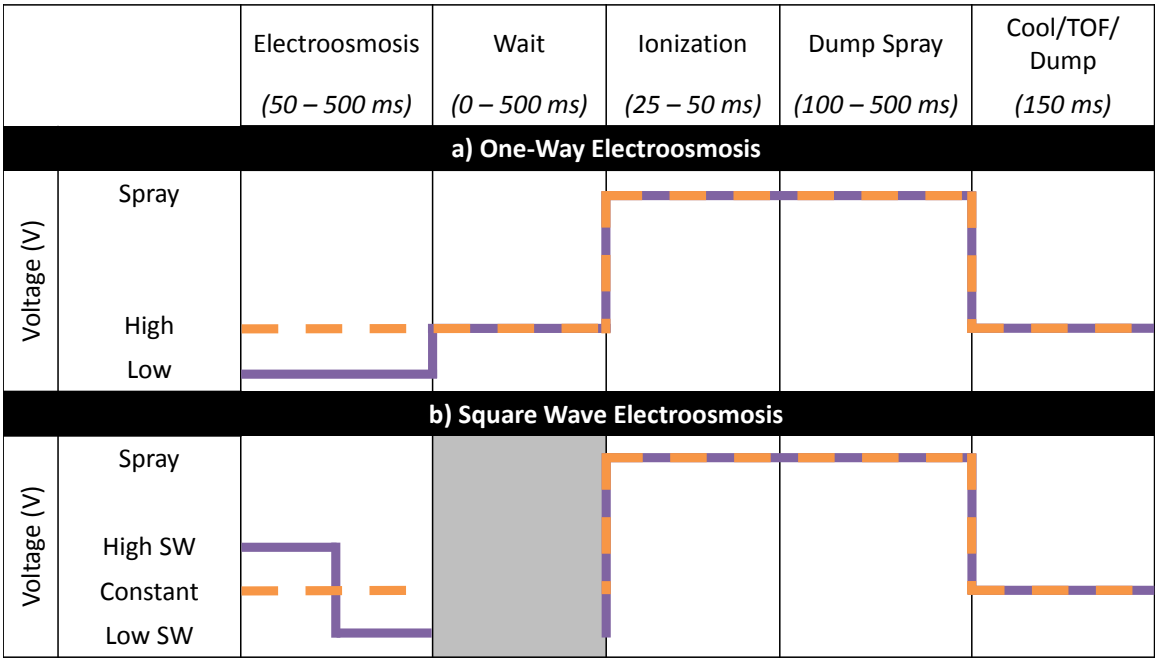

Figure 3.1 Schematic showing the relative voltages applied to each wire electrode during each step of a scan function. The orange dotted line and the purple solid line differentiate the relative voltages applied to each wire electrode individually. The wait step is included in the one-way electroosmosis experiments (a) to match the total time used in the square wave electroosmosis experiments (b) while maintaining a similar mixing volume. The wait step is not used (gray box) for the square wave electroosmosis step (b). The typical range of times used for each step is indicated in italics. High SW and low SW indicate the high and low square wave voltages, respectively.

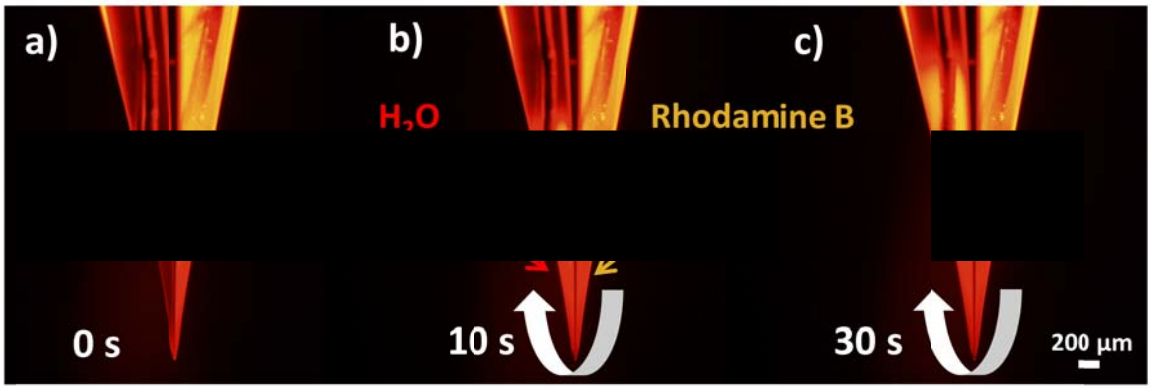

Figure 3.2 Fluorescent images of a theta tip containing water (left channel, +300 V) and an aqueous rhodamine B solution (right channel, +500 V) in opposite channels. Fluorescent images were taken prior to applying potentials to the wire electrodes (a) and after 10 s (b) and 30 s (c) of applying voltages. The curved arrows indicate the observed solution flow direction.

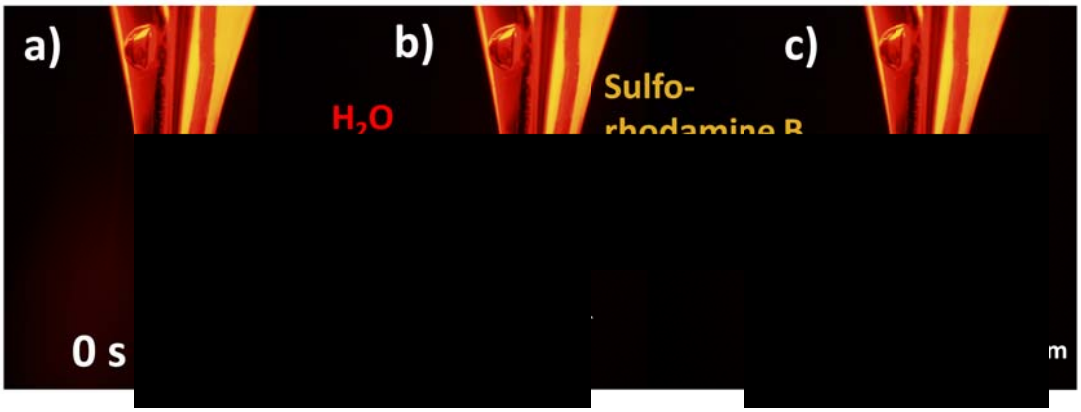

Figure 3.3 Fluorescent images of a theta tip containing water (left channel, +500 V) and an aqueous solution of sulforhodamine B (right channel, +300 V) in opposite channels. Fluorescent images were taken prior to applying potentials to the wire electrodes (a) and after 10 s (b) and 30 s (c) of applying voltages. The curved arrows indicate the observed solution flow direction.

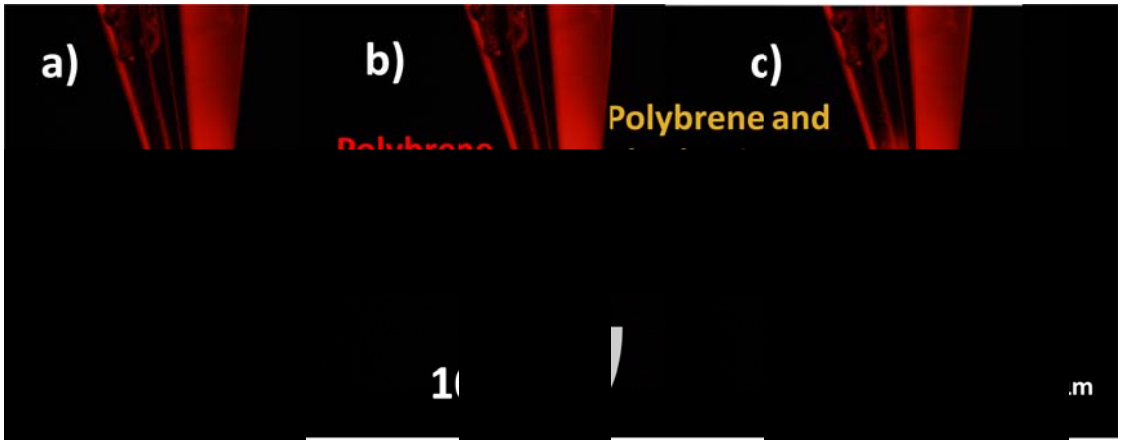

Figure 3.4 Fluorescent images of a theta tip containing an aqueous polybrene solution (left channel, +500 V) and an aqueous rhodamine B and polybrene solution (right channel, +300 V) in opposite channels. Fluorescent images were taken prior to applying potentials to the wire electrodes (a) and after 10 s (b) and 30 s (c) of applying voltages. The curved arrows indicate the observed solution flow direction.

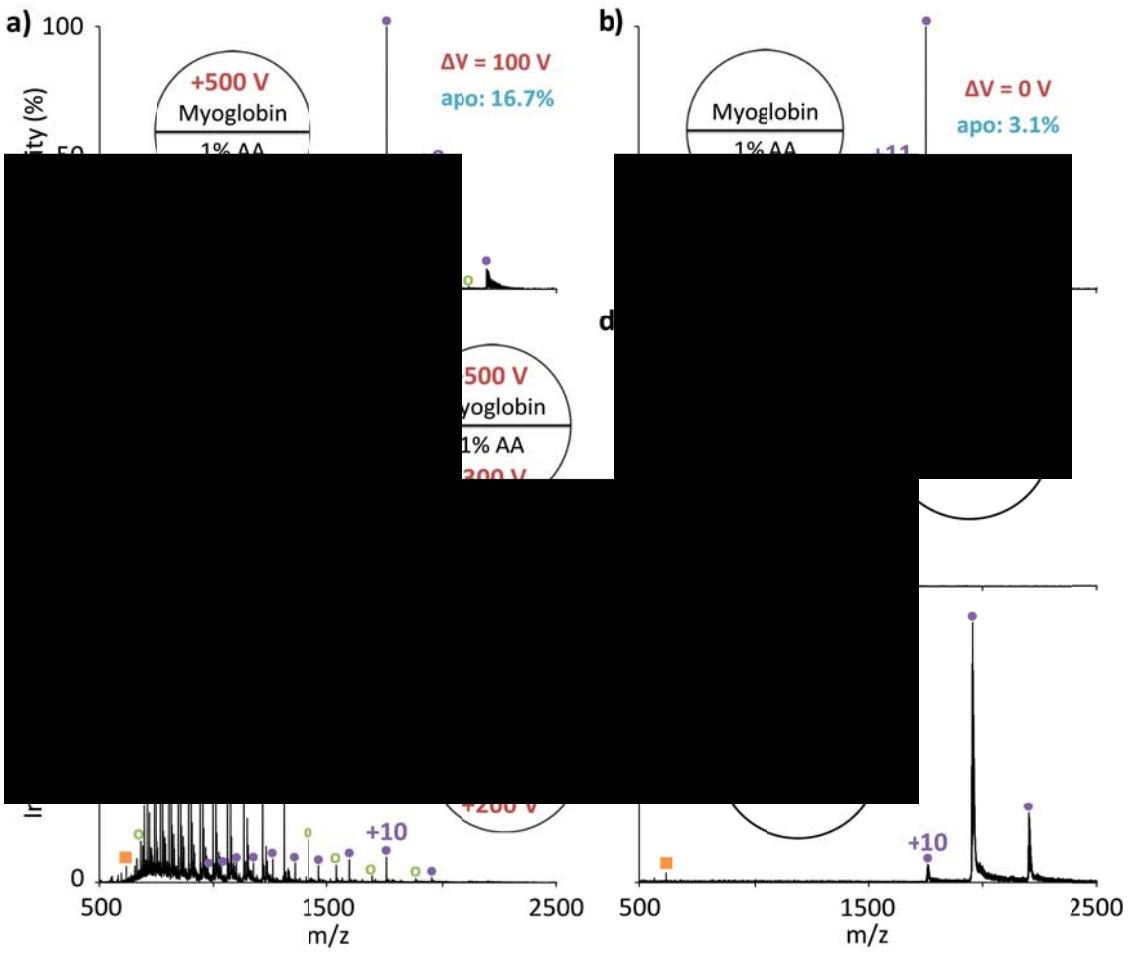

Figure 3.5 Mass spectra of myoglobin mixed with 1% acetic acid in a theta tip via electroosmosis. The wire electrode in the myoglobin side was held at +500 V during the electroosmosis step while the electrode in the 1% acetic acid (AA) side was held at +400 V (a), +300 V (c), and +200 V (e) (red text). The electroosmosis and wait steps were 50 ms each. The spectrum generated by spraying the same theta tip without electroosmosis is given in (b). The control spectra for myoglobin in water (f) and myoglobin mixed with acid in solution (d) are also given. Holomyoglobin peaks: purple filled circles (●), apomyoglobin peaks: green open circles (o), and the heme peaks: orange square (■).

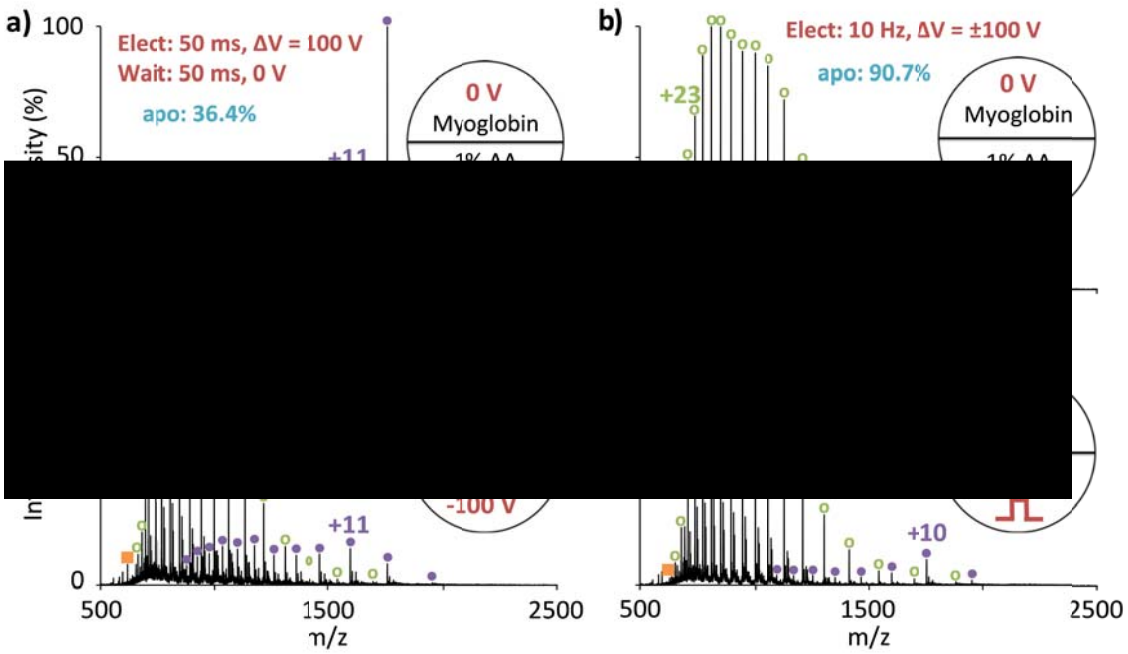

Figure 3.6 Mass spectra of myoglobin mixed with 1% acetic acid via electroosmosis in one direction (a) and (c) and with one cycle of a square wave (b) and (d). The wire electrode in the myoglobin side was held at 0 V during the electroosmosis and wait steps for all spectra. The wire electrode in the 1% acetic acid side was held at -100 V during the electroosmosis step and was switched to 0 V for the wait step of the scan function for (a) and (c). A single cycle of a square wave, oscillating between -100 V and +100 V was applied to the wire electrode in the 1% acetic acid side for (b) and (d).

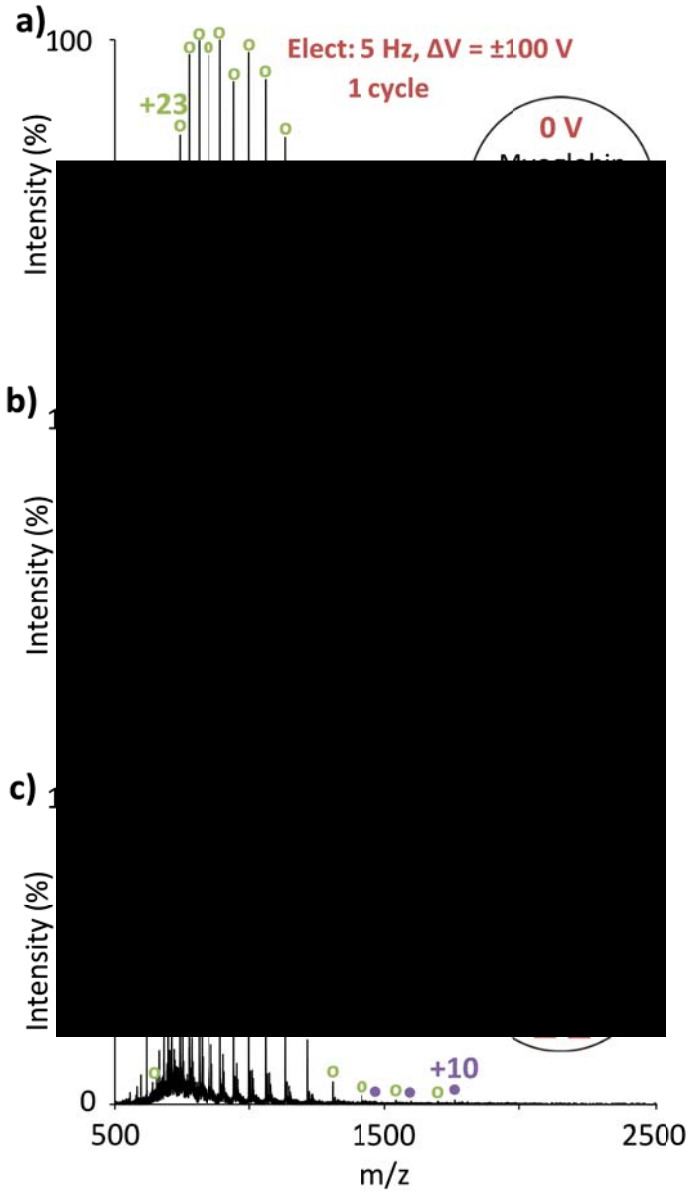

Figure 3.7 Effect of number of square wave cycles during electroosmosis on the denaturation of myoglobin. A 5 Hz square wave ranging from +100 V to -100 V was applied to the acetic acid side of the theta tip for one cycle (a), three cycles (b), and 5 cycles (c). A 0 V DC potential was applied to the myoglobin side of the theta tip during the electroosmosis step.

CHAPTER 4. EXPLORATION OF ALTERNATIVE APPLICATIONS FOR THETA CAPILLARIES AS "LAB IN A TIP" NANOELECTROSRPAY EMITTERS

4.1 Introduction

Electrospray ionization (ESI) has proven to be an immensely useful tool for the analysis of biomolecules, as the soft ionization technique preserves the structure of large molecules as they are ionized and transferred into the gas phase.[1,2] Additionally, the multiply charged ions produced by this ionization method bring the signal of large mass analytes into an *m/z* range that is accessible by many commercial mass spectrometers. Mass spectrometry has become a popular method for the analysis of a variety of biomolecules, particularly with the advent of nanoESI, which has improved ionization efficiency and requires lower sample volumes and concentrations relative to ESI.[3,4] There are numerous methods for determining the structures of biomolecules, ranging from primary to higher order structural information, using mass spectrometry. These methods often include manipulation of the ion types such that tandem mass spectrometry experiments (e.g. fragmentation) can be performed with better efficiency or to generate more complete structural information.

One of the most common methods for analyzing proteins is via enzymatic digestion or modification of the analyte in the bulk solution phase prior to ionization and mass analysis. Protein digestion is commonly used in the "Top Down" proteomic

approach (*vide* supra).[5] Proteins are often digested using various enzymes such as trypsin or pepsin, which cleave at specific residues in the protein. Protein digestions provide smaller fragments of the protein that are often easier to analyze on commercial mass spectrometers compared to the intact protein. The small fragments can be pieced back together to give primary sequence information. However, this method is often slow and missed cleavages (i.e. incomplete digestion) can complicate the resulting mass spectrum.

In addition, solution-phase modifications (to the protein or to the peptide mixture once the protein is digested) are often used to assist in determining the structure of proteins. For example, fixed charge reagents or nonpolar compounds can be added to proteins and peptides to increase their surface activity which improves ionization efficiencies via ESI.[6] There are a variety of reagents that can be used to specifically label protein side chains or the N- or C-terminus of the peptide/protein.[7,8] For example, primary amines can be modified with *N*-hydroxysuccinimide esters to label and identify the N-terminus or lysine side chains in peptides.[9] These reagents have also been used to react two primary amines in a protein with a bifunctional reagent that results in cross-linking of the two sites and provides protein tertiary structure information.[10, 11] These and other reagents can also be used to label the N- or C-terminus of a protein such that fragmentation of the precursor ion will result in a product ion spectrum in which all N- or C-terminal fragments are mass shifted according to the mass of the covalent modification[8,12,13] or to produce only one type of fragment ions (i.e. all y-type fragments).[7] Some modifications are used to alter gas-phase

fragmentation such that certain cleavages are either favored or suppressed.[14,15,16] Other examples include the conjugation of chromophores to biomolecules, which can be more selectively activated with specific wavelengths of light, or can be used to generate radical ions which provide complementary fragmentation information compared to even electron species.[17,18] While these techniques help provide diverse information for structural characterization, they all require modification of the bulk solution and analysis of reaction intermediates is often limited to intermediates with lifetimes on at least the seconds timescale. Additional equipment and/or instrument modifications are often required to analyze intermediates on the sub-second timescale (*vide infra*).

To avoid altering the bulk solution, peptide and protein ion types can also be modified in the gas-phase via ion/molecule or ion/ion reactions.[19] Both methods have been used to alter the observed analyte charge states via charged particle transfers. Recently, a variety of gas-phase covalent modifications via ion/ion reactions have been described by McLuckey *et al*.[20,21,22,23,24] Performing covalent modifications in the gas phase offers several advantages over solution-phase techniques: reaction conditions are easier to tune (i.e. relative amounts of reactant and reaction time), reaction rates are often greater due to the energy associated with the Coulombic attraction of ions of opposite polarity, and adverse solution effects can be avoided.[19] However, ion/ion reactions require more complex instrumentation, and are currently limited to reactions that do not require the presence of solvent molecules for the reaction to proceed.

Solution-phase reactions carried out on short timescales are an increasing area of investigation as technologies such as microfluidics[25,26] and stopped-flow mixers[27,28]

have been coupled with mass spectrometry. These techniques enable the study of reaction kinetics and reaction intermediates with short lifetimes (i.e. sub-seconds timescale) using mass spectrometry. A variety of reactions have been studied using these techniques, including protein folding and unfolding and enzyme catalysis.[27,29,30,31,32,33] Recently, borosilicate theta capillaries have been described as convenient nESI emitters.[34,35,36,37] These capillaries contain a glass septum that separate the barrel into two channels which can be loaded individually with different analyte solutions. As described previously, the solutions can be mixed on the sub-millisecond timescale in the Taylor cone and subsequent droplets while spraying the solutions from the tip. More recently, electroosmosis in the theta tips has been described as a method for mixing analytes on the milliseconds to seconds timescale.[38] Thus far, theta capillaries have been used to show complex formation,[34,36] hydrogen/deuterium exchange,[34] and to manipulate protein charge state distributions.[35,37]

There are a variety of other reactions that occur on short timescales such that intermediates are difficult to detect when performed in the bulk solution phase. For example, peptides and proteins often have multiple reactive sites and it may be desirable to analyze a sample with fewer modifications than reactive sites. In some cases this can be influenced by varying solution conditions (i.e. solution pH), but is usually difficult or time consuming to optimize. Controlling reaction times on the sub-millisecond to seconds time scale can provide a method for controlling the number of modifications. Theta capillaries provide a simple and inexpensive method for performing reactions on these short timescales such that the intermediates and products can be

analyzed via mass spectrometry. Additionally, mixing reagents just prior to MS analysis using theta capillaries is advantageous in that bulk solution modification is not required.

4.2 Experimental

4.2.1 Materials

Bovine serum albumin, cytochrome *c* from bovine heart and from equine heart, melittin from honey bee venom, ubiquitin from bovine erythrocytes, myoglobin from equine skeletal muscle, carbonic anhydrase from bovine erythrocytes, 4-formyl-benzene-1,3-disulfonic acid (FBDSA), propionic anhydride, trimethylamine, piperidine, sodium periodate, and sodium persulfate were purchased from Sigma Aldrich (St. Louis, MO). Glacial acetic acid and ammonium hydroxide were purchased from Malinckrodt Chemicals (Phillipsburg, NJ). Sulfosuccinimidyl acetate (Sulfo-NHS-acetate), sulfosuccinimidyl [4-iodoacetyl] aminobenzoate (Sulfo-SIAB), and *N*-succinimidyl [4-iodoacetyl] aminobenzoate (SIAB) were purchased from Thermo Scientific (Rockford, IL). The peptide ARAMAKA was custom synthesized by NeoBioLab (Woburn, MA). All analyte solutions were prepared using water purified at 15 MΩ using a Barnstead nanopure infinity ultrapure water system from Thermo Fisher Scientific (Waltham, MA). All analyte solutions were prepared without further purification. All protein solutions were diluted in water to a final concentration of 5-20 μM. The peptide solution was diluted to a final concentration of 0.1mg/mL in water with 1% (v/v) acetic acid. All acetic acid solutions were diluted to the designated concentration or percent by volume in

water. All other reagent and peptide solutions were diluted to final concentrations of 0.01-0.1 mg/mL in water.

4.2.2 Nanoelectrospray Ionization Emitters

Borosilicate theta capillaries as well as single-barreled capillaries were purchased from Sutter Instrument Co. (Novato, CA). Both capillaries are 10 cm in length. The theta capillaries have a 1.17 mm I.D., while the single-barreled capillaries have an I.D. of 0.86 mm. Both capillaries were pulled to a 5-10 µm O.D. tip using a Flaming/Brown micropipette puller from Sutter Instrument Co. (Novato, CA) equipped with a heated filament. Analyte solutions were loaded into capillaries, including individual channels of the theta tip, using Seque\Pro pipette tips from Bio-Rad Laboratories (Hercules, CA). Ionization was provided using a wire-in-a-capillary configuration with Pt wire electrodes. For the theta capillary experiments, a single wire electrode was inserted into one channel at a time or two wires were inserted into each channel of the capillary simultaneously. The placement of the wire electrode(s) for each experiment is indicated by the lightning bolt(s) in theta cartoon for each spectrum. All theta tip experiments were performed without electroosmosis (*vide supra*), such that solution mixing occurs in the Taylor cone and subsequent droplets on the sub-millisecond timescale. However, all of these reactions could be performed using electroosmosis to increase the mixing time.

4.2.3 Mass Spectrometry

All protein experiments were performed on a QqTOF tandem mass spectrometer (Q-Star Pulsar XL, AB Sciex, Concord, ON, Canada), which was previously modified for ion/ion reactions. The experiments using the peptide, ARAMAKA, were performed on a QTRAP 4000 hybrid triple quadrupole/linear ion trap mass spectrometer (AB Sciex, Concord, ON, Canada), also previously modified for ion/ion reactions. However, the modifications to allow for ion/ion reactions were not used for the experiments described here.

4.3 Results and Discussion

4.3.1 Adduct Reduction

One disadvantage of ionizing large biomolecules via ESI is adduct formation (e.g. Na^+ and K^+). Adducts result in reduced sensitivity as the analyte signal is spread over various *m/z* ratios. Larger biomolecules tend to be more extensively adducted and tend to be observed at higher charge states. As the charge states increase the adducts become separated by fewer *m/z* units such that many mass spectrometers are unable to resolve the individual adduct peaks, which complicates accurate mass measurements.

There are a variety of methods for adduct reduction, including bulk solution treatment with ion exchange resins,[39,40] bulk solution additives,[41,42] leak-in techniques,[43] and mild collisional activation to heat ions.[44] For example, volatile acids such as acetic acid and formic acid can be added to solution for positive mode analysis such that the

proton concentration in solution is increased relative to the metal cations such as Na^+ and K^+. This shifts the equilibrium toward protonated species as opposed to metal adducted species. However, adding acid into the bulk solution often results in denaturation of the protein, which may interfere with the desired experiment. Similarly, acid vapors can be introduced to the interface of the mass spectrometer to interact with electrospray droplets during the desolvation process.[43] However, the leak-in of acidic vapors also results in denaturation of the protein.[45] As described previously, acids can be sprayed opposite protein solutions from theta capillaries, which results in mixing of the acid with the protein in the Taylor cone and subsequent droplets.[35] The concentration and identity of the acid can be varied to provide more or less denaturation of the protein. Low concentrations of acetic acid (e.g. 1%), can be used to help remove cationic salts while shifting the protein charge state distribution(s) only slightly. This is demonstrated with bovine serum albumin (BSA), a ~66.4 kDa protein that is responsible for transporting various molecules including fatty acids in biological systems.[11] Figure 4.1a shows the resulting spectrum when aqueous BSA is sprayed from a single-barreled tip. The peaks are quiet broad as a variety of unresolved salt adducts are present on the high charge states. The overall signal/noise ratio is also poor due to the spread of signal for each charge state over a large *m/z* range. Adding acetic acid (0.5%) to the solution improves the signal/noise ratio and decreases the peak widths via salt adduct reduction, providing better resolution between charge states (Figure 4.1b). However, the charge state distribution is also shifted to significantly higher charge states. It is well known that higher charge states are indicative of unfolded/denatured

proteins, while more native proteins tend to have lower charge states.[46,47,48] Thus, adding acid to the solution to decrease adducts also prevents the analysis of more native structures. Mixing BSA with 1% acetic acid in the Taylor cone and subsequent droplets on the sub-millisecond timescale by spraying the two solutions from opposite channels of a theta tip results in adduct reduction with only a mild shift to higher charge states (Figure 4.1c).

4.3.2 Protein Refolding

Protein tertiary structure plays an important role in protein function. Therefore, determining the tertiary structure of proteins and understanding their unfolding and folding dynamics is important for understanding the biological function of the protein. Protein folding and unfolding can occur on timescales ranging from sub-microsecond to minutes. As described previously (*vide supra*), proteins can be unfolded on the sub-millisecond timescale by spraying the protein opposite acidic solutions from theta capillaries.[35,37] Under these conditions, short-lived intermediates can be observed (i.e. higher charge states/unfolded holomyoglobin). It is also possible to refold acid denatured proteins by spraying them opposite a buffer solution[37] or basic solutions (as described here) from a theta capillary. Figure 4.2 shows the results of spraying equine cytochrome *c,* denatured with 1% acetic acid, opposite 0.1 M trimethylamine, 0.1 M ammonium hydroxide, and 0.1 M piperidine from a theta capillary (Figure 4.2a, b, and c, respectively). Charge state reduction is observed with each base when compared with spraying the acid denatured protein from a single-barreled capillary (Figure 4.2f),

although the stronger bases (trimethylamine, pKa = 9.8; piperidine, pKa = 11.12) show a greater shift in CSD compared to the weaker base (ammonium hydroxide pKa = 9.25).[49] The shift to lower charge states obtained by spraying the denatured protein opposite the basic solutions from a theta tip is less than that observed by mixing the bases with the denatured protein in solution at equilibrium and sprayed from a single-barreled tip (Figure 4.2d and e). No protein signal was observed when 0.1M piperidine was mixed with the protein in solution and sprayed from a single-barreled tip (data not shown).

It is important to note that shifts to lower protein charge states in the refolding experiment can be caused by gas-phase ion/molecule reactions as well as protein conformational changes in solution. This is not a likely scenario for the unfolding experiment (*vide supra*) because the energy required to overcome Coulombic repulsion to increase protein charge states in the gas-phase is prohibitively high. However, the refolding experiment results in a decrease of protein charge states and the energy associated with gas-phase proton transfer from a multiply protonated protein to a gas-phase basic vapor is much more favorable. Thus gas-phase ion/molecule reactions may contribute to charge state reduction during the refolding experiment. However, multimodal charge state distributions are observed in Figure 4.2b and c and Figure 4.3a and b. If gas-phase ion/molecule proton transfer was the only process contributing to a decrease in the observed charge states, certain charge states would not be favored over others, rather, only a slight shift to lower charge states (relative to no base exposure, Figure 4.2f and Figure 4.3c, d) would be expected. Protein conformational changes however could lead to multimodal charge state distributions, corresponding to multiple

conformations in solution. Therefore, the multimodal charge state distributions indicate protein folding is occurring, although gas-phase proton transfer reactions may also contribute to a decrease in the charge states.

Protein refolding was also studied with carbonic anhydrase and myoglobin, both of which contain non-covalently bound co-factors (Figure 4.3). Carbonic anhydrase contains a zinc co-factor in its holo- form,[50] while myoglobin contains a heme group in its holo- form.[51] The sub-millisecond mixing timescale associated with spraying the solutions from a theta tip does not result in the incorporation of the co-factors into the proteins (i.e. no refolding from the apo- form to the holo- form is observed for either protein). All charge states in the carbonic anhydrase spectra (Figure 4.3a and c) are apocarbonic anhydrase peaks, although refolding of the apocarbonic anhydrase to a more compact form without the Zn co-factor is observed. There are two charge states of holomyoglobin observed when myoglobin is mixed with 0.1% acetic acid (Figure 4.3d), and upon refolding via spraying the denatured protein opposite ammonium hydroxide in the theta tip the amount of holomyoglobin relative to apomyoglobin does not increase (Figure 4.3b). However, as seen with carbonic anhydrase, refolding of apomyoglobin into a more compact structure without heme incorporation is observed.

Protein refolding into the native structure is often a slower process than protein unfolding as refolding usually consists of subsequent folding and unfolding events prior to reaching the specific native or most stable structure. Refolding apocarbonic anhydrase into holocarbonic anhydrase has been found to occur through a series of intermediates and zinc incorporation occurs during one of the initial refolding steps.[52]

However, apocarbonic anhydrase can refold into a structure similar to that of the holo-form prior to zinc incorporation, although this refolding process is slower than that observed with zinc incorporation. Refolding of apomyoglobin into holomyoglobin requires the specific binding of heme followed by a rapid collapse of the protein around the heme. However, the heme group may go through a series of non-specific binding events before the specific interaction is formed, slowing the overall rate of specific heme binding.[53] The various nonspecific interactions of the co-factors with the apoprotein slow the apo- to holo- refolding rate and likely contribute to the fact that refolded holocarbonic anhydrase and holomyoglobin are not observed on the sub-millisecond timescale associated with solution mixing via nESI from a theta tip (Figure 4.3). Protein refolding using electroosmotically-controlled solution mixing in the theta tips (*vide supra*) to provide longer reaction times is currently on ongoing area of research in the McLuckey group.

4.3.3 Complexation and Reactivity

Forming complexes between biomolecules and reactive reagents using theta capillaries is useful for manipulating ion types without modification of bulk solutions. Theta tips have previously been used to demonstrate complex formation between a peptide and vancomycin, although no reactivity was reported.[34] *N*-hydroxysuccinimide reagents are often used to modify primary amines (i.e. lysine side chains and the N-terminus) of proteins resulting in a signature loss of NHS or sulfo-NHS.[9,11] These reagents can be complexed with proteins such as bovine cytochrome *c* by spraying the

reagent and protein from opposite channels of a theta tip as is demonstrated with sulfosuccinimidyl acetate (sulfo-NHS-acetate, SNa), sulfosuccinimidyl [4-iodoacetyl] aminobenzoate (Sulfo-SIAB), and *N*-succinimidyl [4-iodoacetyl] aminobenzoate (SIAB) (Figure 4.4a, b, and c, respectively). Similarly, 4-formyl-benzene-1,3-disulfonic acid (FBDSA) has been shown to react with primary amines in biomolecules via Schiff base formation resulting in a signature loss of water.[54,55] FBDSA was also sprayed opposite cytochrome *c* from a theta tip (Figure 4.4d). A zero charge deconvolution of each spectrum is given (Figure 4.4 e, f, g, and h, respectively) to simplify the spectra such that the extent of adduction is easier to visualize. A variety of numbers of reagent adducts to the protein charge states are observed. Some reactivity is observed with sulfo-SIAB as indicated by the signature loss of sulfo-NHS from the complex mass (Figure 4.4b and f). Complex formation only (i.e. no reaction) was observed with the other three reagents. It is likely the sub-millisecond mixing timescale is too short for covalent modification to occur in addition to complex formation for most of the reagents. However, covalent modification could be driven via mild collision induced dissociation (CID) of the gas-phase complex.

Another common biomolecule modification is the acetylation of primary amines.[56] This reaction is often performed to label the N-terminus such that N-terminal fragments can be identified by the mass shift in top-down proteomics.[57] This reaction can also be performed using theta capillaries to mix acetic anhydride with a peptide or protein in the Taylor cone and subsequent droplets. Although acetylation experiments were performed (data not shown), the present data shows propionylation (using

propionic anhydride) of melittin and ubiquitin, which produces a larger mass shift upon reaction (Figure 4.5). Melittin and propionic anhydride were sprayed from opposite channels of a theta tip (Figure 4.5a). On the sub-millisecond timescale via nESI from a theta tip, fewer reactions are observed when compared to mixing melittin with propionic anhydride in solution at equilibrium (Figure 4.5b). This modification can also be performed on a protein such as ubiquitin. The spectrum produced by spraying ubiquitin opposite propionic anhydride from a theta tip is given in Figure 4.5c with the corresponding zero charge deconvolution in Figure 4.5d. Up to two propionylations are observed on the charge states of ubiquitin. Adduction of the intact propionic anhydride (without reaction) is also observed. Performing the propionylation reaction on the sub-millisecond timescale provides a spectrum that contains both the unmodified precursor as well as the covalently modified signal. It is useful to obtain both species in the same spectrum as each species can be subsequently isolated and fragmented to determine differences in fragmentation that may be caused by the modification, without changing nESI emitters and wasting solution.

4.3.4 Oxidation of Peptides with Peroxy Compounds

Protein oxidation is a common process that occurs in biological systems and has implications for a variety of diseases, especially those associated with aging (e.g. alzheimers).[58] Oxidation can also be used to label peptides and proteins similarly to the covalent modifications described above. It is well known that certain amino acid residues (i.e. methionine and tryptophan) are more susceptible to oxidation via the

addition of peroxy compounds in solution.[59,60] Oxidation of specific residues has also been described as a result from electrochemical reactions during the electrospray process.[61] Recently, oxidation via ion/ion reactions has shown that these same residues are more susceptible to oxidation in the gas-phase as well.[21] Peroxy compounds can be added to peptides or proteins in solution to oxidatively label certain residues, which affects the observed fragmentation of the biomolecule.[62,63] To demonstrate oxidation of a peptide via nESI from a theta tip, ARAMAKA is sprayed opposite periodate and persulfate (Figure 4.6a and b, respectively). Oxidation is observed with both peroxy compounds, however the relative abundance of oxidized peptide vs. the unmodified peptide is greater with persulfate than with periodate, which correlates to the strength of the oxidizing agent (persulfate > periodate). Complex formation of the peptide with the intact peroxy compounds is also observed. It is important to note that some of the easily oxidized residues can become oxidized in older solutions that are exposed to light and the air. As a control, the ARAMAKA sample was sprayed opposite water in a theta tip in Figure 4.6c. No oxidation of the peptide was observed, thus the oxidation observed in Figure 4.6a and b is a result of mixing with the periodate and persulfate solutions, respectively.

4.4 Conclusions

The use of theta capillaries as nESI emitters can be useful for performing a variety of reactions on the sub-millisecond timescale just prior to mass analysis. The simplicity and convenience of theta capillaries makes them a useful technique for the

analysis of reaction intermediates and products from reactions that occur on this short timescale. These reactions can be performed to manipulate ion types, which influences the favored fragmentation pathways and efficiencies. The reactions described here include metal cation adduct reduction with minimal protein denaturation using acids, refolding of acid denatured proteins using basic solutions, complexation of primary amine reactive reagents such as *N*-hydroxysuccinimide esters and a formyl benzene compound, propionylation of a large peptide and a protein, and oxidation of a methionine containing peptide using peroxy compounds. All experiments performed in this chapter were performed by spraying the two reactants from separate channels of a theta tip, such that mixing is limited to the Taylor cone and subsequent droplets. However, future work in this area could include performing all of these reactions (and others) using electroosmosis as described in the previous chapter to extend the mixing/reaction timescale. In many of the experiments in which complex formation was observed without reactivity (NHS reagents and FBDSA), electroosmosis in the theta tips provides additional mixing/reaction time to obtain reaction products. While the propionylation reaction did occur on the sub-millisecond timescale, extending the reaction time via electroosmosis in the theta tips could provide for additional modifications and/or increase the amount of product observed. Controlling the mixing time via electroosmosis provides the flexibility to affect the number of modifications or extent of reaction observed easily and with the same nESI tip. This chapter provides a summary of reactions that show interesting and promising results using the theta tips,

which could be expanded upon to provide additional insights and methods for manipulating ion types.

4.5 References

[1] Yamashita, M.; Fenn, *J. B. J. Phys. Chem.*, **1984**, *88*, 4451-4459.

[2] Fenn, J. B.; Mann, M.; Meng, C. K.; Wong, S. F.; Whitehouse, C. M. *Science* **1989**, *246*, 64-71.

[3] Wilm, M. S.; Mann, M. *Int. J. Mass Spectrom.* **1994**, *136*, 167-180.

[4] Wilm, M.; Mann, M. *Anal. Chem.***1996**, *68*, 1-8.

[5] Kelleher, N. L. *Anal. Chem.* **2004**, *A*, 196-203.

[6] Cech, N. B.; Enke, C. G. *Mass Spectrom. Rev.* **2001**, *20*, 362-387.

[7] Wang, D.; Kalb, S. R.; Cotter, R. J. *Rapid Commun. Mass Spectrom.* **2004**, *18*, 96-102.

[8] Wagner, D. S.; Salari, A.; Gage, D. A.; Leykam, J.; Fetter, J.; Hollingsworth, R.; Watson, J. T. *Biol. Mass Spectrom.* **1991**, *20*, 419-425.

[9] Yang, W.-C.; Mirzaei, H.; Liu, X.; Regnier, F. E. *Anal. Chem.* **2006**, *78*, 4702-4708.

[10] Sinz, A. *J. Mass Spectrom.* **2003**, *38*, 1225-1237.

[11] Huang, B. X.; Kim, H.-Y.; Dass, C. *J. Am. Soc. Mass Spectrom.* **2004**, *15*, 1237-1247.

[12] Chen, W.; Lee, P. J.; Shion, H.; Ellor, N.; Gebler, J. C. *Anal. Chem.* **2007**, *79*, 1583-1590.

[13] Madsen, J. A.; Brodbelt, J. S. *Anal. Chem.* **2009**, *81*, 3645-3653.

[14] Dongré, A. R.; Jones, J. L.; Somogyi, Á.; Wysocki, V. *J. Am. Chem. Soc.* **1996**, *118*, 8365-8374.

[15] Lee, S.-W.; Kim, H. S.; Beauchamp, J. L. *J. Am. Chem. Soc.* **1998**, *120*, 3188-3195.

[16] Gu, C.; Tsaprailis, G.; Breci, L.; Wysocki, W. H. *Anal. Chem.* **2000**, *72*, 5804-5813.

[17] Brodbelt, J. S. *J. Am. Soc. Mass Spectrom.* **2011**, *22*, 197-206.

[18] Brodbelt, J. S. *Chem. Soc. Rev.* **2014**, *43*, 2757-2783.

[19] Prentice, B. M.; McLuckey, S. A. *Chem. Commun.* **2013**, *49*, 947-965.

[20] Gilbert, J. D.; Prentice, B. M.; McLuckey, S. A. *J. Am. Soc. Mass Spectrom.* ASAP.

[21] Pilo, A. L.; McLuckey, S. A. *J. Am. Soc. Mass Spectrom.* **2014**, *25*, 1049-1057.

[22] McGee, W. M.; Mentinova, M.; McLuckey, S. A. *J. Am. Chem. Soc.* **2012**, *134*, 11412-11414.

[23] Prentice, B. M.; Gilbert, J. D.; Stutzman, J. R.; Forrest, W. P.; McLuckey, S. A. *J. Am. Soc. Mass Spectrom.* **2013**, *24*, 30-37.

[24] Mentinova, M.; McLuckey, S. A. *J. Am. Chem. Soc.* **2010**, *132*, 18248-18257.

[25] Figeys, D.; Gygi, S. P.; McKinnon, G.; Aebersold, R. *Anal. Chem.* **1998**, *70*, 3728-3734.

[26] Koster, S.; Verpoorte, E. *Lab Chip*, **2007**, *7*, 1394-1412.

[27] Kolakowski, B. M.; Simmons, D. A.; Konermann, L. *Rapid Commun. Mass Spectrom.* **2000**, *14*, 772-776.

[28] Konermann, L.; Rosell, F. I.; Mauk, A. G.; Douglas, D. J. *Biochem.* **1997**, *36*, 6448-6454.

[29] Wilson, D. J.; Konermann, L. *Anal. Chem.* **2003**, *75*, 6408-6414.

[30] Sogbein, O. O.; Simmons, D. A.; Konermann, L. *J. Am. Soc. Mass Spectrom.* **2000**, *11*, 312-319.

[31] Zechel, D. L.; Konermann, L.; Withers, S. G.; Douglas, D. J. *Biochem.* **1998**, *37*, 7664-7669.

[32] Li, Zhili; Sau, A. K.; Shen, S.; Whitehouse, C.; Baasov, T.; Anderson, K. S. *J. Am. Chem. Soc.* **2003**, *125*, 9938-9939.

[33] Wilson, D. J.; Kondermann, L. *Anal. Chem.* **2004**, *76*, 2537-2543.

[34] Mark, L. P.; Gill, M. C.; Mahut, M.; Derrick, P. J. *Eur. J. Mass Spectrom.* **2012**, *18*, 439-446.

[35] Fisher, C. M.; Kharlamova, A.; McLuckey, S. A. *Anal. Chem.* **2014**, *86*, 4581-4588.

[36] Mortensen, D. N.; Williams, E. R. *Anal. Chem.* **2014**, *86*, 9315-9321.

[37] Mortensen, D. N.; Williams, E. R. *Anal. Chem.* **2015**, *87*, 1281-1287.

[38] Fisher, C. M.; Hilger, R. T.; McLuckey, S. A. *Anal. Chem.* **2015**, submitted.

[39] Huber, C. G.; Buchmeiser, M. R. *Anal. Chem.* **1998**, *70*, 5288-5295.

[40] Liu, C.; Wu, Q.; Harms, A. C.; Smith, R. D. *Anal. Chem.* **1996**, *68*, 3295-3299.

[41] Iavarone, A. T.; Udekwu, O. A.; Williams, E. R. *Anal. Chem.* **2004**, *76*, 3944-3950.

[42] Flick, T. G.; Merenbloom, S. I.; Williams, E. R. *J. Am. Soc. Mass Spectrom.* **2011**, *22*, 1968-1977.

[43] Kharlamova, A.; Prentice, B. M.; Huang, T.; McLuckey, S. A. *Int. J. Mass Spectrom.* **2011**, *82*, 1594-1597.

[44] Chowdhury, S. K.; Katta, V.; Beavis, R. C.; Chait, B. T. *J. Am. Soc. Mass Spectrom.* **1990**, *1*, 382-388.

[45] Kharlamova, A.; Prentice, B. M.; Huang, T.; McLuckey, S. A. *Anal. Chem.* **2010**, *82*, 7422-7429.

[46] Chowdhury, S. K.; Katta, V.; Chait, B.T. *J. Am. Chem. Soc.* **1990**, *112*, 9012-9013.

[47] Kaltashov, I.A.; Eyles, S. J. *Mass Spectrom. Rev.* **2002**, *21*, 37-71.

[48] Fenn, J. B. *J. Am. Soc. Mass Spectrom.* **1993**, *4*, 524-535.

[49] Lide, D. E.; Ed. *CRC Handbook of Chemistry and Physics, 82nd ed.*, CRC Press: Boca Raton, FL, 2001-2002.

[50] Lindskog, S. *Pharmacol. Ther.* **1997**, *74*, 1-20.

[51] Evans, S. V.; Brayer G. D. *J. Mol. Biol.* **1990**, *23*, 885-897.

[52] Yazgan, A.; Henkens, R. W. *Biochemistry.* **1972**, *11*, 1314-1318.

[53] Hargrove, M. S.; Barrick, D.; Olson, J. S. *Biochem.* **1996**, *35*, 11293-11299.

[54] Hassell, K. M.; Stutzman, J. R.; McLuckey, S. A. *Anal. Chem.* **2010**, *82*, 1594-1597.

[55] O'Donnell, M. J.; Polt, R. L. *J. Org. Chem.* **1982**, *47*, 2663-2666.

[56] Riordan, J. F.; Vallee, B. L. *Method. Enzymol.* **1972**, *41*, 494-499.

[57] Mann, M.; Hendrickson, R. C.; Pandey, A. *Annu. Rev. Biochem.* **2001**, *70*, 437-473.

[58] Berlett, B. S.; Stadtman, E. R. *J. Biol. Chem.* **1997**, *272*, 20313-20316.

[59] Clamp, J. R.; Hough, L. *Biochem. J.* **1965**, *94*, 17-24.

[60] Vogt, W. *Free Radical Bio. Med.* **1995**, *18*, 93-105.

[61] Morand, K.; Talbo, G.; Mann, M. *Rapid Commun. Mass Spectrom.* **1993**, *7*, 738-743.

[62] Schey, K. L.; Finley, E. L. *Acc. Chem. Res.* **2000**, *33*, 299-306.

[63] Reid, G. E.; Roberts, K. D.; Kapp, E. A.; Simpson, R. J. *J. Proteome Res.* **2004**, *3*, 751-759.

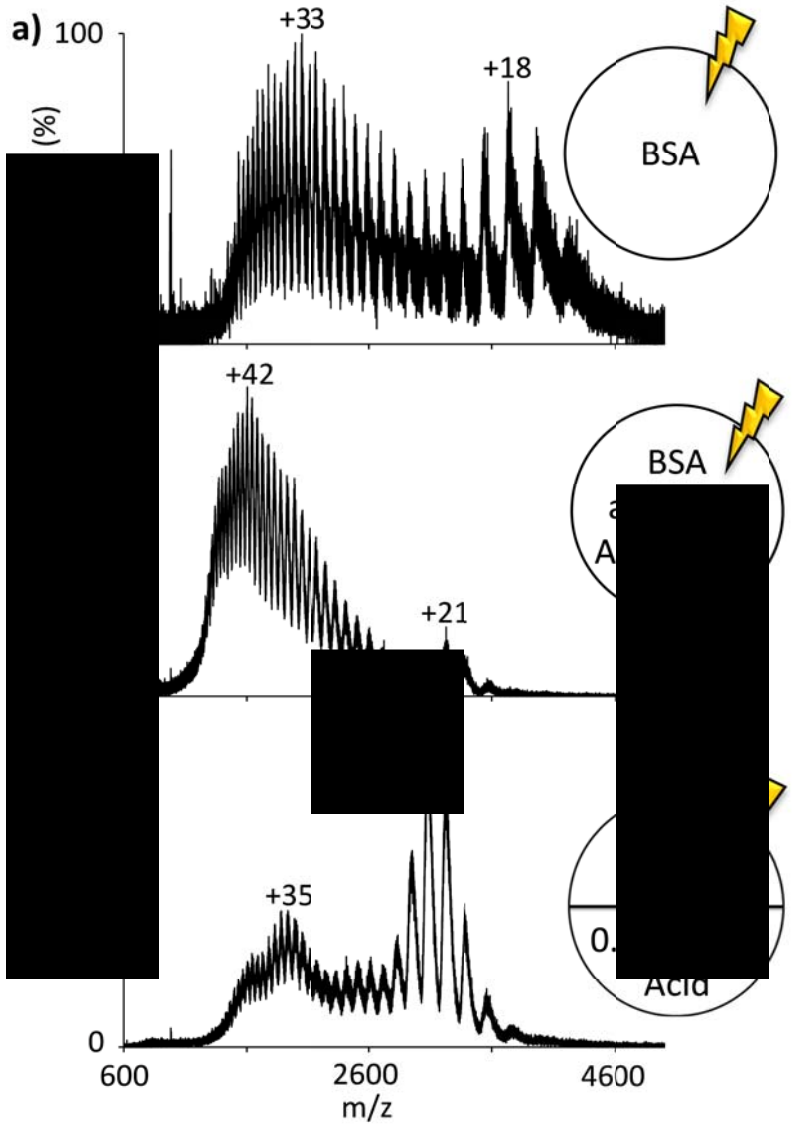

Figure 4.1 Aqueous bovine serum albumin (BSA) dissolved in water and sprayed from a single-barreled tip (a) and mixed with 0.05% acetic acid in solution and sprayed from a regular tip (b) and mixed with 0.1% acetic acid via spraying from a theta tip (c).

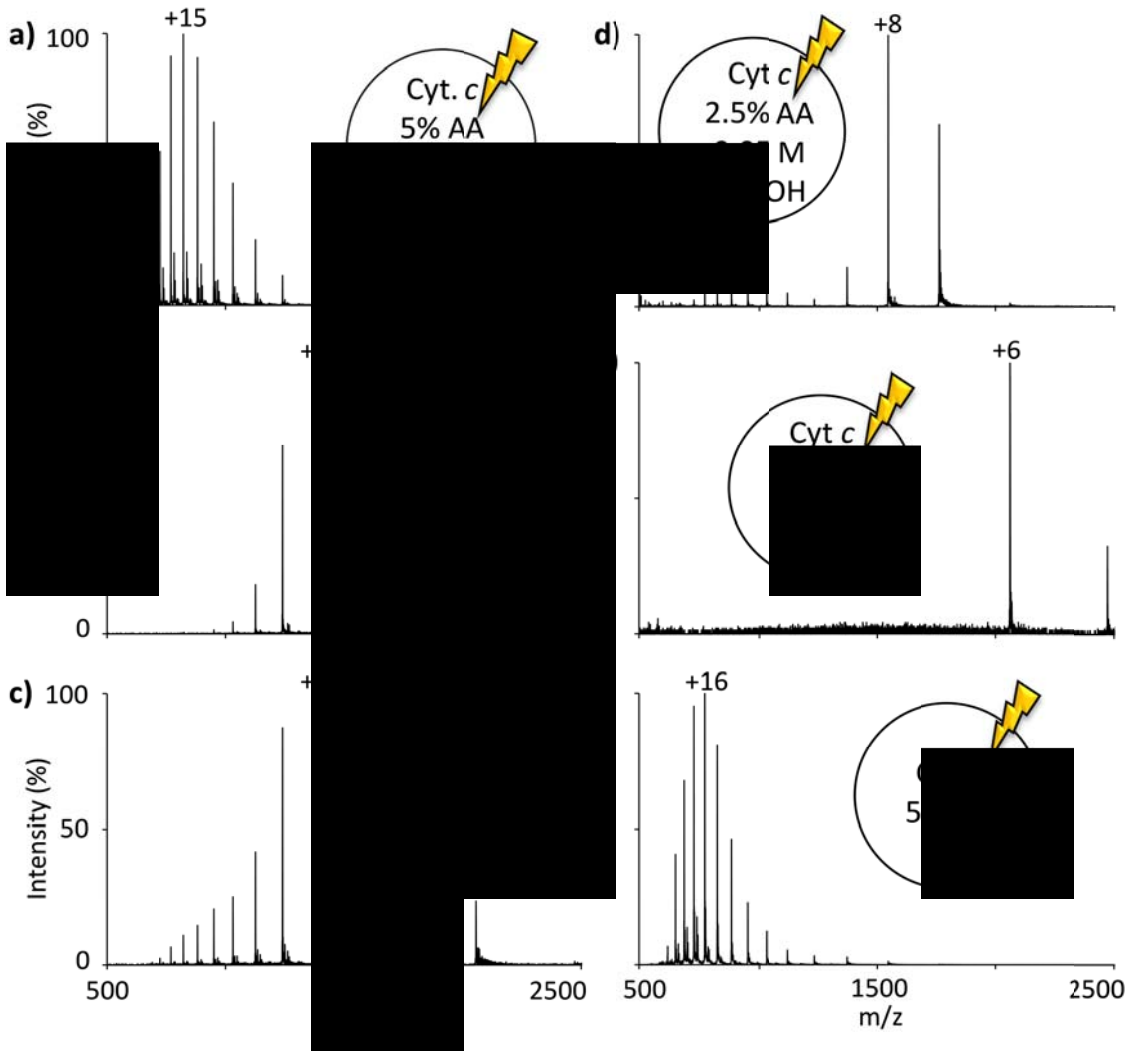

Figure 4.2 Refolding acid denatured (5% acetic acid, AA) equine cytochrome *c* via spraying from theta tips using 0.1 M ammonium hydroxide (NH_4OH) (a), trimethylamine (TMA) (b), and piperidine (pip.) (c). Solution mixtures sprayed from a regular tip for ammonium hydroxide (d) and trimethylamine (e) are given for comparison. The control spectrum in which the acidified cytochrome *c* solution is sprayed from a regular tip is given in (f).

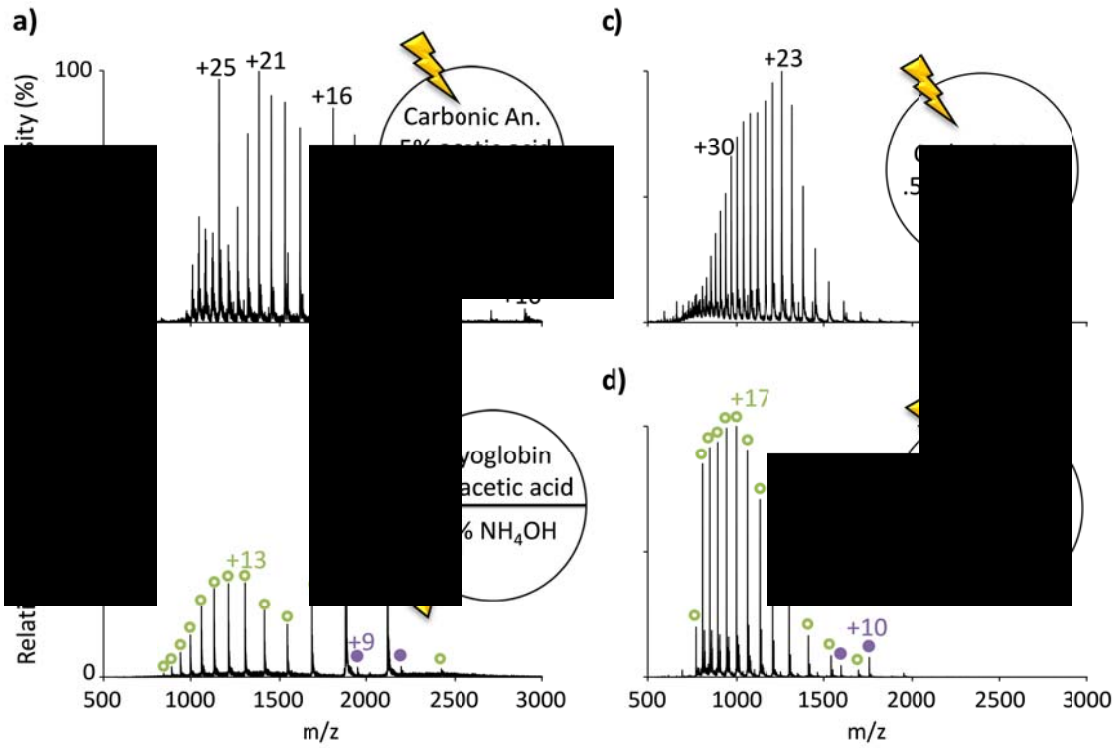

Figure 4.3 Refolding Carbonic anhydrase in 0.5% acetic acid by spraying opposite 1% piperidine from a theta capillary (a) and refolding myoglobin in 0.1% acetic acid by spraying opposite 15% ammonium hydroxide from a theta capillary (b). The charge state distribution produced by spraying the acid denatured proteins from a regular tip are given in (c) and (d), respectively. All peaks in the carbonic anhydrase spectra indicate apocarbonic anhydrase. The green open circles indicate apomyoglobin charge states and the purple solid circles indicated holomyoglobin charge states.

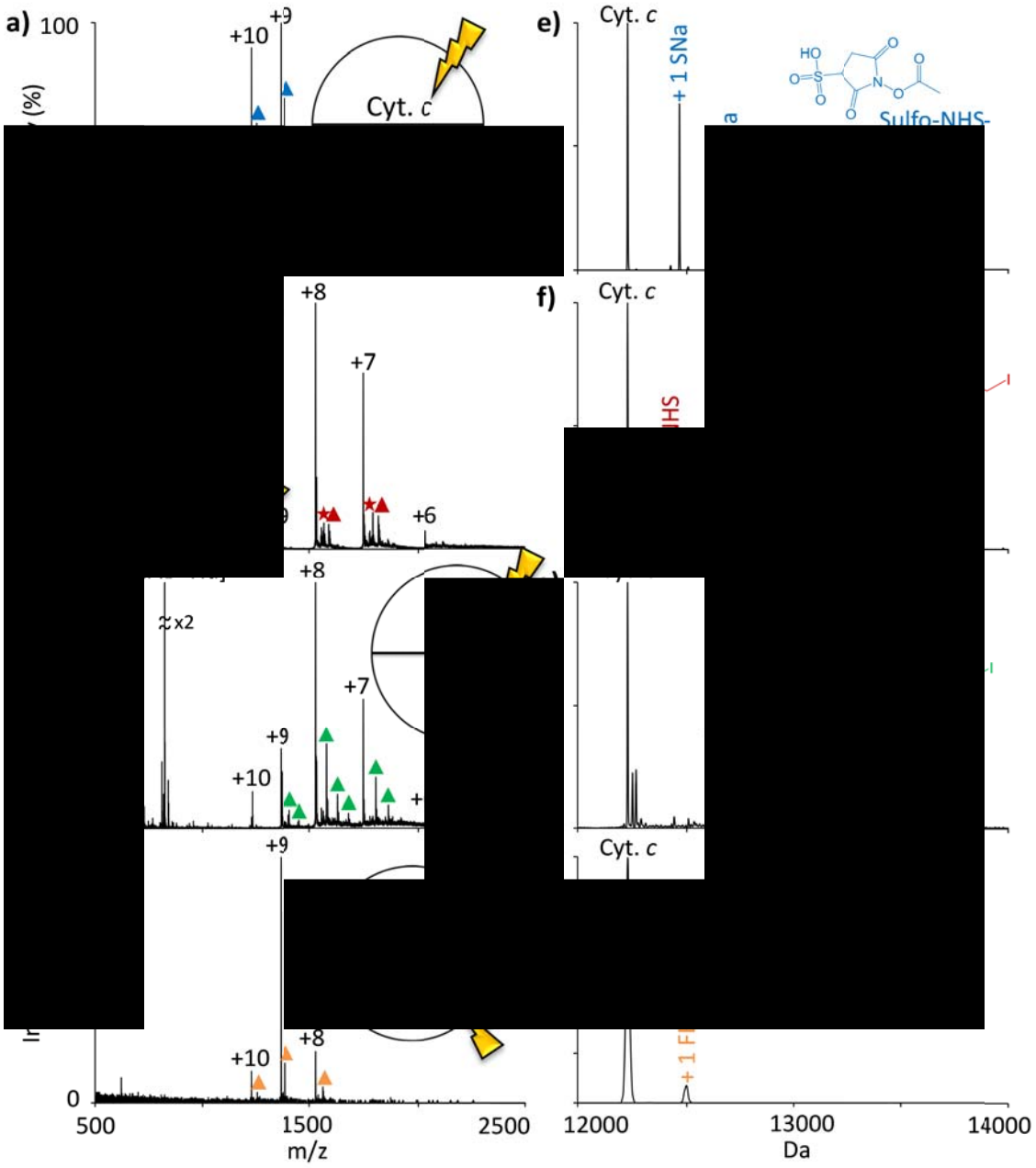

Figure 4.4 Complex formation of bovine cytochrome *c* with sulfo-NHS-acetate (SNa) (a), sulfo-SIAB (b), SIAB (c), and FBDSA (d) when sprayed from opposite sides of a theta tip. Each spectrum is deconvoluted in (e) – (h), respectively. Triangles indicate adducts of the intact reagent. Stars indicate covalent modification (b and f).

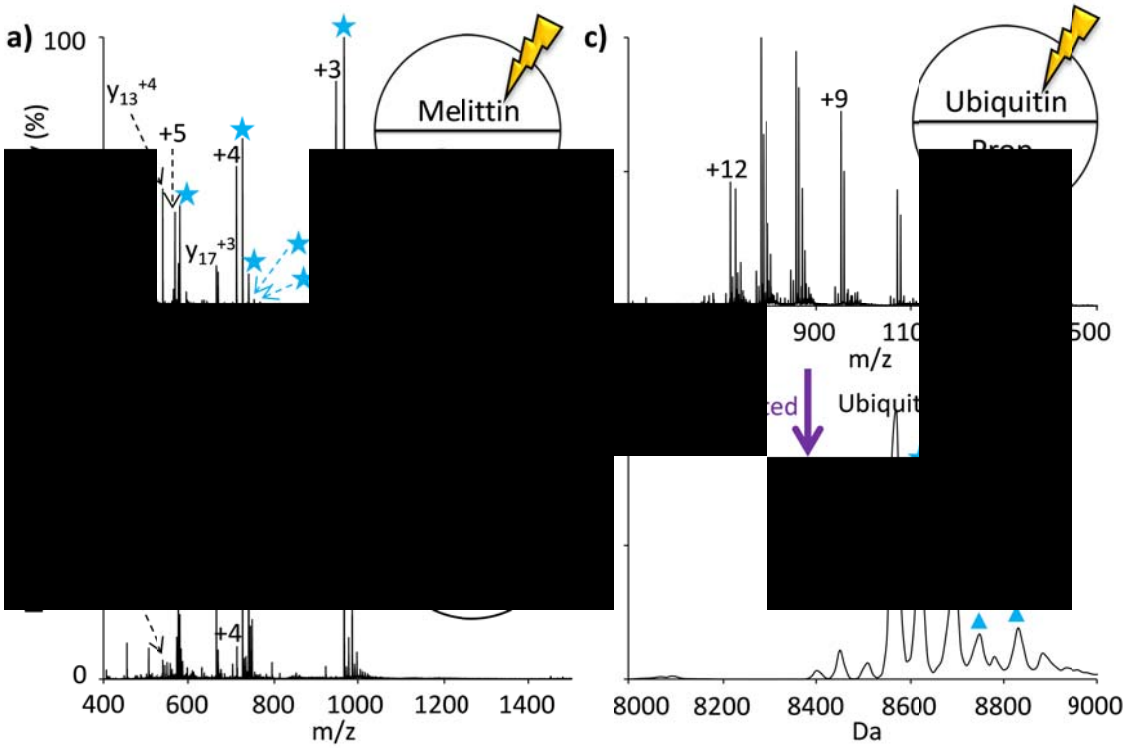

Figure 4.5 Melittin sprayed opposite propionic anhydride (prop. anhy.) in a theta tip (a) and corresponding solution phase mixture sprayed from a single-barreled tip (b). Ubiquitin sprayed opposite propionic anhydride in a theta tip (c) and the corresponding deconvolution (d). Triangles indicate adducts of intact propionic anhydride and stars indicate propionylation.

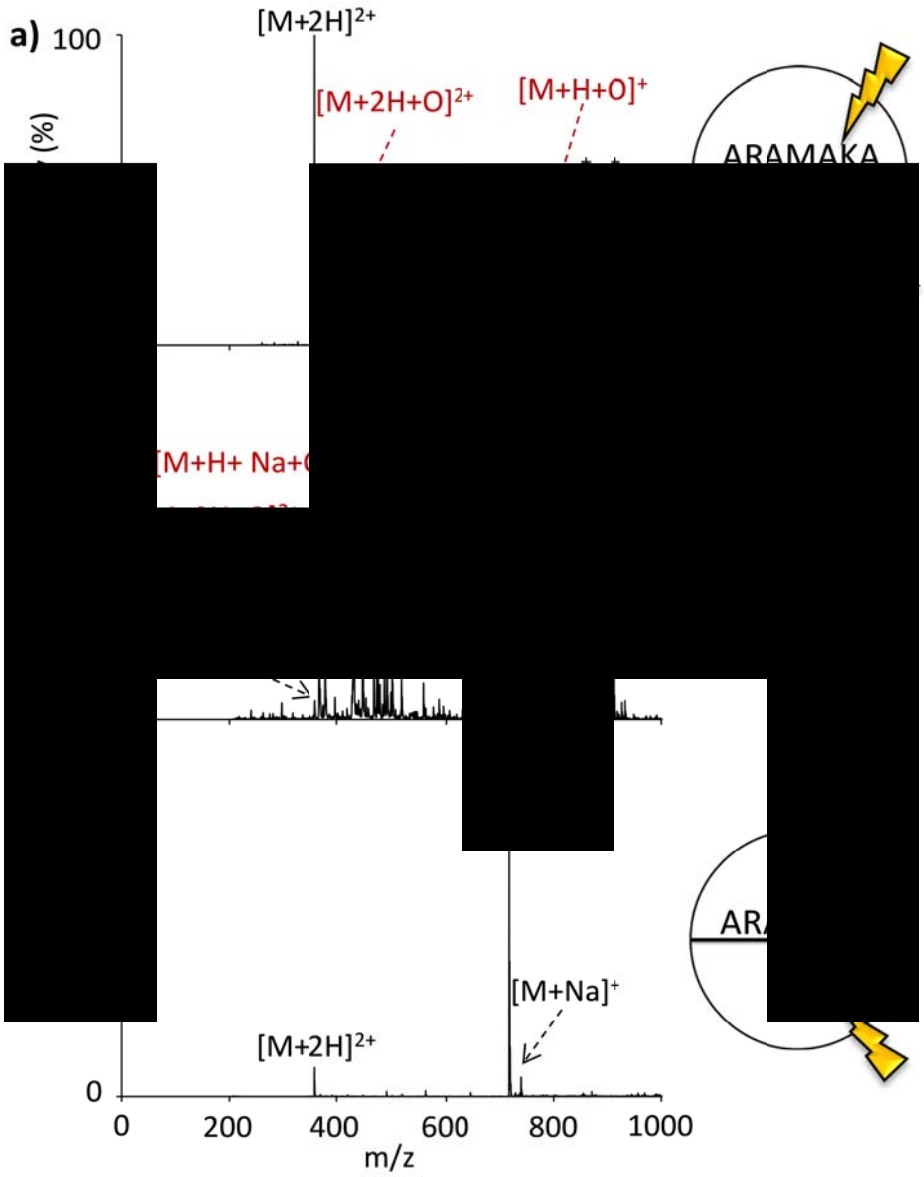

Figure 4.6 Oxidation of the peptide ARAMAKA via spraying opposite periodate (a) and persulfate (b) solutions from a theta tip. A control spectrum in which ARAMAKA is sprayed opposite water from a theta tip is given in (c).Gas-phase Synthesis of peptide radical cations via ion/ion reactions and ultraviolet photodissociation

CHAPTER 5. GAS-PHASE SYNTHESIS OF PEPTIDE RADICAL CATIONS VIA ION/ION REACTIONS AND ULTRAVIOLET PHOTODISSOCIATION

Portions and figures of this chapter were published previously as reference 42, copyright 2015 John Wiley and Sons.

5.1 Introduction

There are a variety of different ionization methods that each produces different types of ions (e.g. protonated, odd-electron). For example, electron ionization (EI) is a high energy ionization technique that often produces $M^{+\bullet}$ ion types as well as extensive fragmentation of the analyte.[1,2] On the other hand, electrospray ionization (ESI) produces either protonated or deprotonated ions which are usually multiply charged.[3,4] ESI is a soft ionization technique that is capable of transferring analytes, including large biomolecules, into the gas-phase with little or no fragmentation. ESI has become a superior ionization method for intact, large biomolecules due to preservation of the intact analyte during ionization and transfer to the gas-phase. Additionally, the multiply charged signal brings their mass to charge ratio (*m/z*) into the operational range of most commercial mass spectrometers.

One of the methods used to analyze biomolecules such as large proteins is to ionize the intact analyte via ESI and interrogate the amino acid sequence via a variety of

activation or dissociation methods. This method has been termed "top-down" proteomics.[5] Both the ion type and the activation method are important in determining the type of structural information that can be obtained via tandem mass spectrometry experiments.[6] Because ESI is the preferred ionization method for the analysis of intact proteins, most studies have been performed on even electron, protonated species via collision induced dissociation (CID). The widely accepted mechanism for fragmentation of protonated proteins and peptides via CID has been termed the "mobile proton theory."[7,8] This fragmentation mechanism relies on the movement of protons along the backbone of the protein/peptide and often results in the formation of b- and y-type ions.

Several methods have been described to produce a variety of biomolecule ion types in an effort to produce complementary fragmentation via CID. One attractive ion type includes odd-electron or radical ions as they afford quite different fragmentation when compared to CID of the even-electron, protonated species as produced via ESI. As described above, using EI or other high energy ionization methods to produce radical ions is not an optimal technique for biomolecules as extensive analyte fragmentation results, which complicates sequence analysis and prevents determination of the intact biomolecule mass.[9] Therefore, a variety of methods have been developed to produce biomolecular ions containing a free radical using ESI.[10] Once the radical ion is generated, CID is performed to induce radical directed dissociation (RDD), which consists of a series of hydrogen abstractions from various locations on the biomolecule and ultimately yields complementary structural information.[11]

One common method of generating radical peptides is through metal-ligand-peptide complexes. A variety of these complexes have been described and have been found to generate $M^{+\bullet}$ species through oxidative dissociation or dissociative electron transfer. [9,12,13,14] A common metal used in these complexes is copper, while a common ligand is salen.[9,15,16] These techniques have been particularly useful in the identification of isomers such as leucine and isoleucine based on differences in side chain fragmentation.[15,17]

Additionally, azo and nitroso functional groups can be homolytically cleaved by CID, yielding free radicals on the R-groups that were on either side of the functional group and a loss of N_2 or NO, respectively. [18,19,20] Reagents containing these functional groups have been conjugated to peptides or proteins in solution and ionized via ESI. CID of the modified ion results in generation of radical peptide/protein ions. A distinct advantage of this method is that proteins can be modified via bifunctional crosslinkers containing an azo group such that a single CID step will produce two free radicals on the analyte ion. The cross-linking experiment can be used to determine protein tertiary structure by varying the length of the crosslinker.[21]

Van Berkel *et al.* have taken advantage of electrochemical reactions that occur during the electrospray process to generate a variety of radical cations.[22] This method has been demonstrated for porphyrin compounds and polyaromatic hydrocarbons.[23] This method has also been used to improve the ionization efficiency of alcohols by conjugating ferrocene-based groups, which are ionizable via electrochemical reactions to the analyte.[24] The generation of radical ions via electrochemical reactions during ESI

is dependent upon the oxidation potential of the analyte as well as the solvent system, which must dissolve the analyte as well as stabilize the radical.[23]

Recently, Julian *et al.* have described a variety of methods using homolytic cleavage of C-I bonds to produce radical peptides and proteins. For example, they have modified tyrosine residues in solution to contain a C-I bond, which is selectively cleaved homolytically with ultraviolet photodissociation (UVPD) at 266 nm to produce a radical peptide.[25,26,27] Julian *et al.* have also generated radical biomolecules via non-covalent complexes formed in solution between biomolecules and crown ethers containing C-I bonds.[28,29] UVPD at 266 nm was used to cleave the C-I bond to produce a radical site on the crown ether.

All of these techniques require modification of the bulk solution and/or solution-phase conjugation reactions. The most common methods for synthesizing radical containing species is by electron capture dissociation (ECD)[30] or by electron transfer dissociation (ETD) in the gas-phase.[31] During ECD, analyte ions are subjected to an electron source such that the analyte captures an electron. ETD is often performed as a gas-phase ion/ion reaction in which an anionic electron transfer reagent (e.g. anthracene) transfers an electron to a multiply protonated analyte (i.e. peptide). When these methods are performed on peptides or proteins, c- and z-type ions are favored, which is complementary to the b- and y-type ions produced via fragmentation of even electron species.

Recently, ion/ion reactions have been used to alter biomolecule ion types via a variety of different covalent modification reactions in the gas-phase. [32,33,34,35,36] Ion/ion

reactions offer several advantages over solution-phase reactions.[37] Solution-phase optimization is not required and reactants can be isolated in the gas-phase prior to reaction to avoid unwanted side reactions with other components in the solution. Additionally, the relative concentrations of each reactant and the reaction time are controlled via the injection time for each ion polarity and the mutual storage time (usually 10's to 100's of milliseconds), respectively, making ion/ion reactions easier to tune compared to solution-phase reactions. Recently, the complexation and conjugation of azo containing compounds to peptides in the gas-phase via ion/ion reactions has been demonstrated as a viable radical cation synthesis method.[38] Upon CID, the complexed or conjugated peptides were shown to yield RDD-specific fragmentation.

In this chapter, two synthetic pathways will be described for the generation of radical peptides via ion/ion reactions coupled with UVPD. Both pathways will consist of an ion/ion reaction between a multiply protonated peptide and a singly deprotonated reagent containing a C-I bond. One pathway contains a reagent that is held near the peptide via a long-lived electrostatic complex. The second pathway consists of covalent modification in the gas-phase via an ion/ion reaction to conjugate the reagent directly to the peptide. In both cases, UVPD at 266 nm is used to homolytically cleave the C-I bond, producing a free radical at a site near the peptide. A final CID step is used to induce radical migration through hydrogen abstraction from the peptide to the reagent, which results in RDD.

5.2 Experimental

5.2.1 Chemicals

Potassium 2-iodo-5-methylbenzene sulfonate (MIBS), bradykinin, 2-iodobenzoic acid, and 1-ethyl-3-(3-dimethylaminopropyl) carbodiimide HCl (EDC) were purchased from Sigma Aldrich (St. Louis, MO). *N*-hydroxysulfosuccinimide (sulfo-NHS) was purchased from Thermo Fisher Scientific (Waltham, MA). The peptide RARARAA was custom synthesized by NeoBioSci (Cambridge, MA). *N,N*-dimethylformamide (DMF) was purchased from Mallinckrodt Chemicals (Phillipsburg, NJ). Methanol (MeOH) was purchased from Macron Chemicals (part of Avantor, Center Valley, PA). All aqueous samples were prepared with water purified at 15 MΩ by a Barnstead nanopure infinity ultrapure water system from Thermo Fisher Scientific (Waltham, MA). All samples were used without further purification.

Iodobenzene sulfo-NHS (IBSN) was synthesized using a procedure similar to that available through Life Technologies (Thermo Fisher Scientific, Inc.). Briefly, IBSN was synthesized by mixing equimolar solutions of 2-iodobenzoic acid, EDC, and sulfo-NHS at room temperature for several minutes. The 2-iodobenzoic acid solution was prepared in DMF. EDC was dissolved in 11% H_2O and 89% DMF. Sulfo-NHS was dissolved in 50:50, H_2O: MeOH. The final solution was ~135 μM in 80% DMF and 20% H_2O. All other reagents and peptide solutions were prepared at a concentration of 0.1 mg/mL in 1:1, H_2O: MeOH. The reaction solution was used directly as the nanoESI reagent mixture without further purification.

5.2.2 Mass Spectrometry and UVPD

All ion/ion reactions were performed using a dual source 3D ion trap mass spectrometer that has been described previously.[39] Briefly, positive peptide ions are generated via one source and are injected into the trap where they are isolated. The negative reagent ions are then generated via the opposite source and are injected into the ion trap where they interact with peptide ions. Alternatively, ions can be injected in the opposite order; usually the order is determined by the complexity of the precursor ion spectrum for each polarity as only one polarity of ions can be isolated using this instrument. In order to perform UVPD experiments, the dual source 3D ion trap mass spectrometer was interfaced with a Nd:YAG laser (Continuum, San Jose, CA) as depicted in Figure 1.2. UVPD was performed with 266 nm photons at a pulse rate of 20 Hz. The 266 nm photons were generated by passing the Nd:Yag fundamental wavelength (1064 nm) through two second harmonic generators. A mechanical beam blocker was controlled by a TTL trigger using the instrument software to allow photons to pass into the instrument only during the desired UVPD segment of the scan function. A series of mirrors were used to direct the laser beam into the instrument through a quartz window. An iris was placed just in front of the quartz window to tune the beam diameter. The laser beam travels along the ion path and enters the 3D ion trap through the entrance endcap electrode (along the z-axis), such that the laser beam will overlap with the ion cloud.

Figure 5.1 shows the two synthesis methods used to generate radical peptides after the desired ion/ion reaction product is isolated. The first method (Figure 5.1a)

shows the synthesis of a free radical through an electrostatic complex (i.e. no covalent modification of the peptide). The doubly protonated peptide forms a long-lived electrostatic complex with the reagent. Upon UVPD, the C-I bond of the reagent is homolytically cleaved. This product is then isolated prior to CID which results in both proton transfer to the sulfonate group of the reagent as well as hydrogen abstraction from a site on the peptide to the reagent, producing a singly positively charged radical peptide and the neutralized reagent. CID of this species produces RDD fragmentation.

The second method (Figure 5.1b) shows the procedure for generating a radical peptide through an ion/ion reaction in which the peptide is covalently modified. The first step involves the reaction of the doubly protonated peptide and a singly deprotonated sulfo-NHS reagent. CID of the initially electrostatic complex yields the loss of a neutralized sulfo-NHS moiety, indicating that covalent modification has occurred.[36] UVPD of the covalently modified peptide results in homolytic cleavage of the C-I bond. This product is then isolated and upon CID, radical migration through a series of hydrogen abstractions along the modified peptide occurs, yielding RDD fragments of the peptide.

5.3 Results and Discussion

UVPD is a selective technique, as only chromophores that absorb at the incident wavelength will be activated.[40] Thus, UVPD offers a distinct advantage over other CID methods. The experiments described below take advantage of the selectivity of UVPD at 266 nm by incorporating C-I bonds into the reagent. C-I bonds selectively absorb 266 nm

light, which results in homolytic cleavage of the bond to yield a radical species. Provided there are no other chromophores that absorb at 266 nm (i.e. peptides and proteins), this is the only site that will be activated.

5.3.1 RDD of an Electrostatically Bound Radical Site

The first method for producing radical peptides via ion/ion reactions coupled with UVPD does so through an electrostatic complex between the peptide and the reagent containing the C-I bond. Method 1 (see Figure 5.1a) is demonstrated with an ion/ion reaction between the doubly protonated peptide, RARARAA, ($[M+2H]^{2+}$) and singly deprotonated reagent, MIBS (Figure 5.2). The structure of MIBS is given in Figure 5.2e. The ion/ion reaction spectrum consists of the unreacted precursor ($[M+2H]^{2+}$), a peak corresponding to proton transfer from the peptide to MIBS ($[M+H]^{+}$), and the ion/ion reaction complex ($[M+2H+MIBS]^{+}$). The desired ion/ion reaction complex was isolated and subjected to UVPD to generate the loss of $I^{\bullet}$ (Figure 5.2a). The radical site generated through the loss of $I^{\bullet}$ is given in Figure 5.2e. This product ($[M+2H+MIBS-I]^{+}$) was isolated and CID was used to induce proton transfer and/or hydrogen abstraction from the peptide to MIBS ($[M+H]^{+}/[M]^{+\bullet}$). The resolution of the 3D ion trap is not sufficient to resolve the two species, which differ by only 1 *m/z*, nor can the species be individually isolated and activated via CID. Therefore, the peak corresponding to both products is isolated and upon CID, RDD fragmentation is obtained (Figure 5.2c). The fragmentation spectrum obtained via CID of the even electron species ($[M+H]^{+}$) is given in Figure 5.2d for comparison. One of the most abundant fragments obtained via RDD

corresponds to an arginine side chain loss ($-R_{86}$), which is not observed when the even electron species is subjected to CID. This is a well-known fragmentation pathway that is favored during RDD.[10]

It is also important to note that there is a trade-off between resolution and the transmission efficiency of the laser beam. It is well known that the resolution of 3D ion traps is dependent upon the size of the apertures in the endcaps. Large apertures create imperfections in the electric field. End cap inserts with various geometries can be used to allow for a more uniform electric field. However, these inserts also decrease the laser and ion transmission efficiency.

5.3.2 RDD of a Covalently Bound Radical Site

Method one, described above, generates a radical site that is able to abstract a hydrogen from the peptide through an electrostatic complex that is formed via an ion/ion reaction. A radical site can also be formed on a reagent that is covalently attached to a peptide via an ion/ion reaction as shown in Figure 5.1b for Method 2. The same doubly protonated peptide, RARARAAA, is reacted with singly deprotonated IBSN, whose structure is given in Figure 5.3e. The ion/ion reaction spectrum (Figure 5.3a) contains three charge states of the precursor peptide (+1, +2, and +3), which are a mixture of the precursor peptide ions and proton transfer ion/ion reaction products. Two ion/ion reaction complexes are also observed: $[M+3H+IBSN]^{2+}$ and $[M+2H+IBSN]^{+}$. CID of the singly protonated complex ($[M+2H+IBSN]^{+}$), without prior isolation, yields the peptide covalently modified with iodobenzene ($[M+H+IB]^{+}$) as indicated by the signature

loss of sulfo-NHS (Figure 5.3b). The covalently modified peptide was isolated and subjected to UVPD at 266 nm (Figure 5.3c) to homolytically cleave the C-I bond, yielding the $[M+H+B]^{+\bullet}$ product. This product was then isolated and RDD was induced via CID (Figure 5.3d). Again, one of the most prevalent fragments observed is the loss of the arginine side chain ($-R_{86}$). There is also a loss of the arginine side chain that contains the benzene modification ($-R_{86}+B$). The sulfo-NHS chemistry used in this ion/ion reaction results in covalent modification to either an unprotonated arginine side chain or the N-terminus of the peptide. Although arginine side chains are usually unreactive in solution, unprotonated arginine side chains have shown reactivity toward NHS esters in the gas-phase.[34] Therefore, it is not surprising that a loss of the arginine side chain containing a benzene modification would be observed. Additionally, two a-type ions are observed, which are also common fragment types observed with RDD. Both the arginine side chain losses and the a-type ions are not observed via CID of the even electron peptide (Figure 5.2d).

5.3.3 Comparison to Other Methods

The peptide, RARARAA, provides a good model system for indicating RDD due to the prevalent arginine side chain loss, which is only present during RDD. However, it is important to demonstrate the utility of ion/ion reactions coupled with UVPD to synthesize radical peptides using a system that is well studied via other RDD methods. Bradykinin (RPPGFSPFR) is a peptide that has been well studied by a variety of other RDD methods. Figure 5.4 shows the RDD spectrum generated using method 1. Briefly,

the doubly protonated peptide was reacted with MIBS to form an electrostatic complex. The reaction complex was isolated and the C-I bond was homolytically cleaved via UVPD at 266 nm. The UVPD product corresponding to the loss of $I^{\bullet}$ was isolated and subjected to CID to induce proton transfer and/or hydrogen abstraction from the peptide to the MIBS reagent. The resulting bradykinin radical cation ($[M+H]^{+}/[M]^{+\bullet}$) was isolated and subjected to another CID step to induce RDD. The RDD spectrum of bradykinin is given in Figure 5.4a. For comparison, the CID spectrum of even electron bradykinin is given in Figure 5.4b. The RDD specific fragments include the loss of the arginine side chain ($-R_{86}$), an abundant c_5 fragment, as well as a series of a-type ions. Similar fragmentation has also been observed by Julian *et al.*[11,41] and Laskin *et al.*[16]

5.4 Conclusions

Two methods have been described for synthesizing radical peptide cations using ion/ion reactions coupled with UVPD. Both methods utilize reagents containing C-I bonds which selectively absorb 266 nm photons, resulting in homolytic cleavage of the bond to form a radical site. The first method generates the radical on a reagent that is electrostatically bound to the peptide via an ion/ion reaction. The second method generates the radical on a reagent after it is covalently linked via an ion/ion reaction to the peptide. Both synthesis methods produce radical peptides as evidenced by RDD specific fragments including the loss of the arginine side chain as well as a-type ions. The first method is also demonstrated on bradykinin which is a well-studied peptide via

mass spectrometry. RDD fragmentation including the same arginine side chain loss and a series of a-type ions was also observed for this peptide.

5.5 References

[1] Bleakney, W. *Phys. Rev.* **1929**, *34*, 157-160.

[2] Bentley, T. W.; Johnstone, R. A. W. in *Advances in Physical Organic Chemistry*, vol. 8, Gold, V. Ed.; Academic Press: London, **1970**, 152-260.

[3] Yamashita, M.; Fenn, J. B. *J. Phys. Chem.* **1984**, *88*, 4451-4459.

[4] Fenn, J. B.; Mann, M.; Meng, C. K.; Wong, S. F.; Whitehouse, C. M. *Science* **1989**, *246*, 64-71.

[5] Kelleher, N. L. *Anal. Chem.* **2004**, *A*, 196-203.

[6] McLuckey, S. A.; Mentinova, M. *J. Am. Soc. Mass Spectrom.* **2011**, *22*, 3-12.

[7] Dongre, A. R.; Jones, J. L.; Somogyi, A.; Wysocki, V. H. *J. Am. Chem. Soc.* **1996**, *118*, 8365.

[8] Wysocki, V. H.; Cheng, G.; Zhang, Q.; Herrman, K. A.; Beardsley, R. L.; Hilderbrand, A. E. in *Principles of Mass Spectrometry Applied to Biomolelcules*, Lifshitz, C.; Laskin, J., Eds.; Wiley-Interscience: Hoboken, NJ, **2006**; *Chapter8*, 301-336.

[9] Hopkinson, A. C. *Mass Spectrom. Rev.* **2009**, *28*, 655-671.

[10] Tureček, F.; Julian, R. R. *Chem. Rev.* **2013**, *113*, 6691-6733.

[11] Sun, Q.; Nelson, H.; Ly, T.; Stoltz, B. M.; Julian, R. R. *J. Proteome. Res.* **2008**, *8*, 958-966.

[12] Barlow, C. K.; McFadyen, W. D.; O'Hair, R. A. J. *J. Am. Chem. Soc.* **2005**, *127*, 6109-6115.

[13] Chu, I. K.; Laskin, J. *Eur. J. Mass Spectrom.* **2011**, *17*, 543-556.

[14] Vaisar, T.; Gatlin, C. L.; Tureček, F. *J. Am. Chem. Soc.* **1996**, *118*, 5314-5315.

[15] Tureček, F. *Mass Spectrom. Rev.* **2007**, *26*, 563-582.

[16] Laskin, J.; Yang, Z.; Lam, C.; Chu, I. K. *Anal. Chem.* **2007**, *79*, 6607-6614.

[17] Wee, S.; O'Hair, R. A. J.; McFadyen, W. D. *Rapid Commun. Mass Spectrom.* **2002**, *16*, 884-890.

[18] Hodyss, R.; Cox, H. A.; Beauchamp, J. L. *J. Am. Chem. Soc.* **2005**, *127*, 12436-12437.

[19] Hao, G.; Gross, S. S. *J. Am. Soc. Mass Spectrom.* **2006**, *17*, 1725-730.

[20] Knudsen, E. R.; Julian, R. R. *Int. J. Mass Spectrom.* **2010**, *294*, 83-87.

[21] Falvo, F.; Fiebig, L.; Schäfer, M. *Int. J. Mass Spectrom.* **2013**, *354-355*, 26-32.

[22] Van Berkel, G. J.; Kertesz, V. *Anal. Chem.* **2007**, 5511-5520.

[23] Van Berkel, G. J.; McLuckey, S. A.; Glish, G. L. *Anal. Chem.* **1992**, *64*, 1586-1593.

[24] Van Berkel, G. J.; Quirke, J. M. E.; Tigani, R. A.; Dilley, A. S.; Covey, T. R. *Anal. Chem.* **1998**, *70*, 1544-1554.

[25] Ly, T.; Julian, R. R. *J. Am. Chem. Soc.* **2008**, *130*, 351-358.

[26] Ly, T.; Julian, R. R. *J. Am. Chem. Soc.* **2010**, *132*, 8602-8609.

[27] Sun, Q.; Yin, S.; Loo, J. A.; Julian, R. R. *Anal. Chem.* **2010**, *82*, 3826-3833.

[28] Tao, Y.; Quebbemann, N. R.; Julian, R. R. *Anal. Chem.* **2012**, *84*, 6814-6820.

[29] Pham, H. T.; Julian, R. R. *Anal. Chem.* **2014**, *86*, 3020-3027.

[30] Zubarev, R. A.; Kelleher, N. L.; McLafferty, F. W. *J. Am. Chem. Soc.* **1998**, *120*, 3265-3266.

[31] Syka, J. E.; Coon, J. J.; Schroeder, M. J.; Shabanowitz, J.; Hunt, D. *P. Natl. Acad. Sci. USA.* **2004**, *101*, 9528-9533.

[32] Gilbert, J. D.; Prentice, B. M.; McLuckey, S. A. *J. Am. Soc. Mass Spectrom.* ASAP.

[33] Pilo, A. L.; McLuckey, S. A. *J. Am. Soc. Mass Spectrom.* **2014**, *25*, 1049-1057.

[34] McGee, W. M.; Mentinova, M.; McLuckey, S. A. *J. Am. Chem. Soc.* **2012**, *134*, 11412-11414.

[35] Prentice, B. M.; Gilbert, J. D.; Stutzman, J. R.; Forrest, W. P.; McLuckey, S. A. *J. Am. Soc. Mass Spectrom.* **2013**, *24*, 30-37.

[36] Mentinova, M.; McLuckey, S. A. *J. Am. Chem. Soc.* **2010**, *132*, 18248-18257.

[37] Prentice, B. M.; McLuckey, S. A. *Chem. Commun.* **2013**, *49*, 947-965.

[38] Gilbert, J. D.; Fisher, C. M.; Bu, J.; Prentice, B. M.; Redwine, J. G.; McLuckey, S. A. *J. Mass Spectrom.*

[39] Wells, J. M.; Chrisman, P. A.; McLuckey, S. A. *J. Am. Soc. Mass Spectrom.* **2002**, *13*, 614-622.

[40] Brodbelt, J. S. *Chem. Soc. Rev.* **2014**, *43*, 2757-2783.

[41] Ly, T.; Julian, R. R. *J. Am. Soc. Mass Spectrom.* **2009**, *20*, 1148-1158.

[42] Gilbert, J. D.; Fisher, C. M.; Bu, J.; Prentice, B. M.; Redwine, J. G.; McLuckey, S. A. *J. Mass Spectrom.* **2015**, *50*, 418-426.

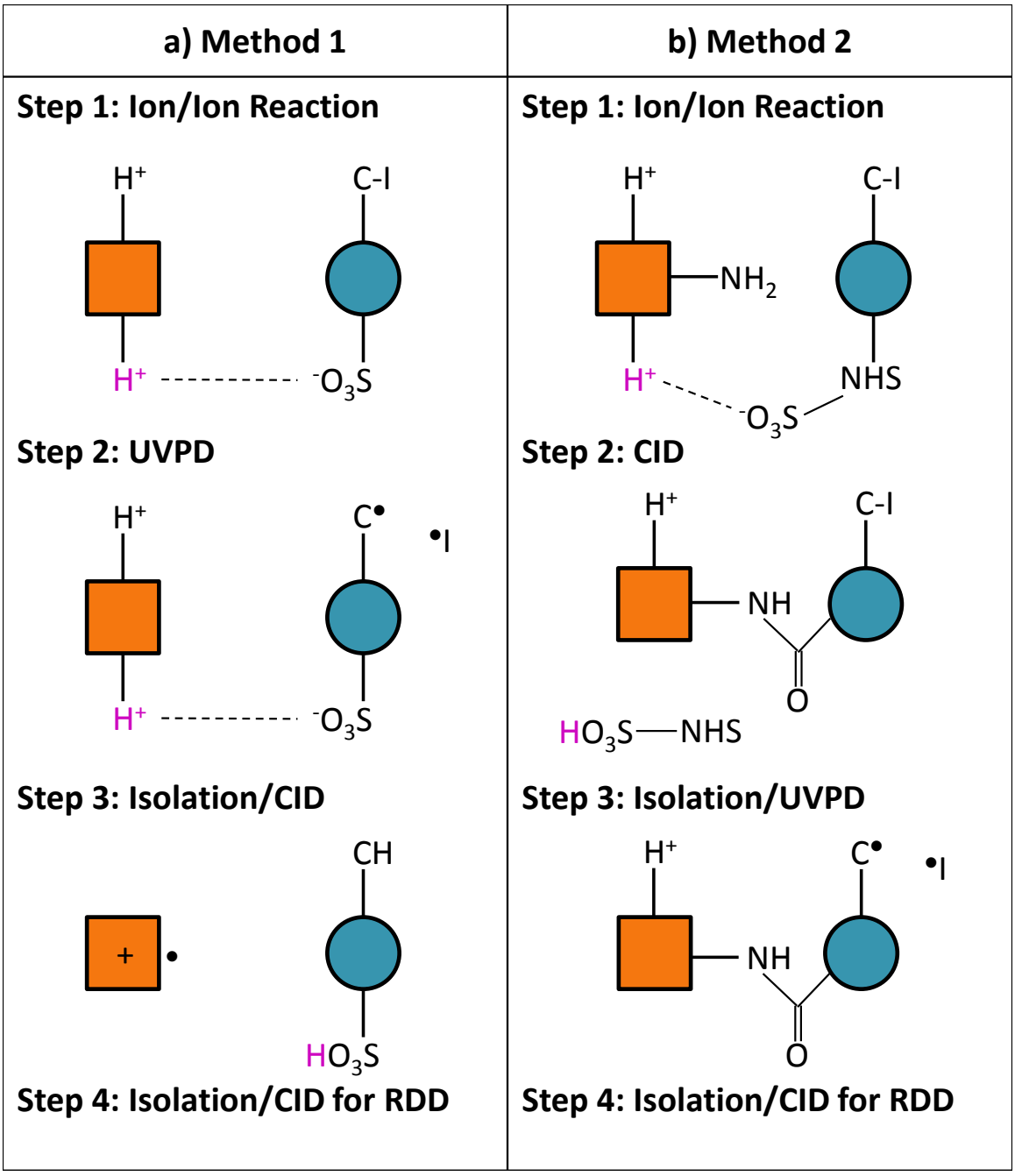

Figure 5.1 Depiction of the steps for each method in which ion/ion reactions and UVPD are combined to synthesize radical peptide ions for RDD. Method 1 consists of an ion/ion reaction to form an electrostatic complex, in which the peptide is not modified (a). Method 2 consists of an ion/ion reaction to form a covalently modified peptide (b).

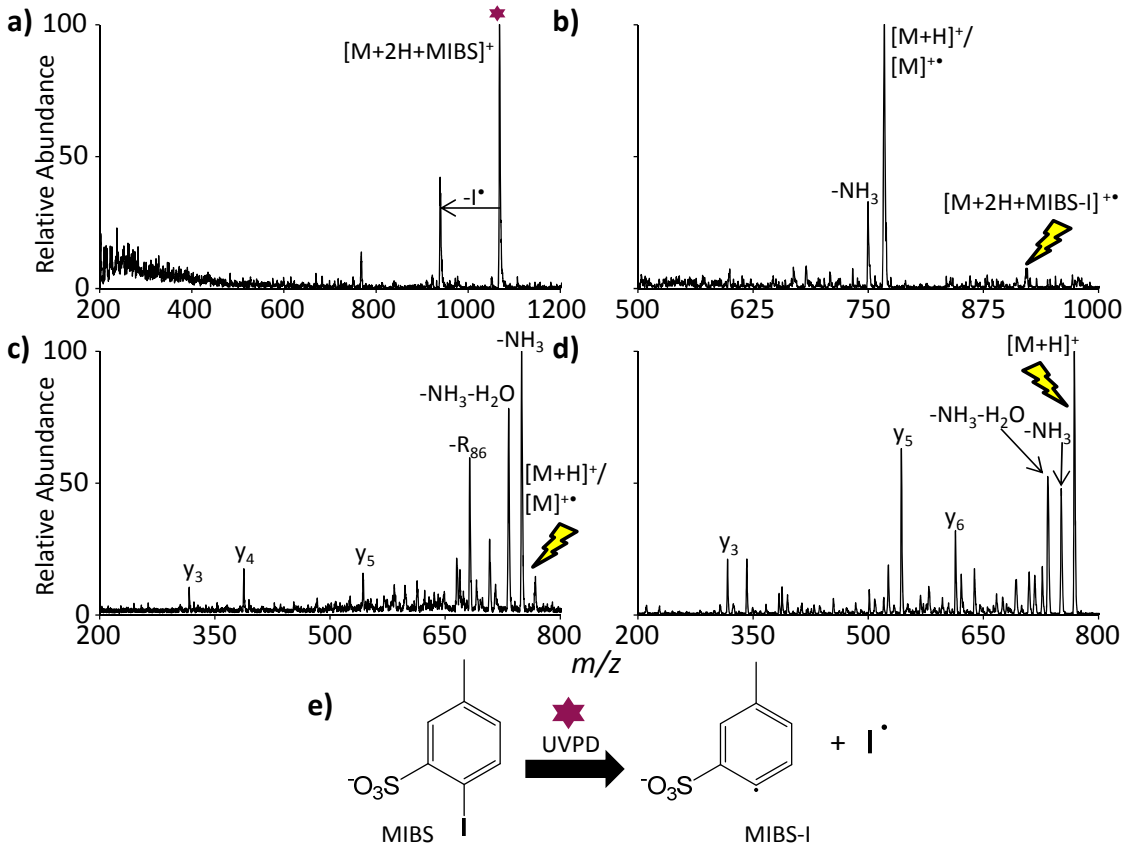

Figure 5.2 A stepwise demonstration of the generation of a radical peptide via UVPD of an electrostatic complex: UVPD of the electrostatic complex between RARARAA (M) and MIBS (a), CID of the resulting $I^{\bullet}$ loss (b), and CID of the radical peptide (c). CID of the even-electron peptide is given for comparison (d). The purple starburst indicates the species subjected to UVPD and the yellow lightning bolts indicate peaks subjected to CID.

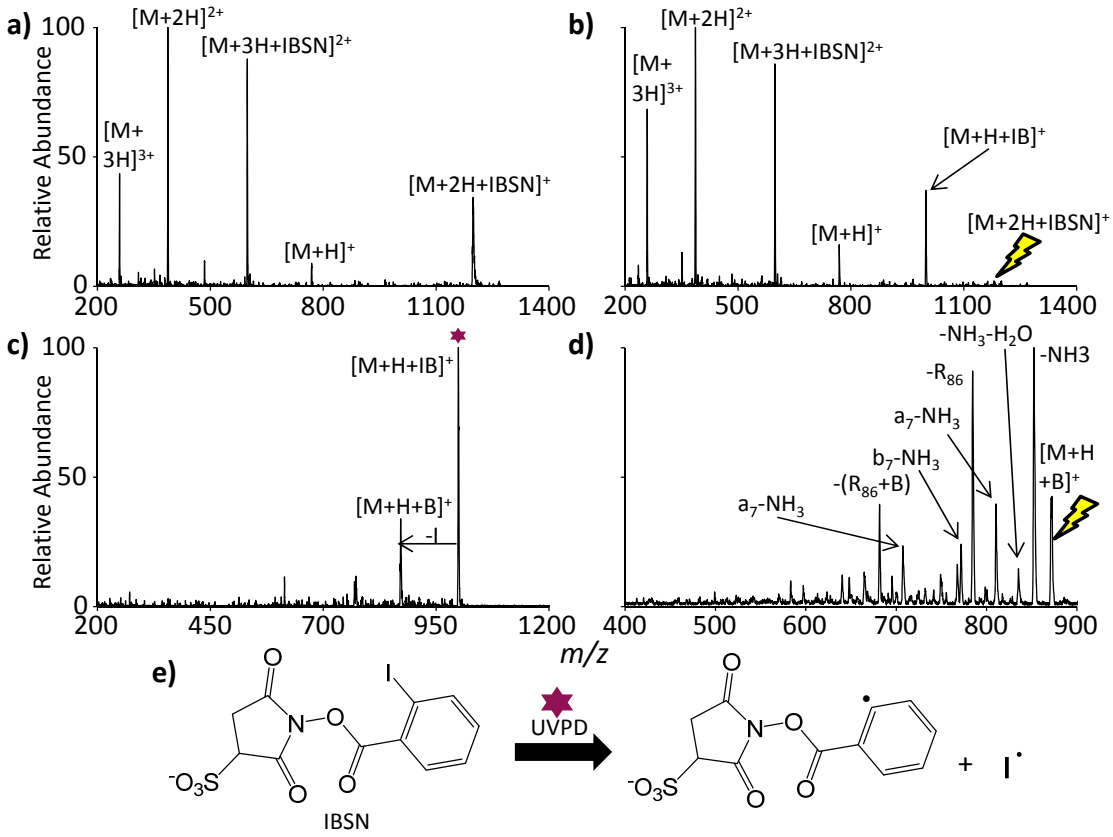

Figure 5.3 A stepwise demonstration of the generation of a radical peptide via UVPD after covalent modification: Ion/ion reaction of RARARAA (M) with IBSN (a), CID of the reaction complex (b), isolation and UVPD of the resulting covalently modified peptide (c), and CID of the resulting odd-electron modified peptide (d). The purple starburst indicates the species subjected to UVPD and the lightning bolts indicate the species subjected to CID.

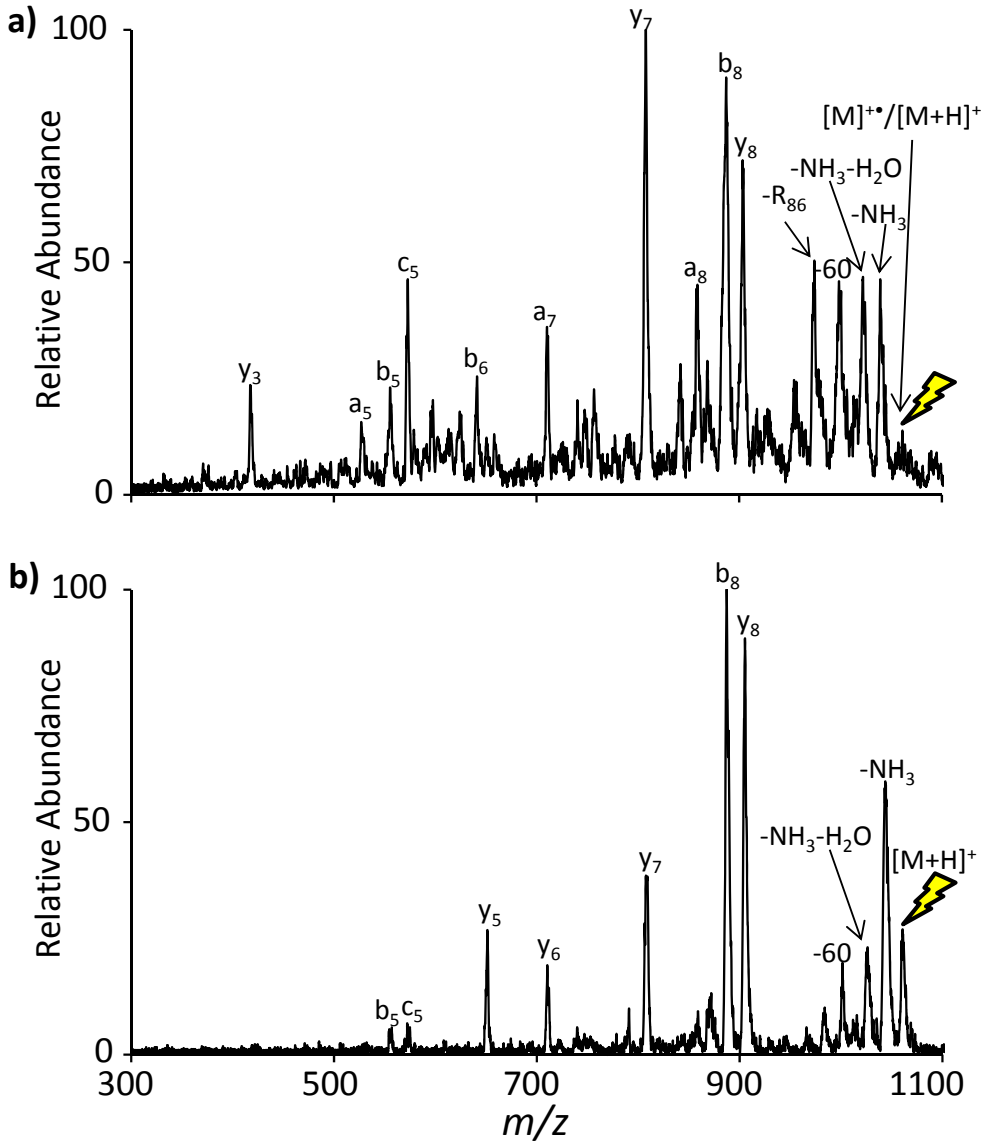

Figure 5.4 RDD of the radical cation of bradykinin (M) generated via UVPD of an electrostatic complex (method 1) between the peptide and MIBS (a). CID of the even electron peptide is also given for comparison (b).

CHAPTER 6. METHOD FOR THE ANALYSIS OF ION/ION REACTION KINETICS USING DIPOLAR DIRECT CURRENT COLLISION INDUCED DISSOCIATION (DDC-CID)

6.1 Introduction

Elucidating the primary structure of biomolecules has been a long sought-after goal.[1] Primary structures of biomolecules can give insight into how biological systems function and are regulated and thus can be useful in developing new methods for treating diseases and other health problems.[2] Tandem mass spectrometry (MS) experiments in which the parent peptide/protein ion is selected and sequentially fragmented have been instrumental in achieving this goal by helping identify proteins, perform *de novo* sequencing, and identify sites of post translational modifications (PTMs).[3] There are many fragmentation techniques that are commonly used including collision induced dissociation (CID),[4] electron capture dissociation (ECD),[5] electron transfer dissociation (ETD),[6] and infrared multiphoton dissociation (IRMPD),[7] and ultraviolet photodissociation (UVPD),[8] each of which provides complementary sequence information. The general mechanism involves the transfer of energy to the ionized protein or peptide via collisions with a bath gas (CID), via ion/electron interactions (ECD), ion/ion reactions in which an electron is transferred between the biomolecule and a reagent ion (ETD), or via absorption of photons (IRMPD).[9] This increases the internal

energy distribution of the ion causing it to fragment at various locations along the backbone, within side chains of the individual amino acids, and/or at near (PTM) sites.[9]

These fragmentation methods provide complementary sequence information as different fragment types are preferentially formed based on the ion type and form of activation. For example, CID usually forms b and y ions, while ECD and ETD usually form c and z ions.[9] Additionally, beam type CID was shown to preferentially fragment the glycosylation site of a glycopeptide while ETD maintained the site of glycosylation, forming only c and z fragments from the backbone of the peptide.[10] Most of these gas phase ion/ion reactions use a reagent to transfer electrons or protons to manipulate the ion type and thus the fragments obtained from the dissociation of biomolecules.

Solution phase derivatization of biomolecules has also been widely used to provide complementary fragmentation in biomolecules to enhance sequence and PTM site identification.[9] Recently the McLuckey group demonstrated that it is also possible to carry out chemical derivatization in the gas phase using various chemical reagents such as 4-formyl-1,3-benzene sulfonic acid derivatives[11] and N-hydroxysuccinimide ester derivatives.[12,13] Based on these experiments, both of these reagents are expected to react with the primary amines of basic amino acids including lysine (K) and arginine (R).

A typical ion/ion reaction involving covalent modification consists of a mutual storage step, where ions of opposite polarity interact with each other, which often results in either proton transfer or the formation of a long-lived reaction complex.[14] The reaction complex is then isolated from all precursor ions and subjected to CID, to yield two main products: proton transfer and covalent modification. The proton transfer

product is a result of proton transfer from the positively charged analyte to the negatively charged analyte which often results in neutralization of one of the ions such that the complex is no longer held together via Coulombic attraction of opposite charges. The covalent modification product is often the desired product in which the analyte has been modified by the reagent. For the Schiff base and sulfo-NHS reactions mentioned above, covalent modification is indicated by a signature loss of water and sulfo-NHS, respectively.[11,12,13] It is not known whether there is enough energy associated with the Coulombic attraction of ions of opposite polarity during an ion/ion reaction to induce chemistry upon complex formation, or if the subsequent CID step provides the additional energy necessary for the reaction to occur. For example, with reactions of protonated peptides with sulfo-NHS reagents, it is possible that the reagent reacts with the peptide upon complex formation, and the subsequent CID step is only responsible for the transfer of a proton from the analyte to the reagent and subsequent disruption of the ion/neutral interaction, which enables the loss of a neutral sulfo-NHS moiety. On the other hand, the CID step may provide the additional energy necessary for the reaction to occur, resulting in a loss of sulfo-NHS. This problem can be investigated by studying the kinetics of ion/ion reactions.

It is desirable to investigate the reaction kinetics for ion/ion reactions to better understand the reaction mechanisms, predict reaction sites in peptides and proteins, and to understand the relative reactivity of various reagents and biomolecular functional groups (i.e. amino acid side chains). A method for measuring peptide ion dissociation rates has been described by Goeringer *et al.*[15] In these studies, the rates of

dissociation of a protonated peptide, leucine enkephalin (YGGFL), were determined from mass spectra taken at various CID activation voltages and activation times using pseudo-first-order reaction kinetics. The equation representing pseudo-first-order reaction kinetics is given in equation 6.1:

$$[\mathrm{M}]_t = [\mathrm{M}]_0 e^{-kt} \quad (6.1)$$

where $[M]_t$ is the abundance of the ion at time *t* and *k* is the depletion rate of the ion. As Goeringer *et al.* have shown, $[M]_0$ can be calculated by summing the abundance of the precursor and all product ions, which normalizes the abundance of the complex to the total ion abundance in the mass spectrum to account for fluctuations in the electrospray.[15] Rearranging Equation 6.1 gives Equation 6.2, which shows how a plot of $ln([M]_t/[M]_0)$ vs. activation time (*t*) gives a slope of -*k*, which is the dissociation rate of the precursor ion.

$$ln\left(\frac{[M]_t}{[M]_0}\right) = -kt \quad (6.2)$$

These dissociation rate experiments[15] were performed using resonant CID, in which a dipolar ac waveform is applied to the ion trap that is in resonance with the secular frequency of the desired precursor ion. Fragmentation via resonant CID is highly dependent upon both the amplitude and the frequency of the ac waveform (i.e. how accurately does the supplementary ac frequency overlap with the secular frequency of the ion). It is possible to induce fragmentation of ions without exciting them at the exact resonance frequency, provided the amplitude and bandwidth is sufficient to cause off-resonance excitation. This aspect of resonant CID gives rise to poor reproducibility.

Recently, dipolar DC (DDC)-CID has been described as an alternative method for performing CID in both linear and 3D ion traps.[16,17] DDC-CID is performed by applying equal and opposite polarity DC potentials to either two rods of a rod pair in a linear ion trap, or to the two endcap electrodes in a 3D ion tap. Unlike resonant CID, DDC-CID is a broadband technique, which obviates the resonance condition and provides more reproducible results. When applied to ion dissociation kinetic studies, DDC-CID results in improved linearity due to improved reproducibility and due to the broadband nature of the technique.

This chapter will describe a method for measuring ion/ion reaction kinetics using a procedure similar to those previously used to measure ion dissociation kinetics. In addition, DDC-CID will be applied as a more reproducible ion dissociation technique when compared to resonance CID. The method will be demonstrated using an ion/ion reaction between doubly protonated KGAGGKGAGGKL and singly deprotonated sulfosuccinimidyl acetate (Sulfo-NHS-acetate). As this is an active area of investigation, future prospects for this research project will also be provided.

6.2 Experimental

6.2.1 Chemicals

Sulfosuccinimidyl acetate (Sulfo-NHS-acetate, SNa) and N-hydroxysulfosuccinimide (sulfo-NHS) were purchased from Thermo Scientific (Rockford, IL). The peptide KGAGGKGAGGKL was custom synthesized by NeoBioLab (Cambridge,

MA). Methanol was purchased from Macron Chemicals (part of Avantor, Center Valley, PA). Water was purified at 15 MΩ using a Barnstead nanopure infinity ultrapure water system from Thermo Fisher Scientific (Waltham, MA). Both the peptide and sulfo-NHS acetate used without further purification and were dissolved in water:methanol at a 1:1 ratio at a concentration of about 0.3 to 0.5 mg/mL.

6.2.2 Mass Spectrometry

All experiments were performed using a home-built, dual source 3D ion trap mass spectrometer that has previously been described.[18] The instrument was previously modified to allow for DDC-CID. Positive and negative ions were ionized and introduced into the 3D ion trap subsequently from separate nanoelectrospray ionization (nESI) sources. The ions were stored in the 3D ion trap simultaneously to allow for ion/ion reaction complex formation. The complex was then isolated from the unreacted precursor ions and from side products (i.e. proton transfer products). DDC-CID was performed at various DDC voltages (measured as the total voltage difference between the two end cap electrodes) and for various times and the resulting ion abundances were used to produce the kinetic plots as described below.

6.3 Results and Discussion

The steps of a typical ion/ion reaction including covalent modification are described in Figure 6.1 for the reaction between the doubly protonated peptide, KGAGGKGAGGKL ($[M+2H]^{2+}$) and singly deprotonated sulfo-NHS-acetate (SNa^-). The

doubly charged peptide was injected into the 3D trap and isolated (Figure 6.1a). The anions were subsequently injected into the 3D trap. Only one ion polarity can be isolated for an ion/ion reaction using this instrument, thus all anions present in the precursor anion spectrum (Figure 6.1b) can interact with the cations during mutual storage in the trap. The ion/ion reaction spectrum (Figure 6.1c) shows the remaining cation precursor, $[M+2H]^{2+}$, the proton transfer product, $[M+H]^{+}$, and the desired reaction complex, $[M+2H+SNa]^{+}$. The complex was then isolated and subjected to DDC-CID at various DDC voltages and for various activation times (see below). An example DDC-CID spectrum is given in Figure 6.1d, which was taken with a DDC voltage of 56 V for 80 ms. The complex peak is quite broad in the spectra. This is due to dissociation of the complex during the mass selective instability RF scan for mass analysis. The abundances of the complex, proton transfer (H^{+} xfer) and covalent modification (cov. mod.) peaks were determined by summing the intensities over the *m/z* range corresponding to the baseline width for each ion peak. The abundances of the complex and both products were determined for each spectrum similar to that given in Figure 6.1d taken at different DDC voltages and with different activation times. These abundances were used to make the kinetic plots described below.

6.3.1 Method for Measuring Ion/Ion Reaction Kinetics

The depletion rate of the complex is determined using a procedure similar to the unimolecular ion dissociation kinetics method described by Goeringer *et al.*[15] Equation 6.2 is used to find the rate of complex depletion where $[M]_t$ is the abundance of the

complex peak at time *t* ($[complex]_t$), $[M]_0$ is the sum of the abundances of the complex and all product ions in the spectrum, and *t* is the duration of the DDC-CID activation step for a given DDC voltage. The duration of the DDC-CID step is varied at a constant DDC voltage. The abundances of the complex and product peaks are measured for each spectrum at each DDC-CID time as described above. An excel macro was written to aid in the calculation of the abundances of all peaks in the spectra, although any programming software could be used to aid with these calculations. A plot of $ln([complex]/[complex+\Sigma products])$ vs. *t* yields a linear relationship (Figure 6.2a). A linear regression is performed to determine the slope of the line which corresponds to the complex dissociation rate (*k*) at that DDC voltage. The experiment is performed at various DDC voltages, which produces multiple dissociation lines, with different slopes (higher DDC voltages usually correspond to larger slopes/faster rates of complex dissociation).

Similar kinetic rate plots can be generated to determine the appearance rate of each product. Appearance rates are calculated similar to the procedure described by Vékey.[19] A reaction that results in two different products can be described according to Equation 6.3:

$$A \overset{k_1}{\leftarrow} M \overset{k_2}{\rightarrow} B \tag{6.3}$$

where *A* and *B* are two different products ions (i.e. proton transfer and covalent modification) that have appearance rates of k_1 and k_2, respectively and *M* represents the ion/ion reaction complex. The sum of the rates of appearance for all products is

equivalent to the rate of depletion of the precursor complex. Thus, the concentration of product *A* can be determined using Equation 6.4:

$$[A] = \left(\frac{k_1}{\sum k}\right)\left(1 - e^{-\sum kt}\right) \quad (6.4)$$

where *Σk* is the sum of all appearance rates, which is equal to the complex depletion rate (*k*), and *[A]* is the normalized abundance of *A* present in the mass spectrum (normalized similar to that described for the complex peak, $[M]_t/[M]_0$) Equation 6.4 can be rearranged to give Equation 6.5, which shows a linear relationship between *[A](Σk)* and *(1-[M])*. The slope of the linear relationship is equivalent to the appearance rate (k_1) for the product *A*:

$$[A](\sum k) = k_2(1 - [M]) \quad (6.5)$$

The same equation can be written for the appearance of product *B*, although only the equations for *A* are given here for simplicity. The appearance rate plots for the proton transfer and covalent modification products are given in Figure 6.2b and c, respectively.

6.3.2 Analysis of *k vs. DDC Voltage* Curves

The rates of complex depletion and product appearance can then be plotted vs. the corresponding DDC voltage to generate a "*k* vs. *E*" curve (Figure 6.3). It is important to note that the DDC voltage does not scale linearly with the ion internal energy (*E*), therefore this will be referred to as a *k* vs. *DDC Voltage* curve. This plot is very similar to those generated for unimolecular dissociation kinetics using RRKM theory.[20,21] There are

many molecules that have been studied via RRKM theory that show a competition between direct cleavages and cleavages that result in a rearrangement.[22] In many of these cases, it is possible to vary the dissociation energy and activation time such that different fragmentation products are favored. For example, direct cleavages tend to occur faster, but at higher energies than rearrangements. Thus rearrangement products can be favored at lower energies and longer activation times. Similarly, generating *k* vs. *DDC Voltage* plots from kinetic studies of ion/ion reaction complexes can provide insights into possible methods for varying the relative amount of proton transfer and covalent modification products.

A *k* vs. *DDC Voltage* curve for the reaction between KGAGGKGAGGKL and sulfo-NHS-acetate is given in Figure 6.3. As expected, the sum of the rates of appearance of proton transfer and covalent modification (green triangles) is roughly equivalent to the rate of complex depletion (purple x's) for all DDC voltages used. The rates of appearance for the proton transfer and covalent modification products are relatively similar at low DDC voltages. However, the rate of appearance of the proton transfer product increases more rapidly compared to the rate of appearance of the covalent modification product as the DDC voltage increases. The *k* vs. *DDC Voltage* curves for the appearance of proton transfer and covalent modification products suggest that performing DDC-CID at lower voltages (i.e. lower energy) for longer times is the optimal condition to favor the covalent modification product. It is not surprising that a covalent modification reaction would be slower than proton transfer reactions, as is indicated by these results.

Additionally, complex dissociation rates from different complexes (i.e. different ion/ion reactions) can be compared, provided the kinetic data was collected under the same conditions (i.e. same pressure). For example, an ion/ion reaction between the doubly protonated peptide KGAGGKGAGGKL and singly deprotonated sulfo-NHS was performed on the same day as the data given above (to ensure the same experimental conditions) and complex depletion rates were determined following the same procedure described for the reaction with sulfo-NHS-acetate. Figure 6.4 provides a comparison of the *k* vs. *DDC Voltage* curves for the dissociation of the peptide-sulfo-NHS complex (blue diamonds) and for the peptide-sulfo-NHS-acetate complex (red squares). The complex depletion rate for the reaction of the peptide with sulfo-NHS-acetate is a convolution of the rates associated with the chemical reaction and with proton transfer from the peptide to the reagent to neutralize the sulfo-NHS group. Therefore, it is not known which step may be rate limiting. Thus, the comparison between complex depletion rates with sulfo-NHS-acetate and sulfo-NHS is interesting because the reaction of sulfo-NHS with the peptide enables the measurement of the kinetics for dissociation of the electrostatic complex via proton transfer to the sulfo-NHS moiety in the absence of rates associated with covalent modification. As shown in Figure 6.4, the rates of depletion for both reactions are similar. Assuming the sulfo-NHS and sulfo-NHS-acetate are similarly “sticky,” this indicates that the proton transfer step may be the rate limiting step and it is possible that the covalent modification reaction occurs during the ion/ion reaction, prior to applying additional heating via CID. If the covalent modification required additional energy (via CID) to occur, and/or was the rate limiting step, then the

rate of complex depletion for sulfo-NHS-acetate would be expected to be slower than that for the complex with sulfo-NHS. There may be some indication of this at the highest DDC voltage used in this data set (i.e. 62 V). Additional work on other systems is currently underway to more definitively answer this question.

6.4 Conclusions

The methods described here can be used to generate k vs. *E* curves for various ion/ion reactions. These curves can be plotted for the appearance rates of two different products, which provides information regarding the competition of the two reactions and may indicate the ideal activation conditions to favor the desired product. Additionally, the comparison of complex depletion rates between different ion/ion reactions can be used to isolate the kinetic rates correspond to certain steps of a multi-step process.

This is an active research project in the McLuckey group. Several systems (different peptides and sulfo-NHS reagents) have been investigated and in many cases have resulted in ambiguous results. However, we have recently investigated the ion/ion reaction between doubly protonated KGAGGKGAGGKL and the singly deprotonated reagets, benzoate-sulfo-NHS (BSN) and sulfo-benzoate-NHS (SBN). The two reagents differ in the location of the sulfonate "sticky" group. For BSN, the sulfonate group is attached to the NHS moiety such that the leaving group will remain electrostatically bound after the reaction occurs. On the other hand, in SBN, the sulfonate group is attached to the benzene group such that the NHS leaving group will not be

electrostatically bound after reaction. This is another method to distinguish the rates associated with covalent modification and proton transfer. Additionally, BSN can be reacted with the peptide in solution to generate the benzene modified peptide. An ion/ion reaction between the modified peptide and sulfo-NHS provides an electrostatically bound complex that should be structurally similar to that generated during the ion/ion reaction between the peptide and BSN after the reaction has occurred. Thus, these reaction rates can be compared to determine if the reaction has occurred prior to the CID step or if the CID step is necessary to provide sufficient energy for the reaction to occur.

The method for measuring ion/ion reaction kinetics described here can be applied to the other ion/ion reaction chemistries that are currently being investigated in the McLuckey group to provide insights for improving reaction efficiencies. The information obtained in these kinetic studies can be combined with density functional theory calculations to determine the energy surface of ion/ion reactions.

6.5 References

[1] Aebersold, R.; Mann, M. *Nature* **2003**, *422*, 198-207.

[2] Patterson, S. D.; Aebersold, R. H. *Nat. Gen. Supp.* **2003**, *33*, 311-323.

[3] De Hoffman, E.; Stroobant, V. *Mass Spectrometry: Principles and Application*, 3rd ed.; John Wiley & Sons, Ltd.: West Sussex, England, 2009.

[4] Wells, J. M.; McLuckey, S. A. *Method. Enzymol.* **2005**, *402*, 148-185.

[5] Zubarev, R. A.; Kelleher, N. L.; McLafferty, F. W. *J. Am. Chem. Soc.* **1998**, *120*, 3265-3266.

[6] Syka, J. E. P.; Coon, J. J.; Schroeder, M.; Shabanowitz, J.; Hunt, D. F. *P. Natl. Acad. Sci. USA* **2004**, *101*, 9528-9533.

[7] Little, D. P.; Speir, J. P.; Senko, M. W.; O-Connor, P. B.; McLafferty, F. W. *Anal. Chem.* **1994**, *66*, 2809-2815.

[8] Tureček, F.; Julian, R. R. *Chem. Rev.* **2013**, *113*, 6691-6733.

[9] Huang, T.; McLuckey, S. A. *Ann. Rev. Anal. Chem.* **2010**, *3*, 365-385.

[10] Han, H.; Xia, Y.; Yang, M.; McLuckey S. A. *Anal. Chem.* **2008**, *80*, 3492-3497.

[11] Hassell, K. M.; Stutzman, J. R.; McLuckey, S. A. *Anal. Chem.* **2010**, *82*, 1594-1597.

[12] Mentinova, M.; McLuckey, S. A. *J. Am. Chem. Soc.* **2010**, *132*, 18248-18257.

[13] McGee, W. M.; Mentinova, M.; McLuckey, S. A. *J. Am. Chem. Soc.* **2012**, *134*, 11412-11414.

[14] Prentice, B. M.; McLuckey, S. A. *Chem. Comm.* **2013**, *49*, 947-965.

[15] Goeringer, D. E.; Asano, K. G.; McLuckey, S. A. *Int. J. Mass Spectrom.* **1998**, *182/183*, 275-288.

[16] Webb, I. K.; Londry, F. A.; McLuckey, S. A. *Rapid Commun. Mass Spectrom.* **2011**, *25*, 2500-2510.

[17] Prentice, B. M.; Santini, R. E.; McLuckey, S. A. *J. Am. Soc. Mass Spectrom.* **2011**, *22*, 1486-1492.

[18] Wells, J. M.; Chrisman, P. A.; McLuckey, S. A. *J. Am. Soc. Mass Spectrom.* **2002**, *13*, 614-622.

[19] Vékey, K. *Int. J. Mass Spectrom.* **1996**, *31*, 445-463.

[20] Rosenstock, H. M.; Wallenstein, M. B.; Wahrhaftig, A. L.; Eyring, H. *Proc. Natl. Acad. Sci. USA* **1952**, *38*, 667-678.

[21] Marcus, R. A. *J. Chem. Phys.* **1952**, *20*, 359-364.

[22] Sleno, L.; Volmer, D. A. *J. Mass Spectrom.* **2004**, *39*, 1091-1112.

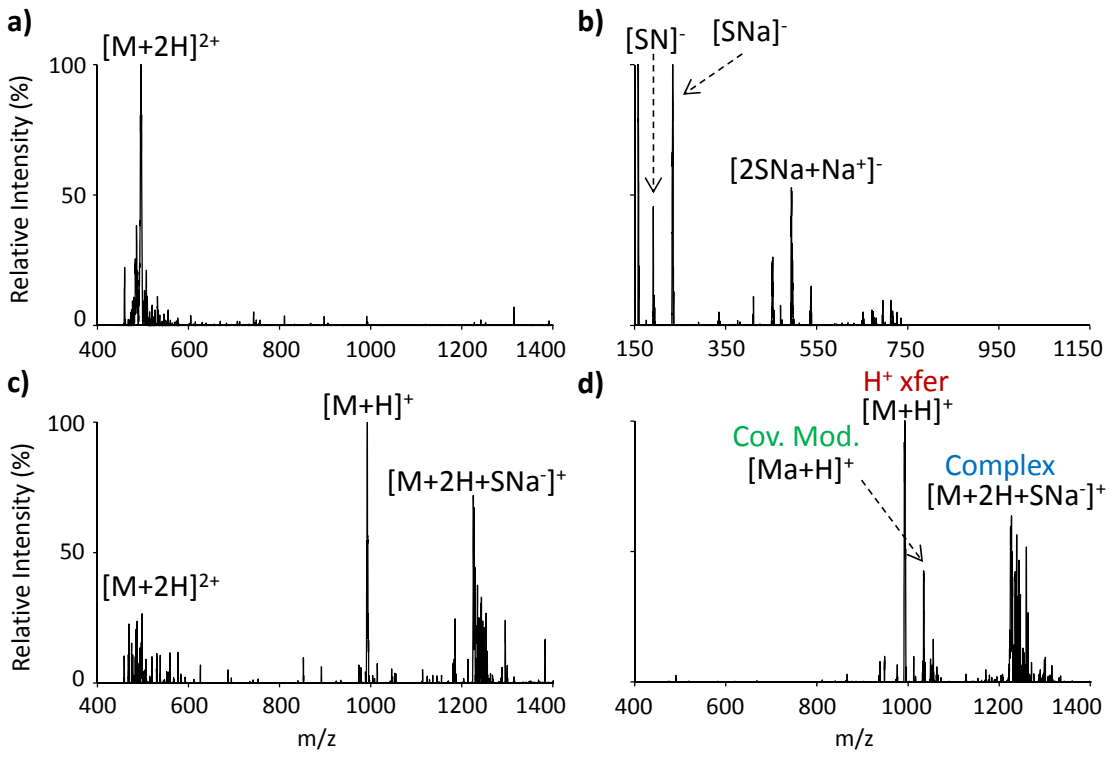

Figure 6.1 Mass spectra depicting the process for generating a covalently modified peptide via an ion/ion reaction. The doubly protonated peptide KGAGGKGAGGKL (M) is isolated (a) and anions produced by –nESI of sulfo-NHS-acetate (SNa^-) are introduced into the trap (b) where they react with the cations (c). The reaction complex (Complex, $[M+2H+SNa^-]^+$, blue) is then isolated and subjected to DDC-CID to produce a proton transfer (H^+ xfer, $[M+H]^+$, red) and a covalently modified peak (Cov. Mod., $[Ma+H]^+$, green) (d). SN indicates sulfo-NHS.

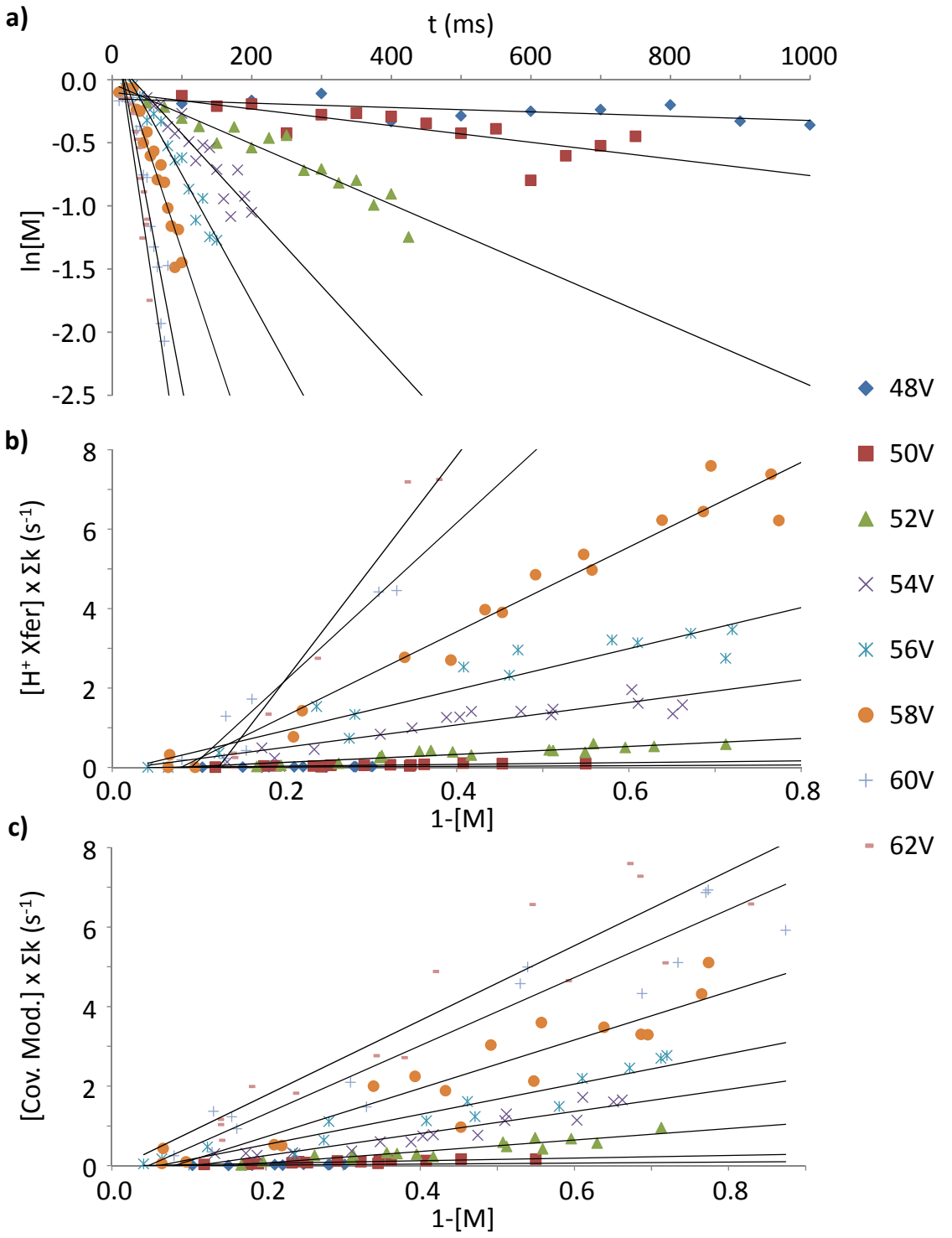

Figure 6.2 Kinetic plots for the depletion of the ion/ion reaction complex ($[M+2H+SNa^-]^+$) (a) and the appearance of the proton transfer product (H^+ xfer, $[M+H]^+$) (b) and covalent modification product (Cov. Mod., $[Ma+H]^+$) (c) upon DDC-CID at the specified voltage and time.

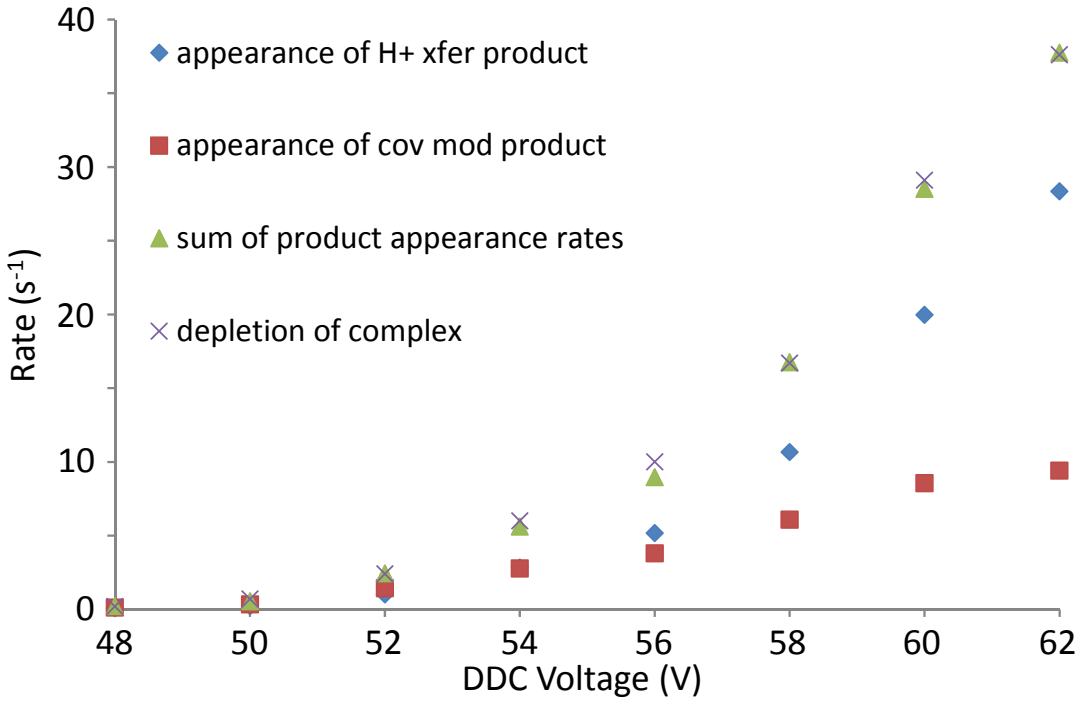

Figure 6.3 Plot of the rates of appearance of the proton transfer (blue diamonds) and covalent modification products (red squares) and rate of depletion of the complex (purple x's) vs. DDC voltage. Rates were determined from the slopes of the linear fits in Figure 6.2. The sum of the rates of appearance for the products (green triangles) is also given for comparison to the rate of depletion.

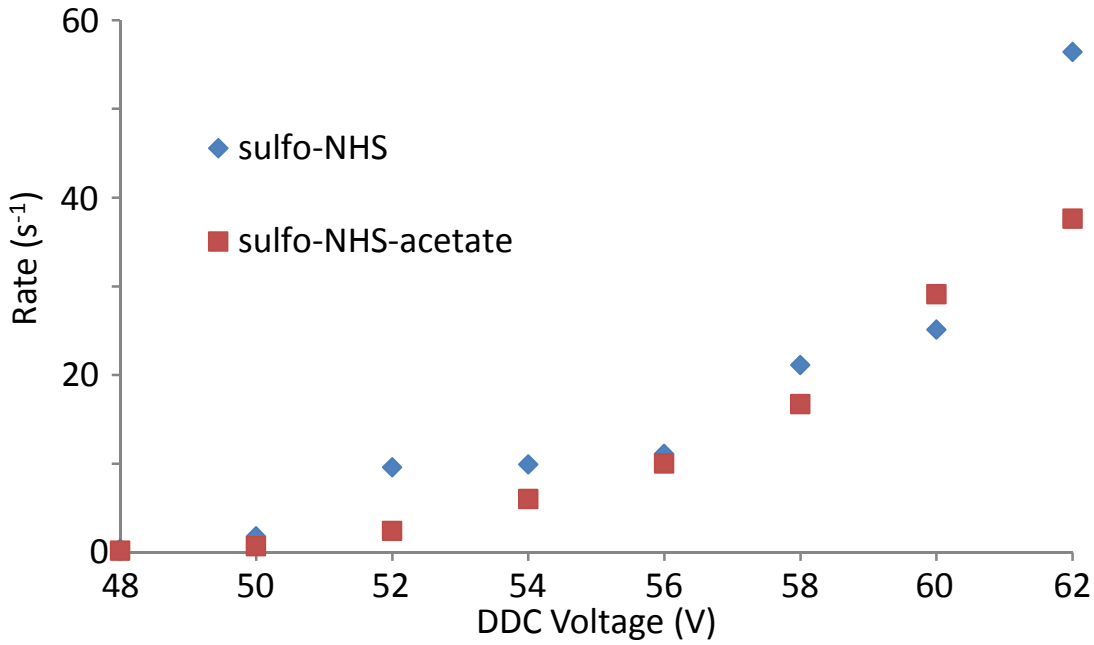

Figure 6.4 Rates of depletion for complexes of the peptide KGAGGKGAGGKL with sulfo-NHS (blue diamonds) and with sulfo-NHS-acetate (red squares).

APPENDIX

APPENDIX

VAPOR TREATMENT OF NANO-ELECTROSPRAY DROPLETS: DETERMINATION OF DROPLET PH

Background: A leak-in system was previously developed by Kharlamova *et al.* to introduce chemical vapors to the interface of a PE/Sciex API QSTAR *Pulsar i* QqTOF mass spectrometer between the curtain plate and the orifice.[1] Briefly, the leak-in set-up consists of a Nitrogen gas flow over a test tube containing a solution of the chemical to be vaporized. As the nitrogen flows over the chemical, it entrains the vapors which are then carried toward the interface where they are further diluted by the curtain gas, a secondary flow of nitrogen just prior to entering the interface.

Initially acidic vapors were used introduced to decrease the amount of metal counter-ions present in spectra for DNA, siRNA, and LNA.[1] More recently, Kharlomova *et al.* have demonstrated that it is possible to alter charge state distributions (CSD) of proteins through the interaction of acidic and basic leak-in vapors with nano-electrospray droplets.[2,3,4] This work has demonstrated that in positive mode the CSD can be shifted to higher charge states upon the leak-in of acids while the leak-in of bases results in lower CSDs.[2,4] Similarly, in negative mode the leak-in of bases results in a shift to a higher CSD[3] and the leak-in of acids leads to a shift to lower charge states.[4] The changes in CSD for various proteins have implied the folding and unfolding of proteins in

which more unfolded proteins can carry more charge resulting in a higher CSD, while more folded proteins carry fewer charges due to Coulombic repulsion resulting in lower CSD's. Similar experiments were performed using nano electrospray ionization (nESI) to generate protein ions from a buffered solution, in which no change in CSD was observed. This supports the authors' hypothesis that the change in CSD is attributed to a pH effect.

It is important to understand the mechanisms of the leaked-in vapor interaction with ions as they are being formed in the interface for reproducibility and to explain the observed phenomenon. Previous studies lead to the conclusion that the observed shifts in CSD are due to a droplet/vapor interaction as opposed to an ion/molecule interaction. Ultimately it is important to develop a mathematical model to describe the effect of the leak-in on the electrospray droplets. Having attributed the effect of the leaked-in acidic/basic vapors to a pH effect, it is important to determine and predict the effective pH of the electrospray droplets with various leak-in reagents. A mathematical model was developed by Prentice *et al.* to calculate the pH of electrospray droplets during the leak-in experiments. The titration experiments described below were used to experimentally test the concentration of acidic vapors in the interface for use with the mathematical model.

Experimental:

Materials: Hydrochloric acid (HCl) was purchased from J.T. Baker (36.5-38.0%, Phillipsburg, NJ). Acetic acid was purchased from (Mallinckrodt Chemicals, Phillipsburg, NJ). Trifluoroacetic acid (TFA) was purchased from Pierce Chemicals (Rockford, IL).

Formic acid was purchased from EM Science (Darmstadt, Germany). Sodium hydroxide (NaOH) was purchased from Mallinckrodt Chemicals (Phillipsburg, NJ). A ~10M NaOH solution was diluted with nano-pure water (obtained from a nano-pure infinity water purifier purchased from Barnstead/Thermo Scientific; Rockford, IL) to the desired concentration using a volumetric flask. The pH 4, 7, and 10 standard solutions were purchased from Aldrich Chemical Company Inc. (St. Louis, MO). The leaked-in acids were not diluted prior to being placed in the leak-in test tube/flask.

Instrumentation: Nitrogen gas was used to entrain headspace vapors of HCl, TFA, or formic acid contained in a test-tube or flask. A flowmeter purchased from OMEGA Engineering Inc. (Stamford, CT) was used to monitor the total flow rate of leaked-in HCl, TFA, or FA vapors and nitrogen gas. The flow was adjusted to a flow rate of about 1.0-1.5 L/min by varying the nitrogen tank regulator and two Swagelok leak valves. An ORION PerpHecT Log R Meter Model 320 pH meter (OMEGA Engineering Inc., Stamford, CT) and glass electrode were used for titrations and the pH was monitored and recorded manually.

Results: A titration method was developed and used to determine the number densities of the acid molecules that are being leaked into the interface of the QSTAR mass spectrometer during leak-in experiments. The leak-in system was removed from the interface of the QSTAR and the end of the leak-in tubing was submerged in a jar of nano-pure water as shown in Figure A.1. The nitrogen gas was turned on and the flow both before and after the leak-in test tube was controlled via two Swagelok leak valves.

A flow meter was placed just before the end of the leak-in tubing to maintain a flow rate of about 0.499-1.5 L/min. The leak-in was bubbled into a jar of nano-pure water for a designated time (usually about 1hr), then titrated to determine the concentration of the leaked-in acid. Both HCl and acetic acid were used for the leaked-in/bubbled titrations. The acidic samples were titrated with varying concentrations of NaOH.

The mole fraction of acid molecules was calculated using Henry's Law and Dalton's Law given below in equations A.1 and A.2, respectively, where P_A is the partial pressure of acid *A* (where acid *A* is either HCl or acetic acid) in the headspace above a solution of concentration C_A, K_H is Henry's Law constant for acid *A*, X_A is the mole fraction of acid *A* in solution, and P_{total} is the total pressure of the system. A range of K_H values for each acid were obtained from those reported on the NIST chemistry web book.[5] The total pressure, P_{total} was assumed to be 1 atmosphere. The acids in the test tube were not diluted and the solution concentration was obtained from the stock bottle. The mole fraction of the acid was calculated using the aforementioned values and Henry's and Dalton's Laws.

$$P_A = K_H * C_A \qquad (A.1)$$

$$P_A = X_A * P_{total} \qquad (A.2)$$

The total moles in the mole fraction was assumed to be ~100% N_2 as the moles of acidic vapors would be relatively low compared to the moles of nitrogen flowing through the leak-in set-up. With this assumption, the molecular weight and density of nitrogen were used to determine the moles of acid *A* per liter of gas in the leak-in system. The flow rate was then used to determine the number of moles of acid *A*

flowing through the tubing per minute. Given a monitored time of bubbling the leaked-in vapors into a given volume of water in a jar (usually 20 mL), the expected concentration of acid molecules in the water was determined.

The bubbled leak-in experiments were typically run for about 1 hour of bubble time into 20 mL of water. The sample was then titrated with NaOH and the concentration was calculated from the concentration and volume of base added at the equivalence point. The equivalence point was determined from the maximum of the first derivative of the titration curve which is given in the plot with the corresponding titration curve in Figure A.2. Figure A.2a and d show the titration curves obtained for HCl and acetic acid leak-ins using the test tube set-up depicted in Figure A.1, respectively. Table A.1 compares the acid concentrations determined from the titration curves to the expected concentration based on the Henry's Law calculation described above with the corresponding conditions.

As can be seen in Table A.1, the concentrations calculated from the titrations in Figure A.2a and d are much lower than the predicted range using Henry's and Dalton's Laws. In addition, the titration curves depicted in Figure A.2a and d have very shallow equivalence points, indicative of very low concentrations. Under these conditions, the titrations are being operated near the limit of detection for a titration. For example, the titrations with HCl often showed two faint equivalence points as can be seen in Figure A.2a. The second equivalence point likely corresponds to the equivalence point for carbonic acid present in the water due to the partitioning of carbon dioxide from the air to the solution. It was hypothesized that the small surface area of the acid solution in

the test tube could explain the discrepancy between calculated and experimental concentrations and the low concentrations obtained with the titrations. To test this hypothesis, a stoppered Erlenmeyer flask was used in place of the test tube, as depicted in Figure A.3, which provides a much larger surface area for the acid molecules to partition between the solution phase and the vapor phase in the headspace. As hypothesized, the larger surface area of the flask resulted in a more concentrated bubbled solution, with a more distinct equivalence point as was observed in Figure A.2b and e. Switching the leaked-in acid vessel also gave titration concentrations within the range of predicted values using Henry's Law. Note, the upper bound concentration predicted from Henry's Law for HCl is not realistic. There is a wide range of reported values for Henry's Law constants for HCl, as can be seen in the NIST Chemistry webBook, and it has been reported that some values used to determine Henry's Law constants are difficult to measure for strong electrolytes such as HCl.

In an effort to determine the maximum concentration that could be obtained, the leak-in set-up with the flask was also used to purge the acidic solution in the flask. This was done by extending the inlet tubing into the flask until the end was submerged in the acidic solution and began bubbling, as indicated by the dotted lines and bubbles in Figure A.3. The titration curves resulting from this leak-in experiment are given in Figure A.2c and f for HCl and acetic acid leak-ins, respectively. The concentration obtained from these titration curves are also given in Table A.1 with the expected concentration range calculated using Henry's Law. As indicated in Table A.1 for acetic acid, the concentration obtained from the titration curve was higher (1.379M) than the

upper-bound of the expected concentration range (1.305M). This is to be expected considering that purging the leaked-in acid solution with a flow of nitrogen brings the experiment outside the range of Henry's Law; which is applicable for determining the headspace concentration of static solutions. However, these findings suggest that using the purging flask set-up could enable the use of chemical vapors in the leak-in that have lower vapor pressures.

The ultimate goal of determining these concentrations is to convert them into number density in the interface of the QSTAR mass spectrometer. The number density is calculated via dimensional analysis using the flow rate, bubble time, volume of water bubbled into, and concentration from the titration curve to obtain the number of molecules per cm^3. The number density is then converted to a partial pressure using the conversion factor: $1molecule/cm^3 = 3 \times 10^{16}$ torr. The calculated partial pressure has been incorporated into a leak-in model that was developed by a fellow lab member using an iterative program in MathCAD. The model is based off of a model previously developed by Schwell *et al.*, in which the concentration of HCl dissolved in a levitated droplet in a 3D trap was determined as HCl vapors were leaked into the trap.[6] The model Schwell *et al.* developed is given in equation A.3 below, where dn^{liq}_{HCl}/t is the growth rate of the droplet due to increased HCl molecule number density inside the droplet with time, r_0 is the initial droplet radius, D^{*}_{HCl} is the "effective diffusion constant" of HCl in the gas-phase and in passage to the solution phase, D^{gas}_{HCl} is the diffusion coefficient of HCl in the gas phase, p^{∞}_{HCl} is the partial pressure of HCl at an infinite distance from the droplet (the calculated partial pressure of HCl in the interface from

the titration data was used for this value), p^{vap}_{HCl} is the vapor pressure of HCl in the droplet, k is the Boltzmann constant, T is the temperature in Kelvin, v_{HCl} is the mean thermal velocity of HCl in the gas phase, and α is an accommodation coefficient (given as 10^{-2} by Schwell *et al.*).[6]

$$\frac{dn^{liq}_{HCl}}{dt} = \frac{3D^{*}_{HCl}}{kTr_0^2}\left(p^{\infty}_{HCl} - p^{vap}_{HCl}\right) \tag{A.3}$$

$$D^{*}_{HCl} = \frac{D^{gas}_{HCl}}{1+{}^{4D^{gas}_{HCl}}\!/_{\alpha\bar{\vartheta}_{HCl}r_0}} \tag{A.4}$$

References:

[1] Kharlamova, A.; Prentice, B. M.; Huang, T.; McLuckey, S. A. *Int. J. Mass Spectrom*. **2011**, *300,* 158-166.

[2] Kharlamova, A.; Prentice, B. M.; Huang, T.; McLuckey, S. A. *Anal. Chem.* **2010**, *82*, 7422-7429.

[3] Kharlamova, A.; Prentice, B. M.; Huang, T.; McLuckey, S. A. *Anal. Chem.* **2011**, *83*, 431-437.

[4] Kharlamova, A.; DeMuth, J. C.; McLuckey, S. A. *J. Am. Soc. Mass Spectrom.* **2011**, *23*, 88-101.

[5] Sander, R. "Henry's Law Constants" in NIST Chemistry WebBook, NIST Standard Reference Database Number 69, Eds. P. J. Linstrom and W. G. Mallard, National Institute of Standards and Technology, Gaithersburg MD, 20899, http://webbook.nist.gov, (retrieved April 26, 2012).

[6] Schwell, M.; Baumgärtel, H.; Weidinger, I.; Krämer, B.; Vortisch, H.; Wöste, L.; Leisner, T.; Rühl, E. *J. Phys. Chem.* **2000**, *104*, 6726-6732.

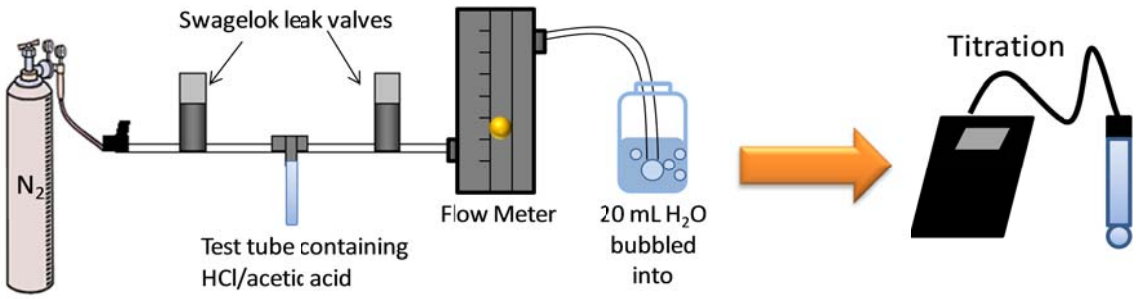

Figure A.1. Schematic for the test-tube leak-in system bubbled into a jar of nano-pure water.

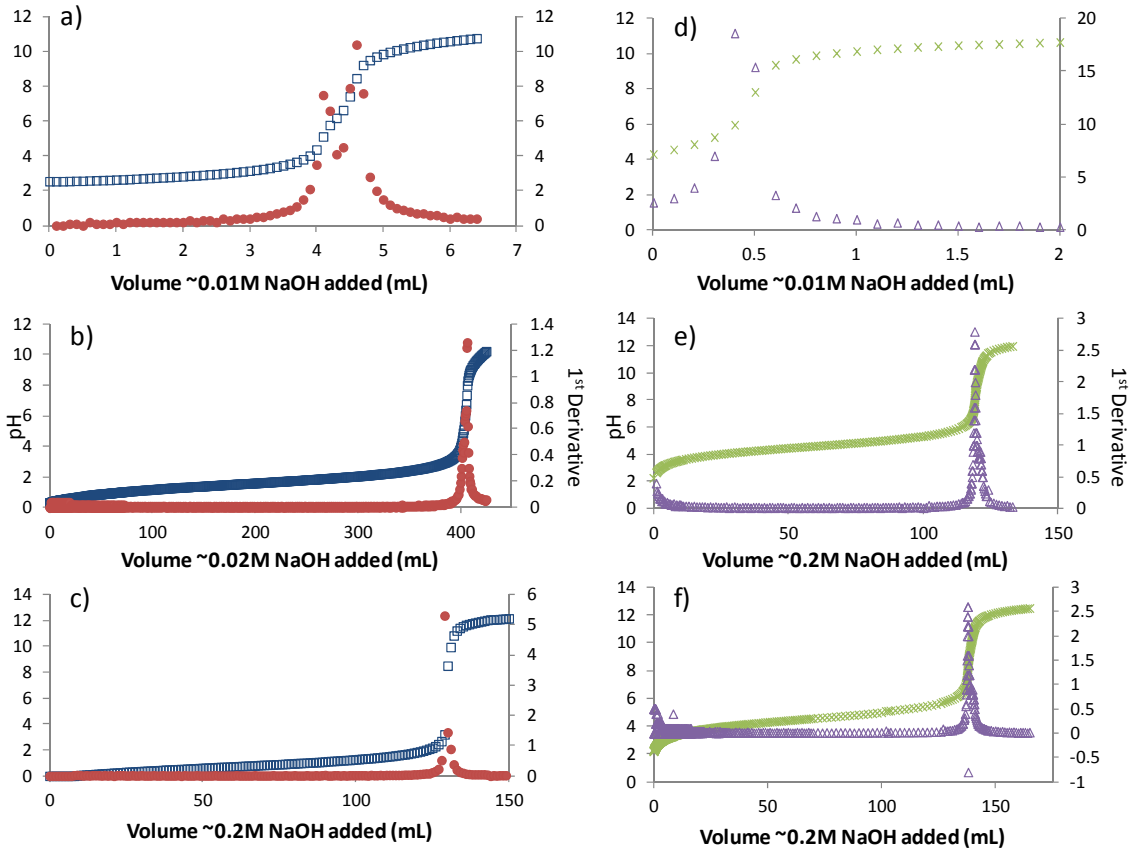

Figure A.2. Titrations of HCl using the test tube (a), flask (b), and purged flask (c) set-ups. Similarly titrations were performed for acetic acid with the test tube (d), flask (e), and purged flask (f) set-ups. Symbols: □ = HCl titration curve, ● = 1st derivative of HCl titration curve, × = acetic acid titration curve, Δ = 1st derivative of acetic acid titration curve

Table A.1. Summary of leak-in titration data including conditions for each leak-in, titrated concentration, and predicted range of concentrations using Henry's Law[31].

Titration Curve as labeled in Figure #	Composition of Leak-In	Flow Rate (converted from flow meter L/min)	Time Bubbled (min)	~Conc. from Titration (M)	Expected Conc. Range from Henry's Law (M)	
a	N_2/HCl	1.03	60.058	0.00205	0.637	1448.495
b	N_2/HCl	0.499	60.040	0.4065	0.309	701.532
c	N_2/HCl	0.499	60.000	1.29	0.308	701.065
d	N_2/acetic acid	1.03	60.037	0.0002	0.224	2.695
e	N_2/acetic acid	0.499	60.037	1.19	0.108	1.306
f	N_2/acetic acid	0.499	60.000	1.379	0.108	1.305

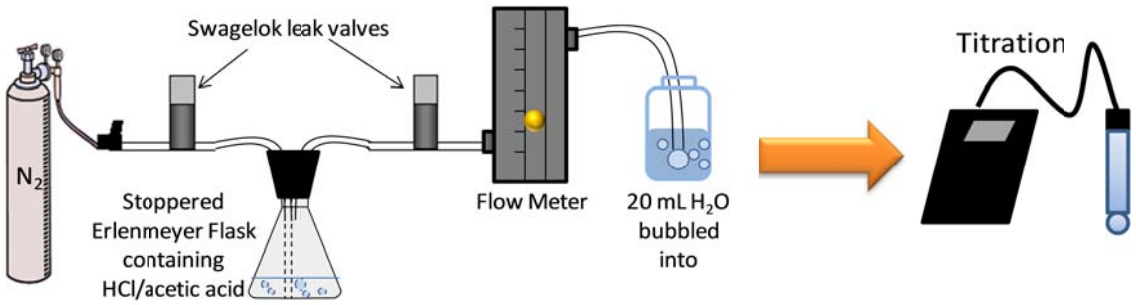

Figure A.3. Leak-in set-up with the flask. The dotted lines show the purged flask set-up in which the inlet tube to the flask is placed below the surface of the acid solution in the flask, and the flow of nitrogen is bubbled into the flask.

VITA

VITA

Christine Marie Fisher was born on September 12, 1988 in Cheyenne, WY. She is the only daughter of Patricia and James Fisher and she has one brother named James C. (J.C.) Fisher. Her father was an officer in the United States Air Force until April 2014. She has lived in several states due to the military lifestyle, including: Wyoming (Cheyenne), Utah (Salt Lake City), Virginia (Woodbridge), Colorado (Colorado Springs), and California (Sand Pedro/El Segundo). She graduated from Woodbridge Senior High School in Woodbridge, VA in June 2006. She moved to Athens, Ohio to attend Ohio University, where she studied forensic chemistry. She had the distinct honor to work with Professor Glen P. Jackson performing simulations for a Loeb-Eiber mass filter using SIMION to be incorporated in a miniaturized mass spectrometer. While at Ohio University, Christine served as a resident assistant and an administrative resident assistant, was a member of Alpha Chi Sigma, and was a teaching assistant for general chemistry. She obtained her Bachelor of Science in Forensic Chemistry with a minor in Biology in June 2010. She then enrolled in the graduate program at Purdue University where she joined Professor Scott McLuckey's research group. During her tenure at Purdue, Christine has been involved with Phi

Lambda Upsilon, the Women in Science Program, and has been elected to several officer positions for Iota Sigma Pi (Social Chair, Secretary, Outreach Co-Chair, and Vice President) and the Graduate Student Advisory Board (Analytical Representative, Newspaper Editor and Co-Chair). She defended her PhD in March 2015 and will begin working as a Senior Scientist in Chemistry at Merck in April 2015.

PUBLICATIONS

PUBLICATIONS

Fisher, C. M.; Hilger, R. T.; Zhao, F.; McLuckey, S. A. “Electroosmotically-controlled solution mixing in borosilicate theta glass nESI emitters.” *J. Mass Spectrom.* **2015**, Submitted.

Gilbert, J. D.; Fisher, C. M.; Bu, J.; Prentice, B. M.; Redwine, J. G.; McLuckey, S. A. “Strategies for generating peptide radical cations via ion/ion reactions.” *J. Mass Spectrom*. **2015**, *50*, 418-426.

Kharlamova, A.; Fisher, C. M.; McLuckey, S. A. “Hydrogen/deuterium exchange in parallel with acid/base induced protein conformational change in electrospray droplets.” *J. Mass Spectrom*. **2014**, *49*, 437-444.

Fisher, C. M.; Kharlamova, A.; McLuckey, S. A. “Affecting protein charge state distributions in nano-electropsray ionization via in-spray solution mixing using theta capillaries.” *Anal. Chem*. **2014**, *86*, 4581-4588.

analytical chemistry

Article

pubs.acs.org/ac

Affecting Protein Charge State Distributions in Nano-Electrospray Ionization via In-Spray Solution Mixing Using Theta Capillaries

Christine M. Fisher, Anastasia Kharlamova, and Scott A. McLuckey*

Department of Chemistry, Purdue University, 560 Oval Drive, West Lafayette, Indiana 47907-2084, United States

Supporting Information

ABSTRACT: Borosilicate theta glass capillaries pulled to serve as nano-electrospray ionization emitters are used for short time-scale mixing of protein and acid solutions during the electrospray process to alter protein charge state distributions (CSDs) without modifying the sample solution. The extent of protein CSD shifting/denaturing can be tailored by acid identity and concentration. The observed CSD(s) are protein dependent, and the short mixing time-scale enables the study of short-lived unfolding intermediates and higher charge states of noncovalent protein complexes, including those of holomyoglobin. Additionally, the theta tips provide a simple and inexpensive method for mixing nonvolatile reagents such as supercharging agents, which cannot be used with previously developed vapor leak-in techniques, with protein solutions during the electrospray process.

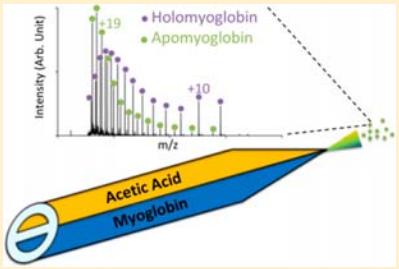

Electrospray ionization (ESI)[1] has been instrumental in enabling the mass spectrometry of proteins due, in part, to the multiple charging of the analyte molecules, which brings the high mass molecule-ions into the operational mass-to-charge range of most mass spectrometers. The conformation of the protein in solution plays a role in determining the charge state distribution (CSD) observed in the mass spectrum. CSDs weighted to high relative charge states correlate with denatured/unfolded forms of a protein, while CSDs weighted to relatively low charge states tend to reflect more native/folded protein conformations.[2−4] The range and magnitudes of charge states can have important implications for mass spectrometry and tandem mass spectrometry experiments. For example, higher charge states are often preferred for protein sequencing studies, as dissociation thresholds tend to decrease with increasing protein charge.[5,6] Dissociation efficiencies, in particular, increase with charge for electron transfer dissociation (ETD)[7] and electron capture dissociation (ECD).[8−10] Many solution additives have been shown to affect protein charge states including acids/bases or various solvents,[11−13] denaturing agents (e.g., urea, guanidine hydrochloride), "supercharging" agents (e.g., tetramethylene sulfone (sulfolane) and *m*-nitrobenzyl alchohol (*m*-NBA)),[14,15] or derivatizing agents.[16] All of these methods require the addition of various agents to the bulk solution which can waste sample, cause deleterious effects on the ESI response, and/or prevent the observation of short-lived intermediates or noncovalent complexes.

To avoid manipulation of the bulk solution, various methods have been developed to alter protein charge states either in the gas phase after the fully desolvated ions are formed or in the solution/droplet phases between the ESI tip and the orifice of the mass spectrometer. Manipulation of protein charge states has been demonstrated in the gas phase via ion/molecule[17,18] and ion/ion[19−22] reactions. Methods of mixing analyte solutions with reagents during ESI include leaking in gaseous reagent vapors into the interface of the mass spectrometer via the counter-current curtain gas,[23−25] placing a plate or a vial of the reagent below the spray region of the interface,[26] and mixing vapors with the nebulizing gas.[27] These methods have been used to manipulate protein charge states,[23−25] decrease salt adducts on biomolecules,[28] and perform on-the-fly hydrogen−deuterium exchange (HDX) studies.[26,29] However, these techniques are limited to the use of volatile reagents and may require instrument modifications for implementation.

Several other techniques have been developed to effect analyte and reagent mixing in the solution/droplet phase between the ESI tip and the orifice of the mass spectrometer, including extractive electrospray ionization (EESI),[30,31] fused droplet-electrospray ionization (FD-ESI),[32,33] and liquid sampling desorption electrospray ionization (DESI).[34] These techniques enable the mixing of nonvolatile reagents with analyte solutions without addition to the bulk solution. One common class of nonvolatile reagents used to manipulate protein charge states is supercharging agents. While the mechanism associated with supercharging remains under study, it has been proposed that the nonvolatile reagent becomes concentrated in the ESI droplet during the evaporation process, thus increasing the surface tension of the droplets.[35] The increased surface tension of the droplet results in an increase in the droplets ability to accommodate charges according to the Rayleigh charge limit theory.[36] The role of protein conformation in solution is also debated

Received: February 14, 2014
Accepted: April 4, 2014
Published: April 4, 2014

   dx.doi.org/10.1021/ac500721r | *Anal. Chem.* 2014, 86, 4581−4588

regarding the supercharging mechanism.[37] Recently, Miladinović et al. employed a dual-spraying microchip which contains two microchannels that cross on-top of each other at the tip of the chip without connecting. Protein and supercharging agent solutions were pumped separately through the two channels, and ionization was affected by applying a voltage to an electrode in contact with the protein solution. Mixing of the protein and supercharging agent solutions occurred at the tip of the microchip and in the spray plume. The authors reported the observation of slightly higher charge states as compared to mixing the analyte solution with additional solvent in the device.[38] Additionally, Konermann et al. have developed a technique to perform time-resolved ESI to monitor the folding and unfolding kinetics of proteins such as myoglobin and cytochrome *c*.[39] This technique combines solution flows from two syringes into a single capillary. Sampling the solution mixture at different lengths of the capillary has been correlated with mixing time, and the observation of short-lived protein intermediates has been reported.[40] These solution/droplet phase mixing techniques enable the use of nonvolatile reagents without adding the reagent to the bulk solution; however, they often require instrument modifications or additional equipment.

Nano-ESI (nESI) is often performed using a borosilicate capillary that has been heated and pulled to a tip. The sample is loaded into the capillary and is sprayed and ionized by applying a voltage to a conductive material that is in contact with the solution. Recently, Mark et al. used theta-shaped borosilicate glass capillaries, which are round capillaries containing a glass septum through the center of the capillary that effectively divides the capillary into two separate channels, for nESI. Electrical contact with the solution was made by hand painting or sputter coating the tips with titanium and/or gold. The authors demonstrated solution mixing via complexation of vancomycin and diacetyl-L-lysyl-D-alanyl-D-alanine when spraying the analytes from opposite sides of a theta tip. The authors also demonstrated HDX between a solution of vancomycin and deuterated vancomycin when sprayed from opposite channels of the tip. The authors believe the solution interactions occur in the Taylor cone of the spray, thus limiting the available mixing time of the solutions.[41]

All of these techniques enable the interaction of the analyte and reagent in the electrospray tip, in the Taylor cone, and/or in the droplets as they evaporate and travel through the interface of the mass spectrometer. Thus, these techniques are well suited for observing short time-scale interactions. Short-lived and/or intermediately unfolded protein conformations can be observed under these conditions. This is particularly advantageous when analyzing noncovalent protein complexes. For example, myoglobin contains a noncovalently attached heme group which is readily lost upon denaturation/unfolding of the protein in solution.[42] However, the limited mixing time involved in most of these techniques makes it possible to observe higher charge states of myoglobin without the loss of the heme group.

Herein, the use of borosilicate theta capillaries, similar to those implemented by Mark et al.,[41] for protein charge state manipulation is reported. The capillaries are heated and pulled to a tip, much like conventional, single barreled nESI capillaries. Rather than painting or sputter coating the tip with a conductive material to effect ionization as described previously,[41] a platinum wire electrode is inserted into one channel of the theta tip to form an electrical contact with the analyte solution. With this configuration, a single wire electrode can be placed in either side of the theta tip, or a dual emitter can be used in which electrodes held at the same potential are placed into both sides of the tip simultaneously. Regardless of electrode placement (each side individually or both sides simultaneously), the generated signal contains characteristics of both solutions loaded into the theta tip. Because the glass septum separates the solutions while they are in the capillary, the majority of solution mixing occurs in the Taylor cone and during droplet evolution and evaporation processes as the droplets travel through the interface of the mass spectrometer. Thus, the resulting spectrum includes species that exist on this short time scale (<1 ms).[43] The relatively short time scale is an interesting platform for studying protein denaturation as the extent of protein unfolding is dependent upon the kinetics of the conformational change, which is protein dependent. The denaturation and/or increased charging of several proteins (including myoglobin, cytochrome *c*, and carbonic anhydrase) on this time scale are reported herein.

EXPERIMENTAL SECTION

Materials. All samples were prepared in water purified by a Barnstead nanopure infinity ultrapure water system (Thermo Fisher Scientific, Waltham, MA). Cytochrome *c* from bovine heart, myoglobin from equine skeletal muscle, carbonic anhydrase II from bovine erythrocytes, oxalic acid, tetramethylene sulfone (sulfolane), and 3-nitrobenzyl alcohol (*m*-NBA) were purchased from Sigma-Aldrich (St. Louis, MO). Protein solutions were used without further purification by diluting aqueous stock solutions to a final concentration of 5−20 μM in water. Sulfolane and *m*-NBA solutions were diluted to final concentrations of 1% and 0.5%, respectively, by volume in water. Acetic acid and formic acid were purchased from Mallinckrodt Chemicals (Phillipsburg, NJ) and were diluted to final concentrations of 0.1% to 10% acid by volume in water or were used without further dilution (100% acid). Hydrochloric acid was purchased from J. T. Baker (Avantor, Center Valley, PA) and was diluted to a final concentration of 0.175 M in water.

Apparatus and Procedures. All experiments were performed using a prototype version of a QqTOF tandem mass spectrometer (Q-Star Pulsar XL, AB Sciex, Toronto, ON) modified to allow for ion trap CID and ion/ion reactions.[44] These features, however, were not employed in this work. Single-barreled borosilicate capillaries and borosilicate theta glass capillaries were purchased from Sutter Instrument Co. (Novato, CA). The single barreled borosilicate capillaries have an internal diameter of 0.86 mm. The theta glass capillaries have an internal diameter of ∼1.17 mm and contain a 0.165 mm thick glass septum that runs the length of the capillary, dividing the capillary into two parallel channels. Both the single-barreled and theta glass capillaries were pulled to a ∼10 μm tip on a Flaming/Brown micropipet puller (Sutter Instrument Co., Novato, CA). Each channel of the theta tip was loaded individually with separate solutions. A platinum wire electrode (∼200 μm diameter) was inserted into one side of the theta tip at a time to effect ionization, or a dual wire electrode was fashioned to apply equal potentials to solutions in both sides of the theta tip simultaneously. The tip of the emitter was placed about 1−2 mm from the orifice, just inside a curtain plate, used to improve the protein signal. The potential applied to the electrode(s) ranged between 1.0 and 1.5 kV. All pH measurements of protein/acid solution mixtures were made

dx.doi.org/10.1021/ac500721r | *Anal. Chem.* 2014, 86, 4581−4588

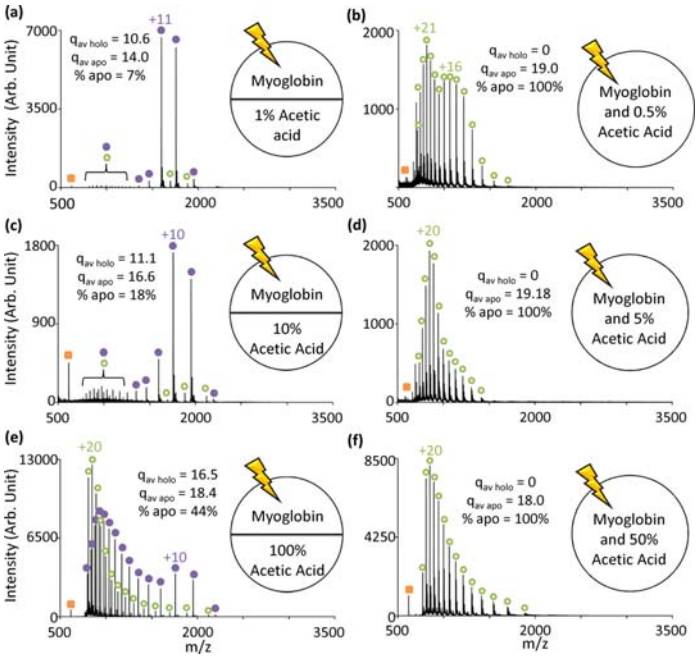

Figure 1. Myoglobin sprayed opposite (a) 1%, (c) 10%, and (e) 100% acetic acid in the theta tips. For comparison, myoglobin was mixed with equi-volume amounts of (b) 1%, (d) 10%, and (f) 100% acetic acid to yield final concentrations of 0.5% (pH 2.9), 5% (pH 2.2), and 50% (pH 0.8) acetic acid, respectively, and sprayed from a regular tip. Purple dots (●) indicate holomyoglobin charge states, green open circles (○) indicate apomyoglobin charge states, and orange squares (■) indicate heme. Lightning bolts indicate emitter location.

with an Orion perpHecT LogR meter, model 320 (Thermo Fisher Scientific; Waltham, MA).

■ RESULTS AND DISCUSSION

Protein solutions were loaded into one side of the theta tip, while reagent solutions were added to the opposite side. Similar results can be obtained by placing the electrode in either side individually or in both sides of the theta tip simultaneously. Additionally, the signal intensities obtained from a theta tip are similar to the signal intensities obtained from a regular tip. An example is illustrated in Figure S-1, Supporting Information, which summarizes a series of experiments with myoglobin and acetic acid. Control spectra in which equi-volume aliquots of the protein and reagent were mixed together in solution and sprayed from a regular tip are provided for comparison. The intensity-weighted average charge state (q_{av}) of the protein charge state distributions (CSDs) in this study are also included in the figure insets. The insets of myoglobin spectra include the average charge state of apo- ($q_{av\ apo}$) and holomyoglobin ($q_{av\ holo}$) species as well as the % of apomyoglobin signal (% apo) in the spectrum. The intensity-weighted average charge state was calculated according to eq 1 in which N is the number of observed i charge states, q_i is the net charge of the ith charge state, and W_i is the signal intensity of the ith charge state.[14]

$$q_{av} = \frac{\sum_i^N q_i W_i}{\sum_i^N W_i} \quad (1)$$

In rare instances, the relative contribution of higher and lower CSDs to the overall spectrum would evolve over time before reaching a steady state spectrum (e.g., several seconds to a minute). The first few spectra would favor a high CSD while over time the more native species at a lower CSD would become more prominent. This observation was most dramatic when using 100% acetic acid on one side of the theta tip with the protein in 100% water on the opposite side. Presumably, this effect is due to diffusion at the solution contact point at the end of the theta tip prior to nESI. All spectra presented here were taken under conditions in which the relative signals in the spectra were not changing over time.

Shifting Protein CSD with Acid Solutions in Theta Tips. Holomyoglobin (pI = 6.8−7.2) is a 17.6 kDa protein that contains a noncovalently bound heme group.[42] The non-covalent complex can be observed under native electrospray conditions.[45−47] However, myoglobin rapidly denatures upon exposure to acidic environments via a short-lived intermediate of unfolded holomyoglobin prior to the loss of the heme group yielding apomyoglobin.[40] Holomyoglobin is observed when spraying myoglobin from water without added acid while the addition of 0.5% acetic acid results in denaturation of the protein such that only apo-myoglobin peaks are observed (see Figure S-1b, Supporting Information, and Figure 1b, respectively). An unfolded holomyoglobin intermediate has been observable under conditions in which the time-scale for mixing of myoglobin with acid is limited (<1 ms).[23,39] Theta tips isolate the solutions in each side until the tip of the capillary where the Taylor cone forms. Presumably, most of the solution mixing occurs in the Taylor cone and in the progeny droplets as they travel toward the orifice of the mass spectrometer, resulting in a short mixing time-scale (<1 ms).

dx.doi.org/10.1021/ac500721r | Anal. Chem. 2014, 86, 4581−4588

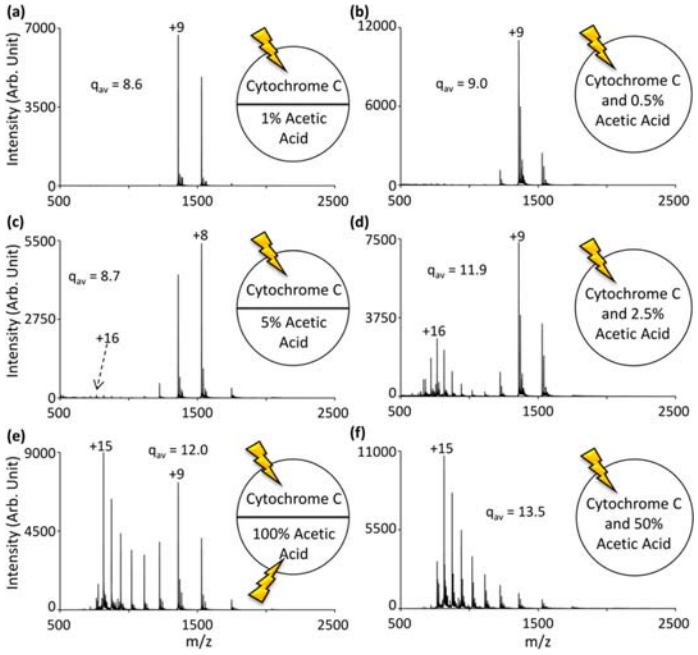

Figure 2. Cytochrome *c* sprayed opposite (a) 1%, (c) 5%, and (e) 100% acetic acid from a theta tip. Cytochrome *c* was mixed in solution with (b) 0.5%, pH 2.9; (d) 2.5%, pH 2.4; and (f) 50%, pH 0.8 acetic acid and sprayed from a regular tip for comparison.

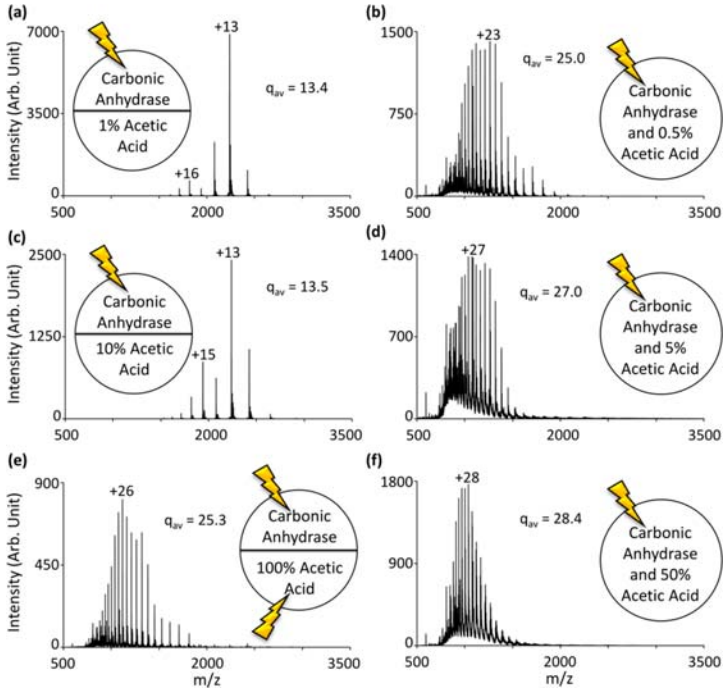

Figure 3. Carbonic anhydrase was sprayed opposite (a) 1%, (c) 10%, and (e) 100% acetic acid from a theta tip. For comparison, carbonic anhydrase was mixed in solution with (b) 0.5%, pH 2.9; (d) 5%, pH 2.2; and (f) 50%, pH 0.8 acetic acid and sprayed from a regular tip.

dx.doi.org/10.1021/ac500721r | *Anal. Chem.* 2014, 86, 4581−4588

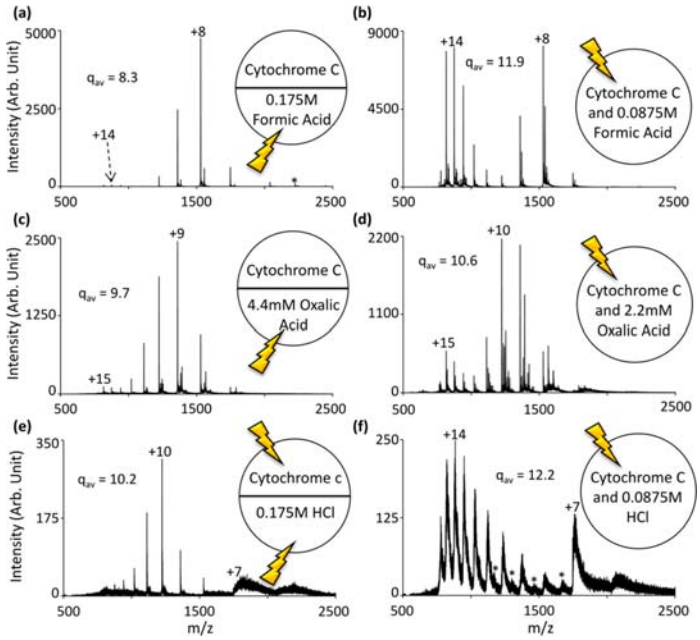

Figure 4. Cytochrome *c* sprayed opposite (a) 0.175 M formic acid, (c) 4.4 mM oxalic acid, and (e) 0.175 M HCl in the theta tips. Cytochrome *c* was also mixed in solution with (b) 0.0875 M formic acid, pH 2.3; (d) 2.2 mM oxalic acid, pH 2.6; and (f) 0.0875 M HCl, pH 1.0 and sprayed from a regular tip. The (∗) indicates cytochrome *c* dimer charge states.

The theta tip spectra support this conclusion as minor contributions from both apomyoglobin and denatured/unfolded holomyoglobin appear in Figure 1a,c,e, where myoglobin is mixed with acetic acid by spraying from a theta tip. The average charge state of holomyoglobin sprayed from water in a regular tip is about +8.3 (Figure S-1b, Supporting Information) compared to +10.6 when mixed with 1% acetic acid in the theta tips (Figure 1a). The acid-induced denaturation of myoglobin in the theta tips is evidenced by the shift of the holomyoglobin CSD to a higher average charge state and by the presence of apomyoglobin peaks. Mixing via the theta tips enables observation of the short-lived unfolded myoglobin without the loss of heme.

The extent of protein CSD shift can be controlled by varying the concentration of the acid. Figure 1a,c,e shows the effect of spraying 1%, 10%, and 100% acetic acid solutions, respectively, opposite myoglobin in a theta tip. The average CSD of apo- and holomyoglobin increases with acetic acid concentration. As shown in Figure 1b, the addition of as little as 0.5% acetic acid to bulk myoglobin solution results in 100% apomyoglobin signal.

Similar experiments were performed using cytochrome *c* (pI = 10−10.5) and carbonic anhydrase (pI = 5.9) as shown in Figures 2 and 3, respectively. Bovine cytochrome *c* is a 12.2 kDa protein containing 104 amino acids and a single heme that is covalently attached via two thioether linkages.[48] The unfolding intermediates and resulting charge state distributions of cytochrome *c* are well-known, including the transition from a more folded, lower CSD (centered around the +8/+9 charge state) to a more unfolded/denatured, higher CSD (centered around the +17 to +19 charge state) upon decreasing the pH below 2−3.[49−53] The observed CSD of cytochrome *c* when sprayed out of water without added acid is +5 to +11 (q_{av} = +7.6, Figure S-2a, Supporting Information). When cytochrome *c* is mixed with acetic acid upon spraying from a theta tip, the higher CSD (centered around the +15 charge state) becomes observable and increases in abundance as the acetic acid concentration is increased from 1% (Figure 2a) to 100% (Figure 2e).

Bovine carbonic anhydrase was also sprayed opposite various concentrations of acetic acid in the theta tips (Figure 3). Carbonic anhydrase (pI = 5.9) is a 29 kDa protein that contains a divalent zinc ion coordinated to 3 histidine residues and a water molecule within the central cavity making up the active site of the enzyme.[54,55] It is well-known that carbonic anhydrase undergoes two transitions in which a partially expanded/loosened intermediate is observable upon acid denaturation occurring within the pH ranges of 4.8−4.0 (transition I) and 3.4−2.5 (transition II).[56,57] The carbonic anhydrase CSD obtained from spraying the protein out of water without added acid from a regular tip (Figure S-2b, Supporting Information) ranged from +9 to +17 (q_{av} = +12.5). Mixing carbonic anhydrase with acetic acid via the theta tips results in an increase in the average charge state. The two lower concentrations of acetic acid resulted in a bimodal distribution centered around the +15/+16 and the +13 charge states, likely indicating the presence of two distinct conformations of the protein. With 100% acetic acid in the theta tip, the CSD shifted to much higher charge states, centered around the +26 charge state, suggesting an extended conformation. In comparison to the control spectra, in which the protein was mixed in solution with acetic acid and sprayed from a regular tip, only the higher CSD was observed with slight variations in the most abundant and average charge states.

dx.doi.org/10.1021/ac500721r | *Anal. Chem.* 2014, 86, 4581−4588

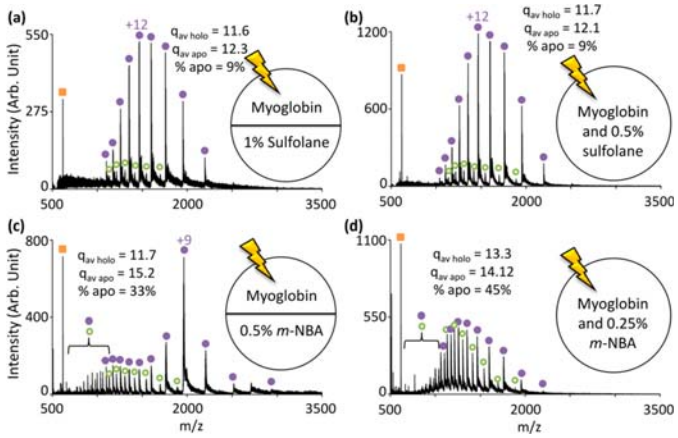

Figure 5. Myoglobin sprayed opposite (a) 1% sulfolane and (c) 0.5% *m*-NBA in a theta tip. Solution mixtures of myoglobin with (b) 0.5% sulfolane and (d) 0.25% *m*-NBA were sprayed from regular tips for comparison.

The short time scale and effective pH/acid concentration play a role in determining the species that will be observed in the mass spectrum. As the acid concentration increases, the protein denaturation rate is expected to increase, which is consistent with the observation of the more denatured protein species (higher charge states and apomyoglobin) when mixed with higher concentrations of acid. The extent of the observed shift in CSD is protein dependent as proteins have different denaturation kinetics under various pH conditions. Even at low concentrations of acetic acid (0.5%) mixed in solution with myoglobin (Figure 1b), almost exclusively apomyoglobin peaks are observed, indicating that a solution pH of 3.3 results in full denaturation at equilibrium. However, all myoglobin theta tip spectra indicate that the protein denaturation kinetics are sufficiently slow on the time-scale of the theta tip experiment that the intermediate (higher holomyoglobin charge states) is observable. This is consistent with stopped flow studies performed by Konermann et al. where they reported lifetimes of 0.38 ± 0.06s for the unfolded holomyoglobin intermediate.[40] Similarly, the solution mixture of acetic acid with carbonic anhydrase sprayed from a regular tip shows only the higher CSD even at lower concentrations of acetic acid (0.5%, Figure 3b), while two CSDs are observable in the theta tip mixing spectra for 1% (Figure 3a) and 10% (Figure 3c) acetic acid concentrations. When 100% acetic acid is mixed with carbonic anhydrase via the theta tip (Figure 3e), only the higher CSD is observed. In contrast, spectra in which cytochrome *c* was mixed with lower concentrations of acetic acid in solution (Figure 2b,d) show two CSDs centered around the +15/+16 and the +9 charge state. The two distinct CSDs indicate that, in the pH range of 2.4 to 2.9, there are multiple conformations of the protein present at equilibrium in solution. The kinetics of cytochrome *c* unfolding upon acid denaturation are not quite fast enough to reach equilibrium on the time scale of the theta tip experiment as evidenced by the lower relative abundance of the higher CSD as compared to the solution mixture at equilibrium (Figure 2a–d). However, the same two CSDs are still present. This provides evidence that there is no partially denatured intermediate observable via CSDs on the time-scale of this experiment (<1 ms). Konermann and Douglas also found only two CSDs for cytochrome *c* on the millisecond time-scale, which indicated the loss of tertiary structure (between pH 2 and 4), while they concluded that protein CSD was not a sensitive measurement for the known change in secondary structure for cytochrome *c*.[49,58]

As indicated above (see Figure 2e), a dramatic shift in the CSD of cytochrome *c* in the theta tip experiments was noted only with the 100% acetic acid experiment. Thus, it may be useful to spray proteins like cytochrome *c* opposite stronger acids to increase the rate of denaturation of the protein. Cytochrome *c* was sprayed opposite formic acid (pK_a = 3.75, vapor pressure (vp) = 35 Torr), oxalic acid (pK_a = 1.25, vp = 0.001 Torr), and HCl (pK_a = −8, vp = 120 Torr) in the theta tips (Figure 4a,c,e, respectively). The solution mixtures of each acid with cytochrome *c* sprayed from regular tips are given in Figure 4b,d,f for formic acid, oxalic acid, and HCl, respectively. Formic acid and HCl were each sprayed with concentrations of 0.875 M for comparison with 1% acetic acid (pK_a = 4.76, vp = 11 Torr) data (1% acetic acid ≈ 0.875 M). Oxalic acid was sprayed at a much lower concentration as comparable concentrations would clog the theta tips due to its low vapor pressure. There is an overall positive correlation between the acid strength and the average charge state observed in the spectra generated from mixing cytochrome *c* with the acids via the theta tips. There are two CSDs for the solution mixture of each acid (Figures 2b and 4b,d,f) and for the theta tip experiments with formic (Figure 4a) and oxalic acid (Figure 4c). The lower cytochrome *c* CSD observed with HCl mixed both in solution (Figure 4f) and via spraying from a theta tip (Figure 4e) is centered around the +7 charge state, as opposed to the +8 or +10 charge state observed with the other acids. The presence of the +7 charge state has previously been attributed to the A-state of the protein in which the protein refolds at low pH into a molten globule structure. The A-state has been observed in solution at equilibrium and on the microsecond time scale.[23,59−63] Goto et al. and Mirza and Chait have found that the acid anion plays an important role in the refolding of denatured proteins upon further decrease in pH as the addition of acid increases the anion concentration sufficiently to counteract the increased repulsive forces of the positive charges at high acid concentration, enabling the protein to refold.[60,62] The counterion effect may underlie the

observation of the lower CSD (centered around the +7 charge state) with HCl at a pH of 1.0 (Figure 4f) while it is not observed with acetic acid at a pH of 0.8 (Figure 2f).

The theta tips are also advantageous for use with nonvolatile acids, which cannot be used with various leak-in/vapor techniques. Oxalic acid is a nonvolatile acid that can be mixed with protein solutions to shift the CSD to higher charge states via spraying from a theta tip (Figure 4c). The cytochrome *c* CSD shifted from +5 to +12 (Figure S-2a, Supporting Information) when sprayed from water in a single-barreled tip to two distinct CSDs centered around the +15 and +9 charge states when mixed with oxalic acid in the theta tip (Figure 4c). The shift in protein CSD indicates solution mixing despite the nonvolatile characteristic of oxalic acid. A disadvantage of nonvolatile acids mixed in solution is the resulting adducts, which decrease the signal intensity of the protonated molecule. However, protein adduction was minimized by mixing the protein and acid solutions in the theta tips as compared to mixing in solution. The greatest difference in protein adducts was observed with oxalic acid and HCl (Figure 4c–f). Thus, the theta tips provide a simple, inexpensive method for shifting protein CSD with various acids and concentrations, including nonvolatile acids, while minimizing protein adducts.

Shifting Protein CSD with Supercharging Agents in Theta Tips. As demonstrated above with oxalic acid, one advantage of using the theta tips to effect analyte and reagent mixing on a short time-scale is their compatibility with nonvolatile reagents. Supercharging agents are a major class of nonvolatile reagents that are used to increase charge states of peptides and proteins. Two of the most commonly used supercharging agents are sulfolane and *m*-NBA. To demonstrate the use of theta tips with supercharging agents, cytochrome *c* (Figure S-3, Supporting Information) and myoglobin (Figure 5) were each mixed with sulfolane and *m*-NBA via spraying from a theta tip and the generated spectra are compared to the respective solution mixture controls.

Cytochrome *c* was sprayed opposite 1% sulfolane (Figure S-3a, Supporting Information) and 0.5% *m*-NBA (Figure S-3c, Supporting Information) in a theta tip. The cytochrome *c* CSD shifted from q_{av} = +7.6 sprayed from water in a regular tip (Figure S-2a, Supporting Information) to q_{av} = +8.7 and +8.2 with sulfolane and *m*-NBA, respectively, sprayed from theta tips. The overall appearances of the theta tip and regular tip spectra are quite similar, in that the CSD was shifted to a slightly higher CSD, but only one distribution is observed for cytochrome *c* for both supercharging agents, unlike the two distinct distributions observed with the acids above.

Similarly, myoglobin was sprayed opposite sulfolane (Figure 5a) and *m*-NBA (Figure 5c) in a theta tip and resulting spectra were compared to the solution mixtures sprayed from a regular tip (Figure 5b,d). As reported previously,[15,64] the addition of sulfolane and *m*-NBA to solutions of myoglobin results in the observation of apo- and holomyoglobin signals, which are also observed in the control spectra and the theta tip spectra reported herein (Figure 5). The percentage of apomyoglobin peaks increases from 9% to 33% with sulfolane and to 45% with *m*-NBA, which is consistent with previous observations in which greater shifts in CSD and denaturation were observed with *m*-NBA than with sulfolane.[64] Similar to the results described above with cytochrome *c*, the overall appearance of the spectra for mixing sulfolane with myoglobin via the theta tips is similar to the solution phase mixture sprayed from a regular tip.

As previously mentioned, the mechanism by which supercharging agents increase the charge state of proteins is still unclear. Lomeli et al. have found that *m*-NBA concentrations below 1.0% do not denature myoglobin in bulk solution.[15] Additionally, Sterling et al. have determined that the addition of sulfolane from 0.0% to 7.5% sulfolane destabilizes the native conformation of myoglobin in solution; however, no loss of helicity was observed at room temperature.[64] The lack of denaturation in bulk solution indicates that the denaturation of the proteins likely occurs during the electrospray process in the droplet. The theta tip results are consistent with this conclusion as the theta tip spectra are similar to the bulk solution mixture spectra, indicating that the equilibrium state of the protein in the bulk solution is not significantly affected by the presence of the supercharging agent. The time-scale of protein denaturation using the supercharging agents appears to be similar in both the theta tip (limited to the microsecond time scale) and regular tip spectra, suggesting that the processes that underlie supercharging occur during the electrospray process.

CONCLUSIONS

The use of pulled borosilicate theta glass capillaries as nESI emitters to effect microsecond time scale mixing of protein and denaturant solutions results in shifts in protein CSD without requiring modification of the bulk solution. The extent of protein CSD shift is determined by acid identity, acid concentration, and the kinetics of unfolding of the protein. Due to the short time-scale of mixing, short-lived intermediate species such as the higher CSD of holomyoglobin can be observed. Theta tips also allow for the use of nonvolatile acids and supercharging agents which are not compatible with other vapor leak-in techniques. No instrument modifications are necessary, which should make this approach widely accessible to the analytical mass spectrometry community.

ASSOCIATED CONTENT

Supporting Information

Additional information as noted in text. This material is available free of charge via the Internet at http://pubs.acs.org.

AUTHOR INFORMATION

Corresponding Author

*E-mail: mcluckey@purdue.edu. Phone: (765) 494-5270. Fax: (765) 494-0239.

Notes

The authors declare no competing financial interest.

ACKNOWLEDGMENTS

This work was supported by the National Science Foundation under CHE-1111389.

REFERENCES

(1) Fenn, J. B.; Mann, M.; Meng, C. K.; Wong, S. F.; Whitehouse, C. M. *Science* **1989**, *246*, 64–71.
(2) Chowdhury, S. K.; Katta, V.; Chait, B. T. *J. Am. Chem. Soc.* **1990**, *112*, 9012–9013.
(3) Kaltashov, I. A.; Eyles, S. J. *Mass Spectrom. Rev.* **2002**, *21*, 37–71.
(4) Fenn, J. B. *J. Am. Soc. Mass Spectrom.* **1993**, *4*, 524–535.
(5) Reid, G. E.; Wu, J.; Chrisman, P. A.; Wells, M.; McLuckey, S. A. *Anal. Chem.* **2001**, *73*, 3274–3281.

(6) Jockusch, R. A.; Schnier, P. D.; Price, W. D.; Strittmatter, E. F.; Demirev, P. A.; Williams, E. R. *Anal. Chem.* **1997**, *69*, 1119−1126.
(7) Syka, J. E.; Coon, J. J.; Schroeder, M. J.; Shabanaowitz, J.; Hunt, D. F. *Proc. Natl. Acad. Sci. USA* **2004**, *101*, 9528−9533.
(8) Zubarev, R. A.; Kelleher, N. L.; McLafferty, F. W. *J. Am. Chem. Soc.* **1998**, *120*, 3265−3266.
(9) Iavarone, A.; Paech, K.; Williams, E. R. *Anal. Chem.* **2004**, *76*, 2231−2238.
(10) Zubarev, R. A.; Horn, D. M.; Fridriksson, E. K.; Kelleher, N. L.; Kruger, N. A.; Lewis, M. A.; Carpenter, B. K.; McLafferty, F. W. *Anal. Chem.* **2000**, *72*, 563−573.
(11) Loo, J. A.; Ogorzalek Loo, R. R.; Udseth, H. R.; Edmonds, C. G.; Smith, R. D. *Rapid Commun. Mass Spectrom.* **1991**, *5*, 101−105.
(12) Iavarone, A. T.; Jurchen, J. C.; Williams, E. R. *J. Am. Soc. Mass Spectrom.* **2000**, *11*, 976−985.
(13) Le Blanc, J. C. Y.; Wang, J.; Guevremont, R.; Siu, K. W. M. *Org. Mass Spectrom.* **1994**, *29*, 587−593.
(14) Iavarone, A. T.; Jurchen, J. C.; Williams, E. R. *Anal. Chem.* **2001**, *73*, 1455−1460.
(15) Lomeli, S. H.; Peng, I. X.; Yin, S.; Ogorzalek Loo, R. R.; Loo, J. A. *J. Am. Soc. Mass Spectrom.* **2010**, *21*, 127−131.
(16) Krusemark, G. J.; Frey, B. L.; Belshaw, P. J.; Smith, L. M. *J. Am. Soc. Mass Spectrom.* **2009**, *20*, 1617−1625.
(17) McLuckey, S. A.; Van Berkel, G. J.; Glish, G. L. *J. Am. Chem. Soc.* **1990**, *112*, 5668−5670.
(18) Ogorzalek Loo, R. R.; Winger, B. E.; Smith, R. D. *J. Am. Soc. Mass Spectrom.* **1994**, *5*, 1064−1071.
(19) Stephenson, J. L., Jr.; McLuckey, S. A. *J. Am. Chem. Soc.* **1996**, *118*, 7390−7397.
(20) Scalf, M.; Westphall, M. S.; Krause, J.; Kaufman, S. L.; Smith, L. M. *Science* **1999**, *283*, 194−197.
(21) He, M.; McLuckey, S. A. *J. Am. Chem. Soc.* **2003**, *125*, 7756−7757.
(22) He, M.; McLuckey, S. A. *Anal. Chem.* **2004**, *76*, 4189−4192.
(23) Kharlamova, A.; Prentice, B. M.; Huang, T.-Y.; McLuckey, S. A. *Anal. Chem.* **2010**, *82*, 7422−7429.
(24) Kharlamova, A.; McLuckey, S. A. *Anal. Chem.* **2011**, *83*, 431−439.
(25) Kharlamova, A.; DeMuth, J. C.; McLuckey, S. A. *J. Am. Soc. Mass Spectrom.* **2011**, *23*, 88−101.
(26) Kostyukevich, Y.; Kononikhin, A.; Popov, I.; Nikolaev, E. *Anal. Chem.* **2013**, *85*, 5330−5334.
(27) Girod, M.; Antoine, R.; Dugourd, P.; Love, C.; Mordehai, A.; Stafford, G. *J. Am. Soc. Mass Spectrom.* **2012**, *23*, 1221−1231.
(28) Kharlamova, A.; Prentice, B. M.; Huang, T.-Y.; McLuckey, S. A. *Int. J. Mass Spectrom.* **2011**, *300*, 158−166.
(29) Takáts, Z.; Schlosser, G.; Vékey, K. *Int. J. Mass Spectrom.* **2003**, *228*, 729−741.
(30) Chen, H.; Touboul, D.; Jecklin, M. C.; Zheng, J.; Luo, M.; Zenobi, R. *Eur. J. Mass Spectrom.* **2007**, *13*, 273−279.
(31) Chen, H.; Venter, A.; Cooks, R. G. *Chem. Commun.* **2006**, *19*, 2042−2044.
(32) Chang, D.-Y.; Lee, C.-C.; Shiea, J. *Anal. Chem.* **2002**, *74*, 2465−2469.
(33) Shieh, I.-F.; Lee, C.-Y.; Shiea, J. *J. Proteome Res.* **2005**, *4*, 606−612.
(34) Miao, Z.; Wu, S.; Chen, H. *J. Am. Soc. Mass Spectrom.* **2010**, *21*, 1730−1736.
(35) Iavarone, A. T.; Williams, E. R. *J. Am. Chem. Soc.* **2003**, *125*, 2319−2327.
(36) Lord Rayleigh. *Philos. Mag.* **1882**, *14*, 184−186.
(37) Lomeli, S. H.; Yin, S.; Ogorzalek Loo, R. R.; Loo, J. A. *J. Am. Soc. Mass Spectrom.* **2009**, *20*, 593−596.
(38) Miladinović, S. M.; Fornelli, L.; Lu, Y.; Piech, K. M.; Girault, H. H.; Tsybin, Y. O. *Anal. Chem.* **2012**, *84*, 4647−4651.
(39) Konermann, L.; Collings, B. A.; Douglas, D. J. *Biochemistry* **1997**, *36*, 5554−5559.
(40) Konermann, L.; Rosell, F. I.; Mauk, A. G.; Douglas, D. J. *Biochemistry* **1997**, *36*, 6448−6454.
(41) Mark, L. P.; Gill, M. C.; Mahut, M.; Derrick, P. J. *Eur. J. Mass Spectrom.* **2012**, *18*, 439−446.
(42) Evans, S. V.; Brayer, G. D. *J. Mol. Biol.* **1990**, *23*, 885−897.
(43) Schneider, B. B.; Baranov, V. I.; Javaheri, H.; Covey, T. R. *J. Am. Soc. Mass Spectrom.* **2003**, *14*, 1236−1246.
(44) Xia, Y.; Chrisman, P. A.; Erickson, D. E.; Liu, J.; Liang, X.; Londry, F. A.; Yang, M. J.; McLuckey, S. A. *Anal. Chem.* **2006**, *78*, 4146−4154.
(45) Katta, V.; Chait, B. T. *J. Am. Chem. Soc.* **1991**, *113*, 8534−8535.
(46) Li, Y.-T.; Hsich, Y.-L.; Henion, J. D. *J. Am. Soc. Mass Spectrom.* **1993**, *4*, 631−637.
(47) Loo, J. A. *Mass Spectrom. Rev.* **1997**, *16*, 1−23.
(48) Margoliash, E.; Schejter, A. *Adv. Protein Chem.* **1966**, *21*, 113−286.
(49) Konermann, L.; Douglas, D. J. *Biochemistry* **1997**, *36*, 12296−12302.
(50) Grandori, R.; Matecko, I.; Müller, N. *J. Mass Spectrom.* **2002**, *37*, 191−196.
(51) Goto, Y.; Hagihara, Y.; Hamada, D.; Hoshino, M.; Nishii, I. *Biochemistry* **1993**, *32*, 11878−11885.
(52) Grandori, R. *Protein Sci.* **2002**, *11*, 453−458.
(53) Bai, Y.; Sosnick, T. R.; Mayne, L.; Englander, S. W. *Science* **1995**, *269*, 192−197.
(54) Lindskog, S. *Pharmacol. Ther.* **1997**, *74*, 1−20.
(55) Saito, R.; Sato, T.; Ikai, A.; Tanaka, N. *Acta Crystallogr.* **2004**, *D60*, 792−795.
(56) Wong, K.-P.; Hamlin, L. M. *Biochemistry* **1974**, *13*, 2678−2683.
(57) Wong, K.-P.; Tanford, C. *J. Biol. Chem.* **1973**, *248*, 8518−8523.
(58) Ikai, A.; Fish, W. W.; Tanford, C. *J. Mol. Biol.* **1973**, *73*, 165−184.
(59) Fink, A. L.; Calciano, L. J.; Goto, Y.; Kurotsu, T.; Palleros, D. R. *Biochemistry* **1994**, *33*, 12504−12511.
(60) Goto, Y.; Calciano, L. J.; Fink, A. L. *Proc. Natl. Acad. Sci. U.S.A.* **1990**, *87*, 573−577.
(61) Bychkova, V. E.; Dujsekina, A. E.; Lenin, S. I.; Tiktopulo, E. I.; Uversky, V. N.; Ptitsyn, O. B. *Biochemistry* **1996**, *35*, 6058−6063.
(62) Mirza, U. A.; Chait, B. T. *Anal. Chem.* **1994**, *66*, 2898−2904.
(63) Jeng, M.-F.; Englander, S. W. *J. Mol. Biol.* **1991**, *221*, 1045−1061.
(64) Sterling, H. J.; Daly, M. P.; Geld, G. K.; Thoren, K. L.; Kintzer, A. F.; Krantz, B. A.; Williams, E. R. *J. Am. Soc. Mass Spectrom.* **2010**, *21*, 1762−1774.